AD-A043 433 ION PHYSICS CORP BURLINGTON MASS F/G 11/4
ELECTRON BEAM TESTING FOR CARBON DYNAMIC RESPONSE PROGRAM (CADR--ETC(U)
MAY 77 R D EVANS F29601-73-C-0075
UNCLASSIFIED IPC-7604-TR-447 AFWL-TR-76-138 NL

1 OF 2
ADA
043433

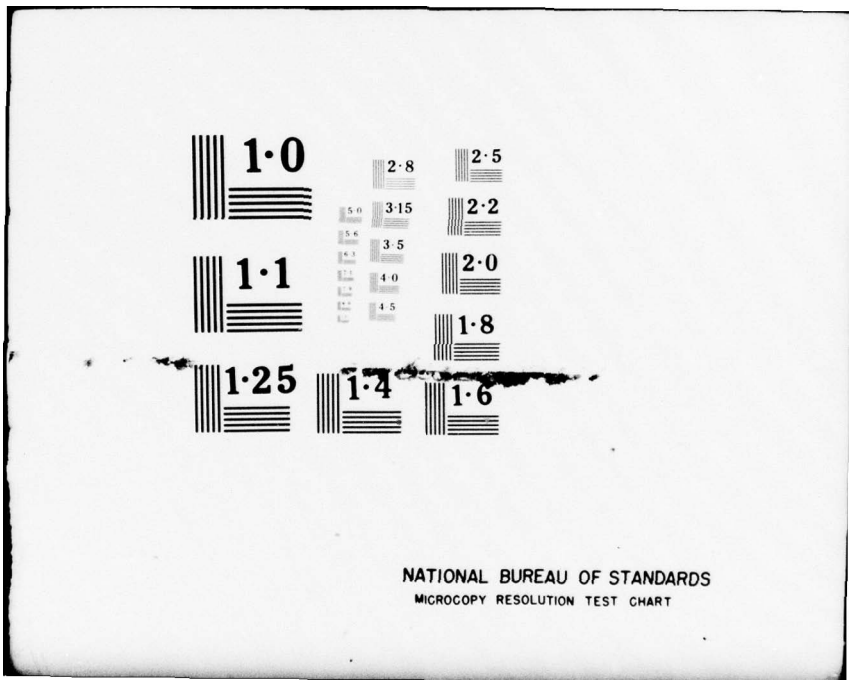
1·0
1·1
1·25
1·4
1·6
1·8
2·0
2·2
2·5
2·8
3·15
3·5
4·0
4·5
5·0
5·6
NATIONAL BUREAU OF STANDARDS
MICROCOPY RESOLUTION TEST CHART

AFWL-TR-
76-138

ELECTRON BEAM TESTING FOR CARBON DYNAMIC RESPONSE PROGRAM (CADRE)

Ion Physics Corporation, Burlington, MA 01803

Avco Systems Division, Wilmington, MA 01887

May 1977

Final Report

This research was sponsored jointly by SAMSO and the Defense Nuclear Agency under Subtask AC304, Work Unit 10, "Carbon-Resin E-Beam Experiments," Subtask AC304, Work Unit 11, "Carbon-Carbon E-Beam Experiments," Subtask AX888, Work Unit 16, "Response Correlation (Ming Blade)," and Subtask AC304, Work Unit 16, "Carbon Resin Material Response."

Prepared for

Director
DEFENSE NUCLEAR AGENCY
Washington, DC 20305

SPACE AND MISSILE SYSTEMS ORGANIZATION
Los Angeles, CA 90009

AIR FORCE WEAPONS LABORATORY
Air Force Systems Command
Kirtland Air Force Base, NM 87117

This final report was prepared by Ion Physics Corporation, Burlington, Massachusetts, and Avco Systems Division, Wilmington, Massachusetts under Contract F29601-73-C-0075, Job Order WDNA0406 with the Air Force Weapons Laboratory, Kirtland Air Force Base, New Mexico. Previous project officers were Capt Theodore D. Lynch, Capt Ronald G. Powell, Capt Charles M. Snow, and Lt John A. MacFarlane. Mr. David Newlander (DYV) is the Laboratory Project Officer-in-Charge.

When US Government drawings, specifications, or other data are used for any purpose other than a definitely related Government procurement operation, the Government thereby incurs no responsibility nor any obligation whatsoever, and the fact that the Government may have formulated, furnished, or in any way supplied the said drawings, specifications, or other data is not to be regarded by implication or otherwise as in any manner licensing the holder or any other person or corporation or conveying any rights or permission to manufacture, use, or sell any patented invention that may in any way be related thereto.

This report has been reviewed by the Information Office (OI) and is releasable to the National Technical Information Service (NTIS). At NTIS, it will be available to the general public, including foreign nations.

This technical report has been reviewed and is approved for publication.

C. David Newlander
C. DAVID NEWLANDER
Project Officer

FOR THE COMMANDER

Rand E. Rensvold
RAND E. RENSVOLD
Lt Colonel, USAF
Chief, Material & Structures
Engineering Branch

John S. DeWitt
JOHN S. DeWITT
Lt Colonel, USAF
Chief, Analysis Division

DO NOT RETURN THIS COPY. RETAIN OR DESTROY.

UNCLASSIFIED

SECURITY CLASSIFICATION OF THIS PAGE *(When Data Entered)*

REPORT DOCUMENTATION PAGE		READ INSTRUCTIONS BEFORE COMPLETING FORM
1. REPORT NUMBER AFWL-TR-76-138	2. GOVT ACCESSION NO.	3. RECIPIENT'S CATALOG NUMBER
4. TITLE *(and Subtitle)* ELECTRON BEAM TESTING FOR CARBON DYNAMIC RESPONSE PROGRAM (CADRE)		5. TYPE OF REPORT & PERIOD COVERED Final Report. 6. PERFORMING ORG. REPORT NUMBER IPC-7604-TR447
7. AUTHOR(s) Robert D. Evans		8. CONTRACT OR GRANT NUMBER(s) F29601-73-C-0075
9. PERFORMING ORGANIZATION NAME AND ADDRESS Ion Physics Corporation South Bedford Street Burlingotn, MA 01803		10. PROGRAM ELEMENT, PROJECT, TASK AREA & WORK UNIT NUMBERS 62707H & 63311F WDNA0406
11. CONTROLLING OFFICE NAME AND ADDRESS Director Defense Nuclear Agency Washington, D.C. 20305 SAMSO, POB 92960, WWPC Los Angeles, CA 90009		12. REPORT DATE May 1977 13. NUMBER OF PAGES ~~124~~ 229
14. MONITORING AGENCY NAME & ADDRESS*(if different from Controlling Office)* Air Force Weapons Laboratory (DYV) Kirtland AFB, NM 87117		15. SECURITY CLASS. *(of this report)* UNCLASSIFIED 15a. DECLASSIFICATION DOWNGRADING SCHEDULE

16. DISTRIBUTION STATEMENT *(of this Report)*

Approved for public release; distribution unlimited.

17. DISTRIBUTION STATEMENT *(of the abstract entered in Block 20, if different from Report)*

18. SUPPLEMENTARY NOTES

The subcontractor for this report was Avco Systems Division, Wilmington, Massachusetts.

19. KEY WORDS *(Continue on reverse side if necessary and identify by block number)*

Electron Beam Testing
Impulse
Shock Waves
Carbon Phenolic
Carbon-Carbon

20. ABSTRACT *(Continue on reverse side if necessary and identify by block number)*

Electron beam testing performed under the Carbon Dynamic Response Program is described. Results are presented for a simulated tape wrapped carbon phenolic and for a three dimensional carbon-carbon composite.

188 000

DD FORM 1 JAN 73 1473 EDITION OF 1 NOV 65 IS OBSOLETE

UNCLASSIFIED

SECURITY CLASSIFICATION OF THIS PAGE *(When Data Entered)*

18. SUPPLEMENTARY NOTES (Continued)

This research was sponsored jointly by SAMSO and the Defense Nuclear Agency under Subtask AC304, Work Unit 10, "Carbon-Resin E-Beam Experiments," Subtask AC304, Work Unit 11, "Carbon-Carbon E-Beam Experiments," Subtask AX888, Work Unit 16, "Response Correlation (Ming Blade)," and Subtask AC304, Work Unit 16, "Carbon Resin Material Response."

PREFACE

The author wishes to acknowledge the assistance of Captain Richard Scammon who functioned as liaison between ourself and the AFWL computer center and who unstintingly gave of his time to see that this interface was a smooth one. Recognition is also due Mr. David Newlander (AFWL) who offered technical and administrative aid throughout the course of the work.

At Ion Physics, the laboratory crew consisting of Messrs. Gerald Guse and Ted Norton was instrumental in making the experimental program a success. Substantial portions of the testing were supervised by Drs. R. S. Wenstrup and S. G. Oston; it was a pleasure to work with these gentlemen.

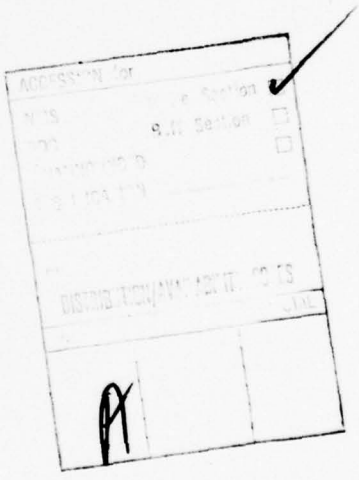

CONTENTS

ILLUSTRATIONS

TABLES

SECTION I

INTRODUCTION

The objective of the Carbon Dynamic Response (CADRE) Program was to understand and learn how to predict the thermomechanical behavior of carbon phenolic and carbon-carbon composites. To meet this objective, an effort was undertaken to meld new and existing data from underground testing, electron beam experiments, and gas gun measurements into a comprehensive whole; these results were than used to test the predictive ability of impulse and stress propagation models. Materials studied were two dimensional carbon phenolic (2DCP) and three dimensional carbon-carbon (3DCC). Simultaneously, a study was undertaken at Systems, Science, and Software, La Jolla, California, to examine three dimensional carbon phenolic (3DCP).

CADRE was carried out in an experimental and an analytical task. The experimental work consisted of obtaining impulse and stress-time data on 2DCP and 3DCC in a variety of electron beam environments, and of attempting to determine the Gruneisen parameter for both materials under conditions of quasi-isovolumetric heating. During the course of the program it became clear that Hugoniot data available from the literature were insufficient to support a careful modeling effort, and additional gas gun data were accordingly taken at the Air Force Weapons Laboratory (AFWL) impact facility.

The analytical portion of CADRE endeavored to develop a semi-empirical model for stress propagation in 2DCP based upon a modified version of PUFF. Correlation between impulse predictions and measurements were made for several models using underground test and electron beam data.

Because the work fell naturally into experimental and analytical phases, this division has been maintained for purposes of reporting. This document presents results of electron beam measurements; modeling and analysis of material behavior will be covered in a separate report.

SECTION II

ELECTRON BEAM TESTING MATRIX

This report describes electron beam testing carried out on 2DCP and 3DCC using the facilities of Ion Physics Radiation Effects Laboratory. Additional work on these same materials, sponsored by AFWL, was conducted at the Naval Research Laboratory (NRL) as a supporting effort and has been reported upon in reference 1. At NRL, impulse and rear surface stress-time histories were measured at an electron fluence near 300 cal/cm^2 with a beam whose mean energy was nominally 500 keV.

A matrix of the CADRE experiments, exclusive of those undertaken at NRL, is shown in Table 1. In 2DCP, this matrix was designed to provide for a progression of dose levels ranging from the vaporization threshold of phenolic up to and beyond the point at which both resin and graphite vaporize simultaneously. It therefore provided for data under conditions from pure thermal shock to vapor dominated blowoff; contributions to impulse and stress histories from non-blowoff, from front surface spallation or "jumpoff", from single phase vaporization, and from vaporization of both phases could all be studied.

Tactical situations for which the response of 2DCP would be dominated by thermal shock or blowout of the resin alone correspond to substantial in-depth heating with relatively low surface doses. These conditions are represented by the 30, 60, and 100 cal/cm^2 750 keV testing in our matrix. The fluences indicated correspond to peak doses of about 200 cal/gm (incipient vaporization of phenolic), 300 cal/gm, and 450 cal/gm (two points in the region of in-depth single phase blowout of the resin).

Vapor dominated intercepts are defined by high surface doses and relatively shallow penetration. Testing at electron energies near 200 keV was included to examine cases of this type. At 20 cal/cm^2, 200 keV peak doses

TABLE 1

EXPERIMENT MATRIX

Target Material	Mean Energy, keV	Fluence, cal/cm^2	Measurement Types*
TWCP	200	20	I, σ
		60	I, σ
		130	I, σ
3DCC	200	60	I, σ
		100	I, σ
		130	I, σ
TWCP	750	30	I, σ
		60	I, σ
		100	I, σ
TWCP	3000	10	γ
		40	γ
3DCC	3000	10	γ
		40	γ

*I = Impulse

σ = Stress time

γ = Gruneisen stress measurement

were about 600 cal/gm; this value was close to that achieved at 100 cal/cm^2, 750 keV, and provided a point of near overlap between testing with a surface dose and in-depth heating.

From this point at 20 cal/cm^2, the matrix indicates an increase to 60 cal/cm^2 (or about 1500 cal/gm), which is at or near the incipient vaporization energy of graphite. At this fluence, sensitivity to threshold effects in refractories should be greatest, and blowoff of graphite will be accompanied by violent removal of superheated phenolic. The highest surface dose which can presently be achieved with electron beams over a reasonable working area corresponds to 130 cal/cm^2 on Neptune (approximately 4500 cal/gm over a 0.75-inch diameter spot). It was the objective of this point in the matrix to study the response of 2DCP when impulse produced by both phases is vapor dominated.

Testing of 3DCC was limited to conditions in the vicinity of or higher than the vaporization threshold of graphite; therefore experiments using 200 keV mean energy electrons were emphasized. Fluences chosen ranged from a value designed to give surface doses near the point of incipient vaporization up to 130 cal/cm^2, corresponding to the highest dose which could be consistently achieved over a reasonable working area. When 3DCC testing was initiated, first measurements were made at 130 cal/cm^2 because largest responses were expected at this level. In practice, it was found that signals generated were not substantially above background. From this result it became apparent that the value of testing at lower fluences would be negligible, and the 60 and 100 cal/cm^2 portions of the 3DCC matrix were accordingly deleted.

Quantities recorded in experiments conducted at 200 and 750 keV were impulse and rear surface stress-time histories. Impulse was measured with a ballistic pendulum using sample construction and mounting methods developed under a previous program and discussed in reference 2. A variety of stress gaging techniques were examined during the course of the effort, including interferometry, piezoresistive elements, and quartz crystals, but

bulk of the histories reported here were taken with the latter.

The primary exception to this was the need for interferometry to read the low stresses associated with isovolumetric heating experiments made on 2DCP and 3DCC using a 3 MeV beam. The purpose of these experiments, carried out at 10 and 40 cal/cm^2, was to determine dynamic Gruneisen parameters for the two materials.

Testing utilized Ion Physics FX-35 and upgraded Neptune facilities, both of which have been described in detail elsewhere[2,3]. Neptune-C is a low impedance pulser which can produce electron spectra having mean energies in the range 100 to 500 keV; it will store up to 15,000 joules and will deliver 5,000 joule electron beam at the diode. With a matched load, currents in excess of 200 kiloamperes can be generated. Using neutral gas beam drifting techniques, energy fluences up to 150 cal/cm^2 can be placed into a 3 cm^3 spot, 100 cal/cm^2 into 5 cm^2, and 30 cal/cm^2 into 18 cm^2. With bar cathodes it has been possible to irradiate rectangular areas 1 cm wide by 10 cm long with fluences up to 25 cal/cm^2. Width of the power pulse is about 70 nanoseconds at half maximum.

Because of its unique design, Neptune has proven to be a very reproducible and trouble free machine. Shot-to-shot variation in beam energy is ± 5 percent or less, making possible carefully controlled experiments. Command switching at all stages of energy flow allows jitter between the initial firing signal and beam emergence to be held to a ± 5 nanoseconds RMS. Mechanical transients at firing are minimized by conducting all switching operations in gas; this consideration can be important for experiments that must be placed in proximity to the machine or that must remain aligned during the pulse.

The FX-35 was designed as a source of high voltage bremsstrahlung photons. In the electron beam mode, spectra ranging in mean energy from 500 keV to 3.6 MeV can be obtained. Fluences depend on the degree of pinch; typical values are 100 cal/cm^2 over 1 cm^2, 60 cal/cm^2 over 2 cm^2, 30 cal/cm^2 over 3 cm^2, and lower fluences over correspondingly larger areas. Pulsewidth in the beam mode is about 40 nanoseconds.

FX-35 stores 2.5 kilojoules and under matched conditions will give a current of 55 kiloamperes. Like Neptune, FX-35 offers excellent shot-to-shot reproducibility.

Details of experiment chamber configurations for both machines have been described in reference 2; setups used throughout this work were similar to those discussed in the reference.

SECTION III

GRUNEISEN EXPERIMENTS

3.1 Experiment Design

The Grueneisen parameter is defined as

$$G(E,V) = V\left(\frac{\partial P}{\partial E}\right)_V \qquad (1)$$

where E = energy density

V = specific volume

P = pressure

Assuming reference states of zero pressure and internal energy, equation (1) can be approximated by:

$$G = \frac{1}{\rho_o}\left(\frac{P}{E}\right)_V \qquad (2)$$

The Gruneisen parameter could therefore be determined directly from an experiment in which material was heated isovolumetrically to a uniform energy density E and the corresponding internal pressure recorded. In practice, this idealized experiment can only be approximated. Qausi-isovolumetric heating can be obtained by injecting energy into the target in a pulse whose width is short compared to the time required for substantial stress relief; relief becomes "substantial" when the thickness of material affected roughly the same as the thickness which is being heated. For electron beam heating, the conditions necessary to approximate isovolumetric heating can therefore be quantified by insisting that the distance relief waves travel

during the pulse is small compared to the electron range, or

$$\frac{c\,\tau}{R} << 1 \qquad (3)$$

Here c is sound speed in the target material, τ electron beam pulse width, and R range. If it is demanded that

$$\frac{c\,\tau}{R} = 0.1$$

the necessary range can be calculated and the corresponding mean energy determined, thus specifying the type of electron environment needed.

Taking the sound speed of carbon phenolic as 4.2×10^{-4} cm/ns, the value given by Kohn[4], and using 50 ns as being typical of electron beam pulsewidths, then it is found that range must satisfy the requirement

$$R = 0.21 \text{ cm}$$

Spencer[5] gives range-energy relations for monoenergetic electrons incident at zero angle from a planar source; his data have been plotted in Figure 1 for carbon. Entering this figure with a range of 0.21 cm shows that the corresponding energy is about 1 MeV. A relatively high energy beam is therefore required to meet the requirement for quasi-isovolumetric heating.

A high energy beam is also necessary to approximate the condition of uniform heating throughout the target volume. Figure 2 shows deposition profiles plotted for 2.6 MeV and 4.5 MeV electron beams. This plot shows that it is possible to obtain a deposition profile which is very nearly flat over a substantial depth by going to a high energy beam. The 4.5 MeV profile is uniform to within 10 percent or better from the surface to a depth of about 1.4 gm/cm^2.

Figure 2 shows that a 2.6 MeV beam will give a profile flat to within ± 10% over the region reaching to about 0.5 gm/cm^2. For material whose density is in the vicinity of 1.5 gm/cm^3, 0.5 gm/cm^2 corresponds to

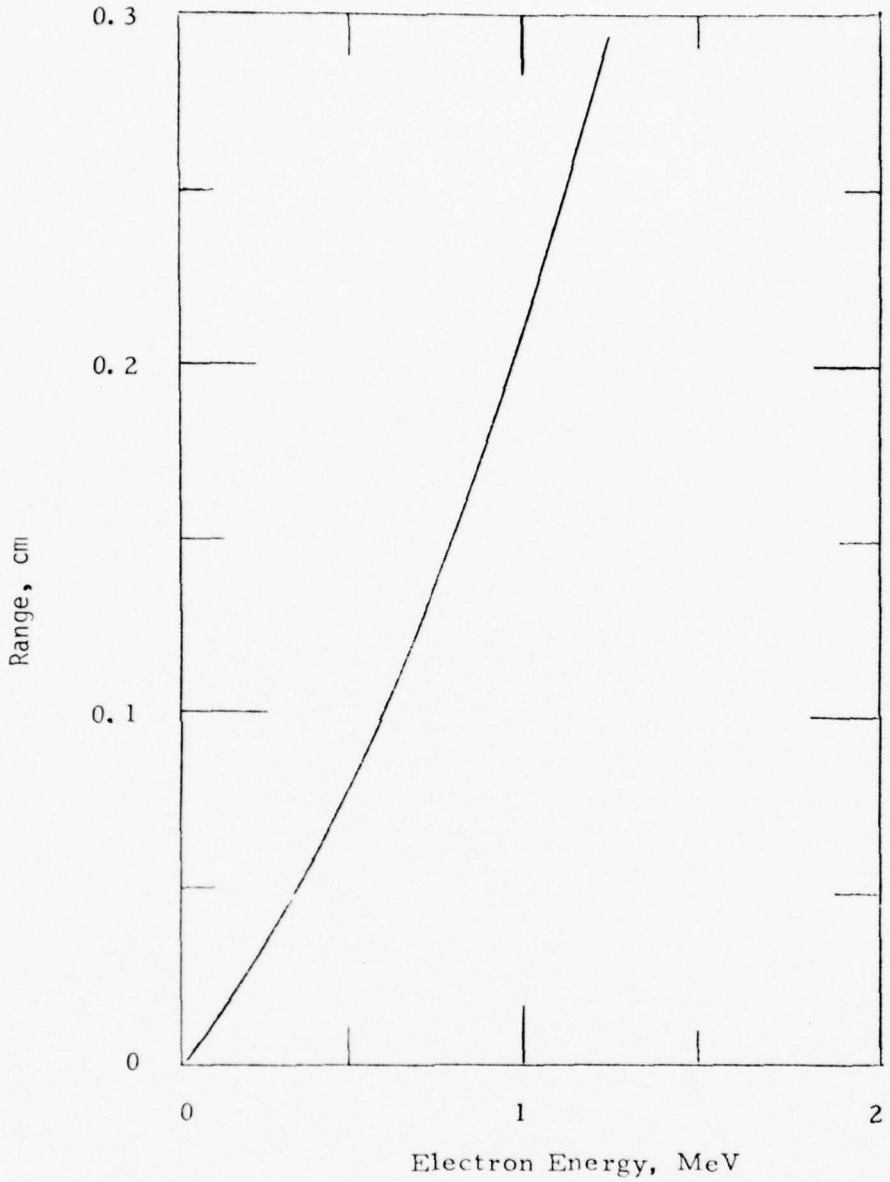

Figure 1. Range-Energy Relation for Monoenergetic Electrons Incident on Carbon

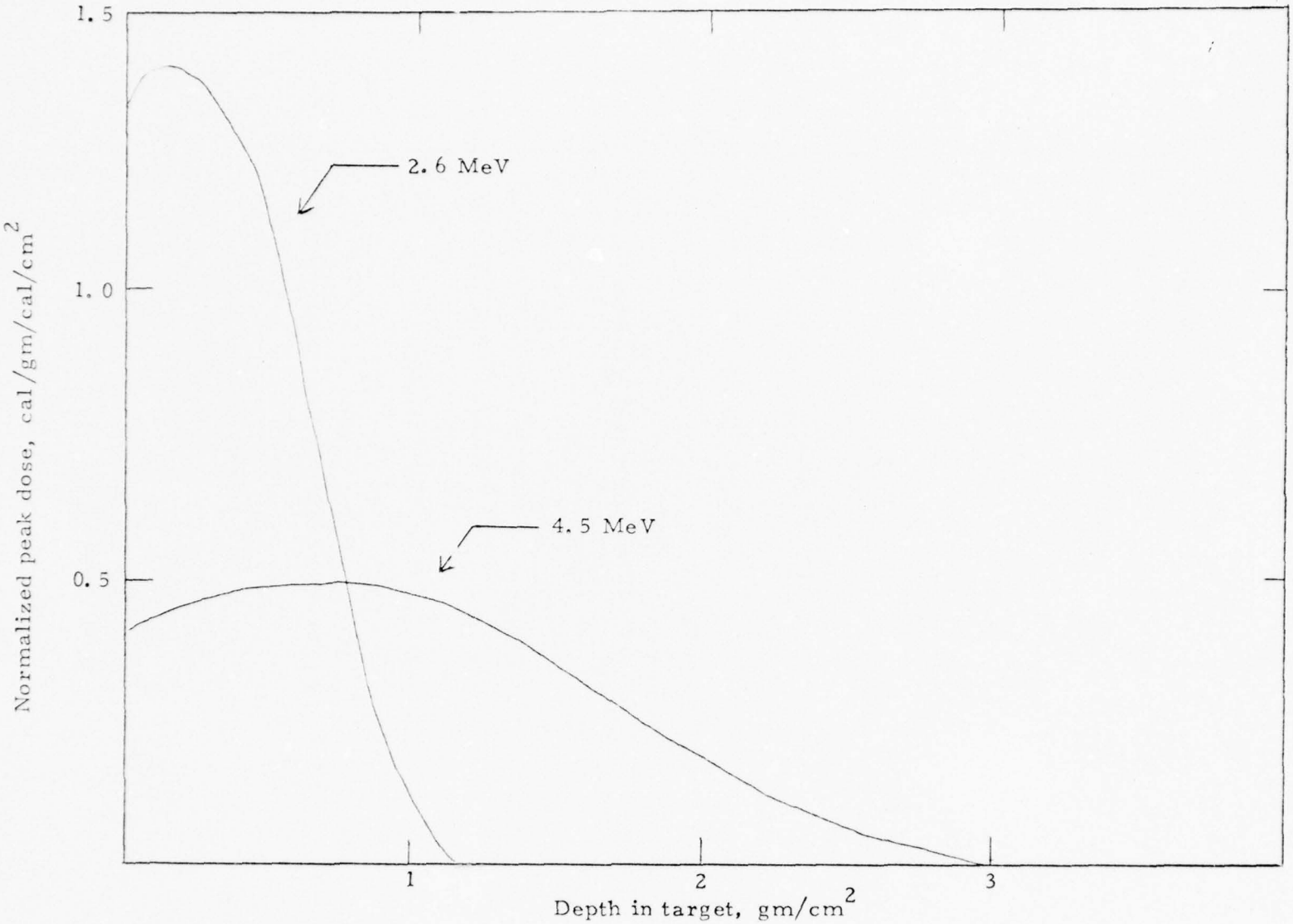

Figure 2. Depth-Dose Profiles for High Mean Energy Beams

a thickness of about 0.33 cm. This would be the maximum carbon phenolic thickness usable at 2.6 MeV without exceeding a dose variation of ± 10%. Employing Kohn's value of sound speed with the 40 ns baseline-to-baseline pulsewidth of the FX-35 gives a relief depth of 0.017 cm. The ratio of target thickness to relief depth would therefore be about

$$\frac{X}{c\tau} \cong 20 .$$

While this calculation shows that either dose profile depicted in Figure 2 provides acceptable dose uniformity over material depths adequate for the experiment, it would appear at first glance that the 4.5 MeV beam enjoys an advantage because it is flat over a larger region. In practice it is the case that a compromise must be struck between uniformity and depth of penetration; for beams of limited diameter, deeper penetration implies a reduction in one dimensional read time at the measuring point if this point must be outside range. Because the interferometric technique used here required an undisturbed reflecting surface, use of a 4.5 MeV beam would have placed the measuring point in a region of very short read time. For this reason the lower mean energy beam was preferred.

To study energy dependence of the Gruneisen parameter, dose should be varied from near zero to a value high enough to verge on the production of impulse by vaporization. Measurements made at very low doses serve as a check on the experimental method by giving a Gruneisen constant close to the room temperature value determined by standard methods. High dose experiments are necessary to characterize material behavior up to the threshold of the transition from thermomechanically dominated to blowoff dominated response.

Conditions actually chosen were limited to fluences which could be obtained reliably with good spatial uniformity over a beam diameter great enough to provide an acceptable read time. For the FX-35 operating at 3 MeV, the highest fluence found to meet these criteria was 40 cal/cm^2. A hundred cal/cm^2

would be necessary to reach the point of transition from thermomechanical dominated to blowoff dominated response in 2DCP, and 1000 cal/cm^2 to reach this same point in 3DCC.

The lowest dose which can reasonably be specified is dependent upon the minimum stress level measurable with the technique selected to monitor shock histories. A laser interferometer operating in the displacement mode appears to be the most sensitive of these techniques. An estimate of the lowest dose which will produce a stress measurable with a position-mode interferometer can be made as follows. Ideally, at least one oscillation from minimum to maximum light level should occur during the shock pulse-width; this corresponds to a change in position of the surface being monitored of a quarter wavelength and produces half a fringe in the interferometer output. It is desirable to record more than half a fringe, but this represents a minimum. The expression relating mirror velocity and fringe rate for a position interferometer is:

$$u = \frac{\lambda}{2} \dot{F} \qquad (4)$$

where λ is the laser wavelength and $\dot{F}$ the fringing rate.

Therefore, assuming a shock pulse width equal to the relief wave transit time across the thickness of the uniform dose region, and demanding that at least half a fringe be read during the pulse gives as a minimum particle velocity

$$u_{min} = \left(\frac{\lambda}{2}\right)\left(\frac{1/2}{\frac{x}{c}}\right) = \frac{\lambda c}{4x} \qquad (5)$$

The symbols are x = target thickness and c = sound speed.

In linearized theory, this minimum particle velocity can be related to stress in the target by the expression:

$$P_{min} = \left(\frac{Z_T + Z_B}{2}\right) u_{min} \qquad (6)$$

where Z_T is the target impedance and Z_B is the impedance of the substrate upon which the target is placed. We can also write:

$$P_{min} = \rho G E_{min} = \rho G E^{*} \phi_{min} \qquad (7)$$

where E_{min} is the minimum dose, ϕ_{min} the minimum fluence, and E^{*} the normalized peak dose characteristic of the beam being considered. Using (5) in (6) and equating (6) and (7) gives:

$$\phi_{min} = 0.125 \frac{(Z_T + Z_B)}{GE^{*}} \left(\frac{c}{\rho x}\right) \qquad (8)$$

For IPC's FX-35 the parameters which go into equation (8) are given below:

Laser wave length, cm = 6.3×10^{-5}

Target thickness, gm/cm^2 = 0.5

Normalized peak dose, $\frac{cm^2}{gm}$ = 1.4

Equation (8) shows that minimum fluence is inversely proportional to the value of the Gruneisen constant; an estimate of G is needed to estimate ϕ_{min}. Chabai* has determined that the Gruneisen constant for carbon is about 0.3; using this value with the numbers tabulated above and the other parameters listed below gives a minimum fluence for the FX-35 of about 8 cal/cm^2. A reasonable minimum fluence was therefore chosen to be about 10 cal/cm^2.

*Personal communication, Dr. A. Chabai, Sandia Laboratories, Albuquerque, New Mexico.

Property	Value	Comment
Z_T, Target impedance	0.63×10^6 $\frac{gm}{cm^2 - sec}$	Kohn's value for CP
Z_B, Backer impedance	1.52×10^6 $\frac{gm}{cm^2 - sec}$	Kohn's value for quartz
c, Target soundspeed	$.42 \times 10^6$ cm/sec	Kohn's value for CP

3.2 Beam Diagnostics for Gruneisen Experiments

A high energy beam was produced by fixing the FX-35 diode and drift chamber parameters to the following values:

Charging voltage:	: 4.2 megavolts
Anode material	: 2 mil titanium
Anode-Cathode gap	: 2 centimeters
Cathode	: 16° stainless steel
Cathode shank	: 3/8-in diameter
Drift Chamber Pressure	: 1.3 torr
Drift pipe	: 1.5-in diameter by 14.5-in long

The beam was characterized by a normalized peak dose of about 1.5 cm^2/gm and a range of approximately 1.0 gm/cm^2 in graphite. In shape the depth-dose profile closely resembled that for a "2.6 MeV" beam except that it fell off more sharply near the front surface.

Diagnostic measurements which were made are the following:

- reproducibility
- beam uniformity
- depth-dose profile
- spectrum and power curve

3.2.1 Reproducibility

Reproducibility was determined at 10 and 40 cal/cm^2 through a series of shots on single element total stopping graphite calorimeters. Calorimeter diameter was varied to give information on the radial variation of fluence as well; diameters used corresponded to 1, 2, and 2.85 square centimeters. At 40 cal/cm^2, shots were also made into a calorimeter whose diameter was greater than that of the drift pipe to determine total beam energy. Tables 2 and 3 give results of successive calorimeter measurements at each level. Fluence was found to be reproducible within about 5 percent at both stations, the beams appearing to represent exceptionally stable conditions.

3.2.2 Uniformity

First attempts to probe for beam uniformity were made with a twenty-five element graphite calorimeter at 40 cal/cm^2. Results obtained for two shots are shown in Figure 3. The array is one inch square, individual elements being 4 mm on a side with about a half mm gap between adjacent blocks. Thermocouple output was read with a 20 channel Vidar digital microvoltmeter. Results of the mappings shown in Figure 3 and of others obtained on earlier beams led us to believe that the calorimeter was malfunctioning, and uniformity was subsequently studied with the three single probe elements for which data are given in Table 4.

Measurements made over several different areas show that at the high level station mean fluence dropped from 42 cal/cm^2 at 1 cm^2 to 39 at 2.85 cm^2, a change of about 8 percent (based on the larger area). In the largest area monitored, only about 110 calories were stopped; this is less than half of the total beam energy and suggests that fluence may fall relatively slowly beyond the limits investigated. A usable spot of 3/4-inch diameter, however, should give adequate one dimensional read time[6], and therefore no effort was made to resolve beam uniformity beyond this point.

Inside the 3/4-inch diameter, both the 10 and 40 cal/cm^2 beam appeared to be quite flat.

TABLE 2

REPRODUCIBILITY OF 10 cal/cm^2, 2.6 MeV BEAM

Shot Number	Calorimeter Area, cm^2	Fluence, cal/cm^2
2086	2.85	10.
2087	2.85	10.
2088	2.0	10.
2089	1.0	10.
2090	2.85	10.
2091	2.85	13.
2100	2.85	10.
2101	2.0	11.
2102	1.0	10.

TABLE 3

REPRODUCIBILITY OF 40 cal/cm^2, 2.6 MeV BEAM

Shot Number	Calorimeter Area,* cm^2	Fluence, cal/cm^2
1761	1	41
1762	2	41
1763	2.85	40
1764	∝	250 calories
1765	∝	242 calories
1766	1	42
1767	2	45
1768	2.85	39
1769	2.85	39
1770	2	40
1771	1	42
1772	∝	242 calories

* ∝ implies that the calorimeter intercepted the entire beam, thus the reading corresponds to the result which would be obtained by integrating the radial distribution to ∞ .

-	25	-	21	-
23	26	29	28	-
19	22	25	X	23
24	34	25	31	-
-	24	-	30	-

Shot 1759

-	30	-	25	-
25	37	42	37	X
25	29	36	X	29
29	36	36	43	-
-	29	-	40	-

Shot 1760

Note: X = probe inoperative at time of measurement

\- = probe not monitored

Figure 3. High Resolution Calorimeter Maps for FX-35 2.6 MeV Beam at 40 cal/cm^2

TABLE 4

SPATIAL UNIFORMITY OF 2.6 MeV BEAMS

Area, cm^2	Fluence, cal/cm^2	
	10 cal/cm^2 Beam	40 cal/cm^2 Beam
1	10.0	41.7
2	10.3	42.0
2.85	10.6	39.3

3.2.3 Depth-Dose Profile

Efforts were made to measure depth-dose profiles by several techniques. These included:

- the use of thin foil titanium and graphite calorimeter stacks, and
- radiation sensitive cellophane film sandwiched between layers of graphite.

The use of graphite should give a profile more nearly representative of that to be expected in 3DCC and TWCP because the absorbing medium makes a close match in atomic number and density. In general it would be expected that measurements in titanium would show a coupling coefficient higher than that obtained in graphite (Spencer's calculations[5] predict peak normalized dose in titanium at 3 MeV should be about 20 percent higher than that in graphite). More substantial differences can occur in depth, however, because the profile in titanium falls off rapidly and is characterized by a shorter range.

Figure 4 plots normalized dose versus depth in titanium measured for a shot on the multiple foil stack. The stack was made of twenty 2-mil foils having an overall thickness of just over 0.4 gm/cm^2; the remainder of the profile was not investigated because the stack was thought to span the depth of interest.

The measurement was made at 40 cal/cm^2 under the same beam conditions for which reproducibility and uniformity data were obtained.

A second dose profile was measured using a compressed stack of alternating layers of 10 mil thick Poco graphite (density 1.8 gm/cm^2) and Dupont MSC-300 radiation sensitive blue cellophane. Under irradiation the optical density of the cellophane decreases with dose, and this change can be read with a scanning densitometer. In theory a dose curve could be constructed directly from an appropriate calibration of the cellophane; in practice, cellophane was used to give the shape of the depth-dose curve and this was normalized to calorimeter measurements to determine amplitude. The profile

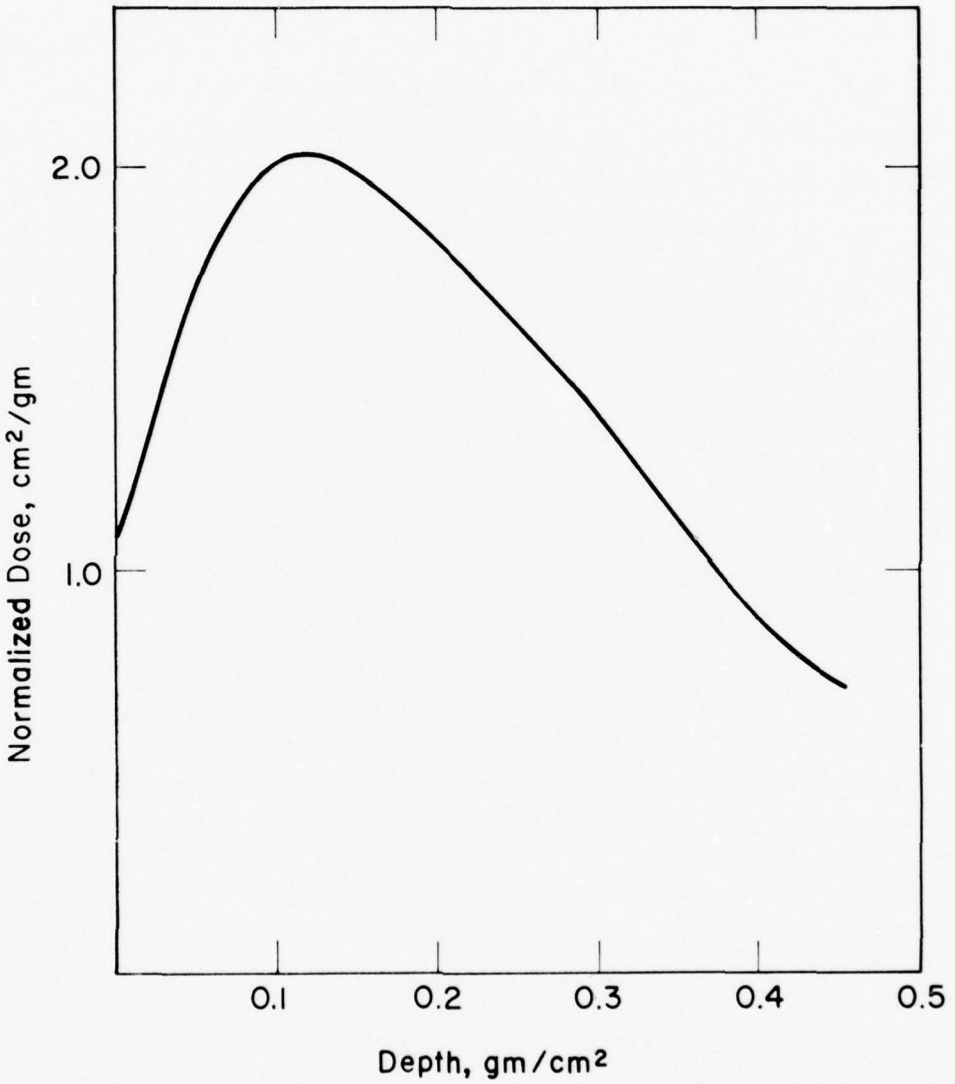

Figure 4. Normalized Dose in Titanium for 3 MeV Beam

was carried to a depth of about 0.9 gm/cm^2. At this depth, approximately 4 percent of the incident energy was transmitted through the rear of the stack. A two layer graphite calorimeter,consisting of an outer slab equal to the stack depth and an underlying absorber, were constructed to permit the normalization process to be carried out.

First attempts to employ this approach were made at 40 cal/cm^2, but it was found that the cellophane saturated to a depth well past peak energy density; fluence was therefore dropped to about 20 cal/cm^2 by altering the drift chamber pressure from 1.5 to 0.035 torr. All other parameters remained the same. Measurements reported here for cellophane were made with this 20 cal/cm^2 beam.

Upon disassembling the graphite-cellophane stack it was found that carbon dust had accumulated on the film, and it was necessary to remove this with acetone before a true reading of the change in optical density could be obtained. Preliminary readings showed that transmission was unaltered by washing films in acetone.

Results of the measurement are shown in Figure 5. Peak normalized dose is about 1.5 cm^2/gm, and range is in the vicinity of 1 gm/cm^2.

Comparison with the titanium measurement shows a difference in peak doses of 29 percent, titanium being higher. This result is consistent with that expected from Spencer's predictions as they were quoted earlier.

Because it could be used directly at 40 cal/cm^2 and because it should give a close approximation to actual profiles in 2DCP and 3DCC, a graphite foil stack was developed and used as the basic instrument for recording dose profiles. Frequent profile measurements were interspersed among data shots, and it was found that profiles were consistently reproducible and were consistent with the cellophane record.

Table 5 lists normalized dose as a function of depth in graphite for a series of shots at 40 cal/cm^2.

To drop fluence to 10 cal/cm^2, charging voltage was reduced somewhat and this lowered the effective mean energy of the beam, increasing the coupling coefficient from 1.4 to 1.8 $\frac{cm2}{gm}$. Table 6 gives normalized dose

TABLE 5

DEPTH-DOSE SUMMARY FOR 40 cal/cm^2

Depth in Graphite gm/cm^2	Shot #								
	Dose, cal/gm/cal/cm^2								
	1979	1980	1994	1999	2000	2010	2019	2026	2060
.0457	1.096	1.066	1.278	1.199	1.335	1.337	1.230	1.148	1.140
.0914	1.271	1.193	1.319	1.246	1.374	1.337	1.302	1.262	1.246
.1371	1.315	1.236	1.401	1.291	1.413	1.376	1.375	1.339	1.318
.1828	1.315	1.279	1.360	1.291	1.413	1.337	1.338	1.301	1.318
.2285	1.358	1.321	1.401	1.338	1.413	1.337	1.375	1.339	1.353
.2742	1.358	1.321	1.401	1.338	1.413	1.337	1.338	1.339	1.353
.3199	1.358	1.321	1.360	1.338	1.374	1.337	1.338	1.339	1.353
.3656	1.358	1.321	1.319	1.338	1.335	1.298	1.302	1.301	1.318
.4113	1.315	1.321	1.278	1.292	1.296	1.258	1.266	1.301	1.282
.4570	1.271	1.279	1.237	1.246	1.217	1.219	1.230	1.263	1.246
.5027	1.227	1.236	1.154	1.199	1.139	1.140	1.157	1.186	1.175
.5484	1.139	1.193	1.113	1.153	1.060	1.101	1.121	1.148	1.104

Table 5 continued
Depth-Dose Summary for 40 cal/cm^2

Depth in Graphite gm/cm^2	Shot #								
	Dose, cal/gm/cal/cm^2								
	1979	1980	1994	1999	2000	2010	2019	2026	2060
.5941	1.096	1.108	1.031	1.061	0.982	1.023	1.049	1.071	1.068
.6398	1.008	1.023	0.948	1.015	0.903	0.944	0.977	0.995	0.997
.6855	0.876	0.938	0.824	0.876	0.824	0.865	0.868	0.918	0.890
.7312	0.789	0.852	0.742	0.784	0.707	0.747	0.796	0.803	0.819
.7769	0.701	0.725	0.660	0.692	0.628	0.669	0.687	0.727	0.712
.8226	0.613	0.639	0.536	0.600	0.550	0.590	0.579	0.612	0.641
.8683	0.482	0.511	0.453	0.507	0.432	0.472	0.470	0.497	0.534
.9140	0.307	0.341	0.288	0.323	0.275	0.315	0.326	0.306	0.321

TABLE 6

NORMALIZED DOSE PROFILE
FOR 10 cal/cm^2 (Shot 2093)

Mass Depth, gm/cm^2	Normalized Dose, cm^2/gm
.0457	.957
.0914	1.826
.1371	1.739
.1828	1.826
.2285	1.826
.2742	1.652
.3199	1.565
.3656	1.652
.4113	1.478
.4570	1.131
.5027	1.044
.5484	.957
.5941	.870
.6398	.783
.6855	.696
.7312	.522
.7769	.435
.8226	.261
.8683	.348
.9140	.174

values for a typical measurement made at 10 cal/cm^2.

3.2.4 Spectrum and Power Curve

Diode current and voltage were reduced for Shot Number 1771, a calorimeter shot from the 40 cal/cm^2 level, to obtain a spectrum and power curve. Raw diode current and voltage are shown in Figure 6. With the cathode geometry and anode-cathode gap spacing used here, a load impedance of about 150 Ω is produced, overmatching the output impedance by about a factor of four. This causes current and voltage to ring down in a series of steps rather than in a single pulse, and increases the baseline-to-baseline pulsewidth somewhat.

The spectrum and power curve determined from diode diagnostics are shown in Table 7 (spectrum) and in Figure 7 (power curve). Points to note from these are that the mean energy was about 3 MeV and width of the power pulse at half maximum was 35 ns.

3 MeV Beam

P = 35 μ
L = 14.5-inches

3/8" pointed cathode
V_c = 4.2 mv

gap = 2 cm
anode = 2 mil Ti

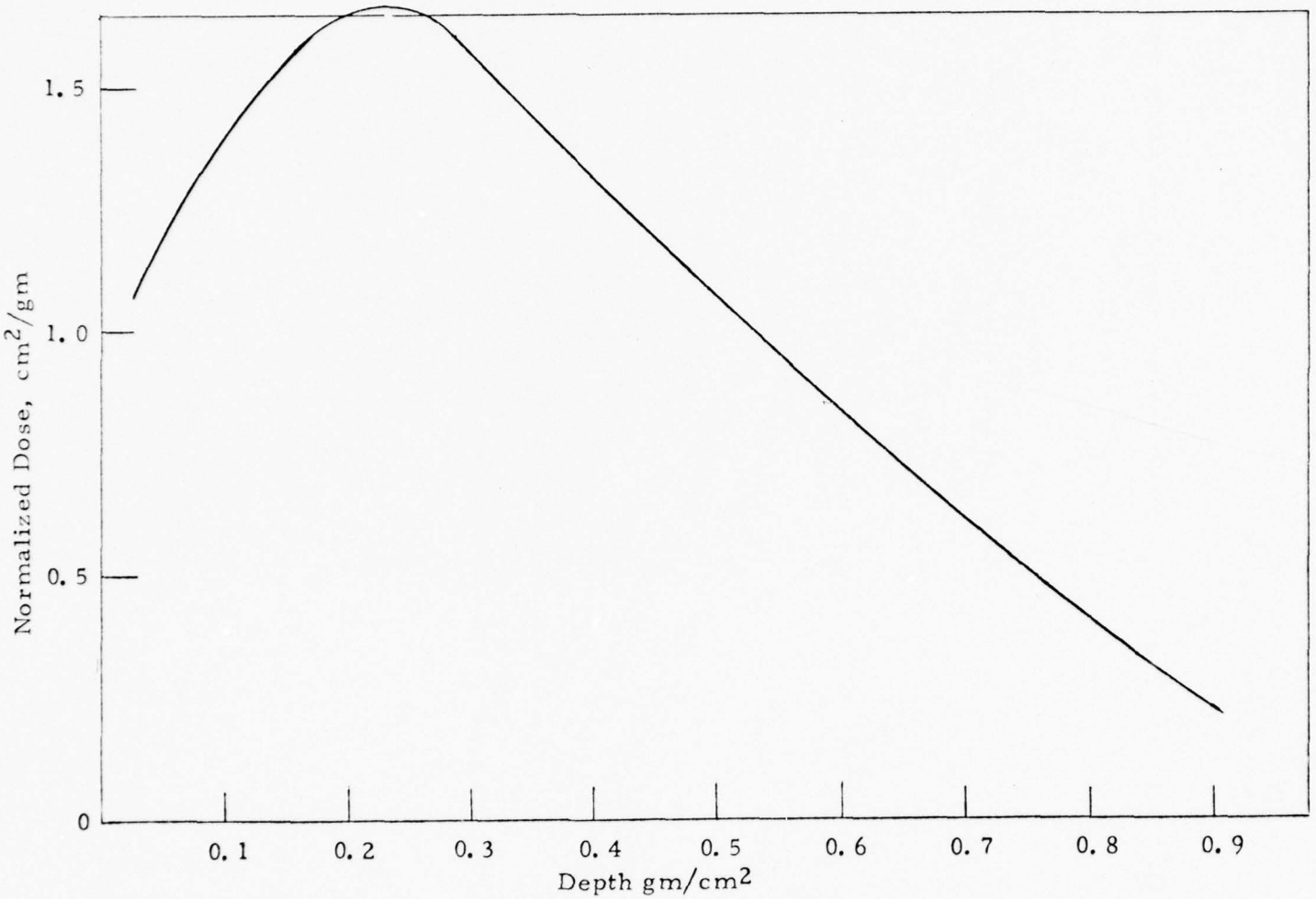

Figure 5. Dose Profile for 2.6 MeV Beam in Graphite

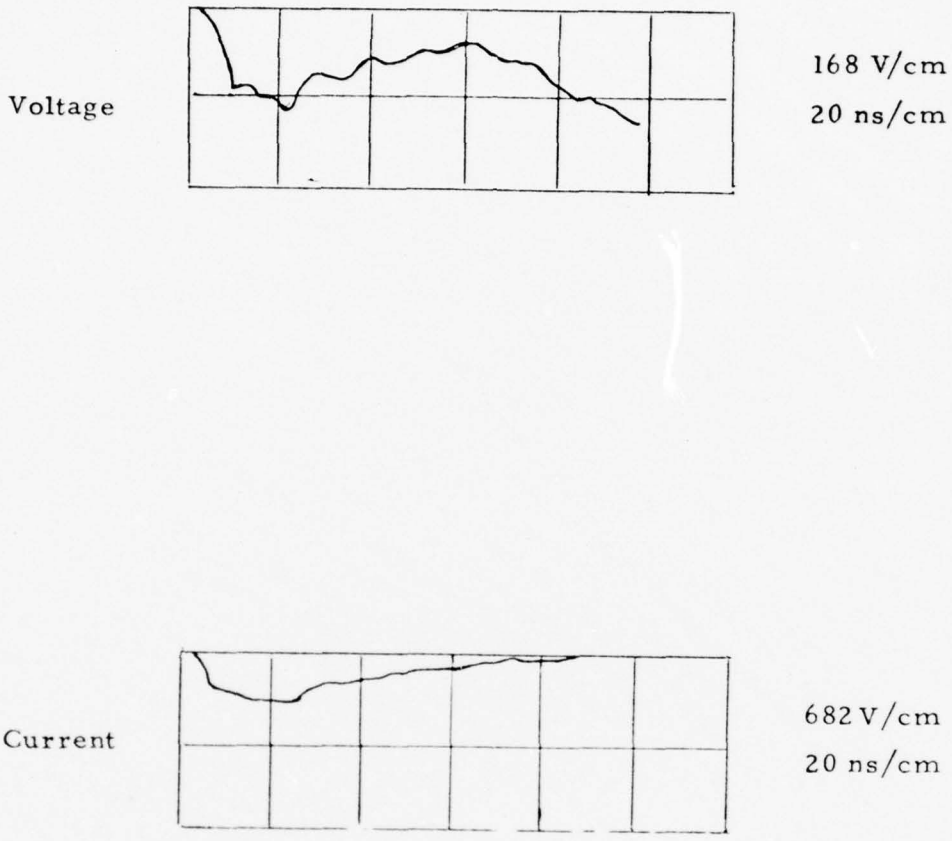

Figure 6. Diode Current and Voltage Traces for FX-35 Shot Number 1771

TABLE 7

ELECTRON NUMBER SPECTRUM

FOR FX-35 SHOT 1771

Energy, MeV	$N(E)/N_{TOTAL}$
0 - 1.75	0
1.75 - 2.0	.0647
2.0 - 2.25	.1323
2.25 - 2.50	.1810
2.50 - 2.75	.0908
2.75 - 3.0	.0437
3.0 - 3.25	.1477
3.25 - 3.50	.1379
3.50 - 3.75	.0344
3.75 - 4.0	.0359
4.0 - 4.25	.0407
4.25 - 4.50	.0491
4.50 - 4.75	.0461

Mean energy: 2.96 MeV

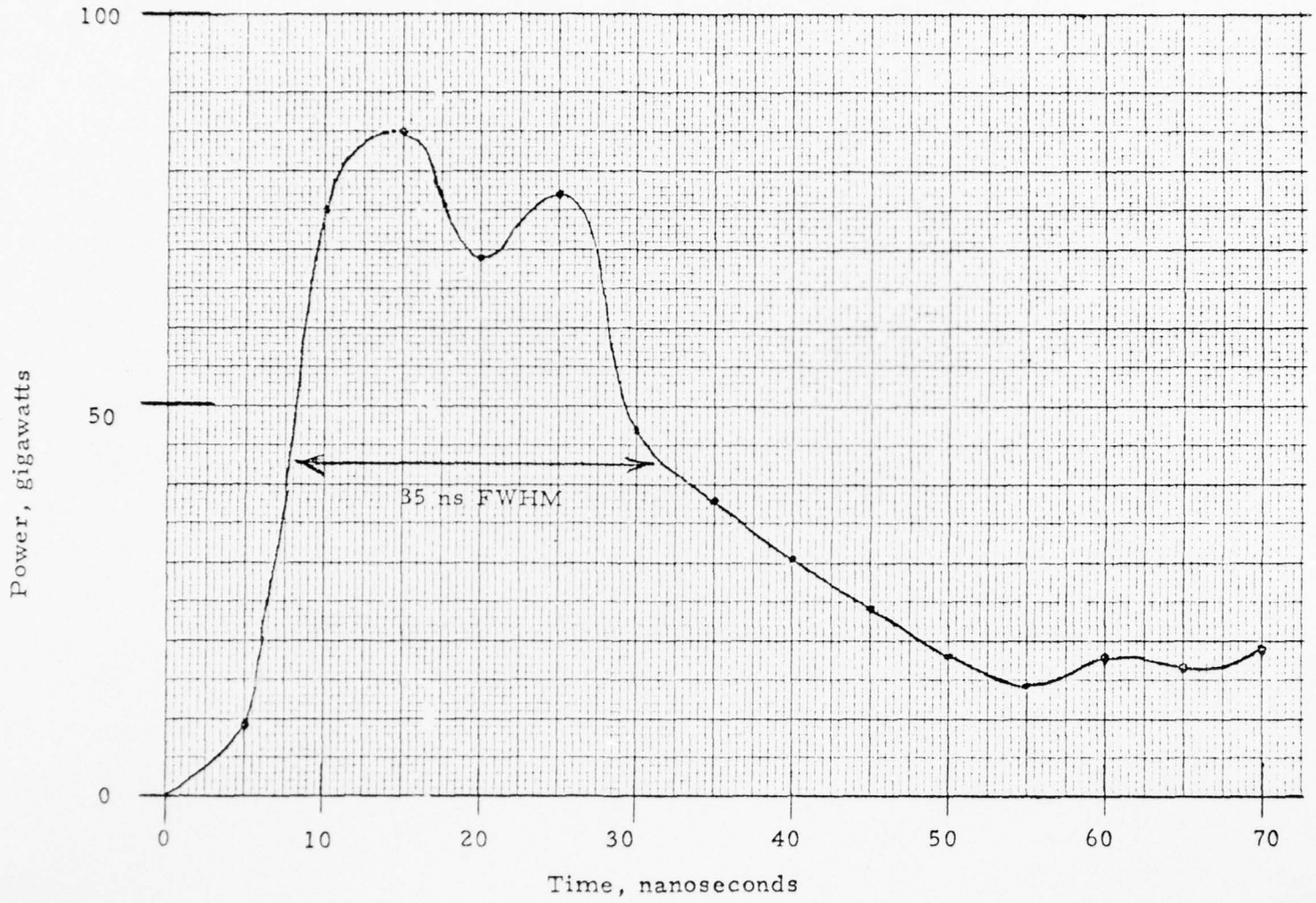

Figure 7. Power Curve for 3 MeV Beam (Shot Number 1771).

3.3 Target and Beam Stop Sizing

Targets sized to assure a minimum variation of dose with depth should be less than a range thick, hence electrons would shine through and directly irradiate any stress monitoring device secured to the rear. This made it necessary to bond the target to a beam stop which was sufficiently thick to bring the total target assembly to just over a range in depth. It was a requirement on this beam stop that it not generate a large thermomechanical shock in its own right due to electron deposition, so that the main wave from the target would not be obscured. It should also be fairly dense so that it could be made thin, thus maximizing planar read time, and its stress propagating characteristics should be well known. Fused silica represents a good choice on all these counts.

The Gruneisen parameter of fused silica at room temperature is known to be small at low energies, measurements made at PI under the BASE II program have confirmed this. The equation-of-state of fused silica has been thoroughly studied by Barker and Hollenbach at Sandia[7].

In addition to meeting the requirements indicated above, fused silica is optically transparent and can therefore be used as the substrate upon which a mirror can be mounted for interferometry; a perfect impedance match can be made across the mirror, thus eliminating a possible additional complication in the reduction of data to values of the Gruneisen constant.

The depth-dose profile of Figure 5 can be used to determine dimensions of targets and beam stops. Criteria which control target thickness are:

- the beam should be relatively flat in the target
- target must be thick compared to the distance traveled by a relief wave during the power pulsewidth
- one dimensional read time must be adequate.

The latter constraint should be met if thickness is held to 0.5 gm/cm^2 or less, this being the maximum dimension employed in pretest calculations.

These calculations showed that, with this thickness, read time was adequate.

Refief distances for 2DCP and 3DCC are given approximately by the product of sound speed and pulsewidth. Because acoustic velocities in the materials are different, relief distances are not the same. Hydrodynamic sound speed can be estimated from the coefficient of the first order Hugoniot term, C, using the expression

$$c \cong \sqrt{\frac{C}{\rho}} \qquad (9)$$

where ρ is the normal density. For 2DCP and 3DCC, applying (9) results in the velocities indicated below. We have referred to reference 6 for values of density and modulus. Using these sound speeds and a pulsewidth

Material	Modulus, dynes/cm^2	Density, gm/cm^2	Hydrodynamic Sound Speed, cm/μsec
2DCP	$.196 \times 10^{12}$	1.44	0.37
3DCC	$.378 \times 10^{12}$	1.67	0.48

of 35 nanoseconds gives relief depths of 0.013 cm for TWCP and 0.017 cm for 3DCC; these correspond to mass thicknesses of 0.019 and 0.029 gm/cm^2 respectively. Demanding that targets be made ten relief depths thick, we find that 2DCP targets should be sized at about 0.19 gm/cm^2 and 3DCC at 0.29 gm/cm^2. For the sake of convenience, both targets of both materials were fabricated to the larger thickness; at this dimension 2DCP was about fifteen relief depths thick.

Referring to Figure 5, it can be seen that normalized dose varies from a minimum of 1.3 to a maximum of 1.5 cm^2/gm over the range of depths from 0.1 gm/cm^2 to 0.4 gm/cm^2. It appears, therefore, that a 0.3 gm/cm^2 target placed at this point in the profile would be subject to a variation in fluence of about ± 7 percent from the mean value. This was a sufficiently close approximation to a flat profile for purposes of the experiment.

Material	Thickness, cm	Thickness, inches
2DCP	0.278	0.11
3DCC	0.240	0.95

To provide for an interferometer mirror location which is outside the electron range, a fused silica beam stop 0.125-inches (0.7 gm/cm^2) thick was placed behind the target. Overall sample configuration was that shown in Figure 8.

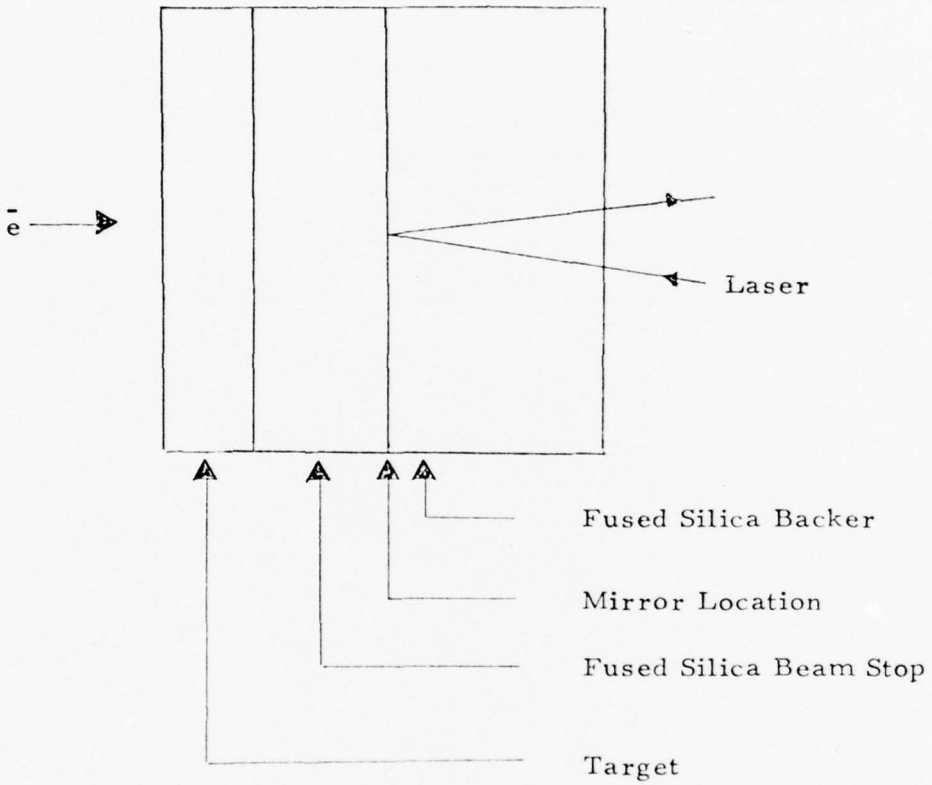

Target Thickness: 0.4 gm/cm^2

Backer Thickness: 0.7 gm/cm^2

Beam Stop Thickness: 516 gm/cm^2

Figure 8. Schematic of Target Configuration for Gruneisen Experiments

3.4 Results

The relationship between target stress and measured fringing rate is

$$P_t = \left(\frac{Z_{bs} + Z_t}{4} \right) \lambda \dot{F}$$

Here Z is acoustic impedance and the subscripts t and bs refer to target and beam stop respectively. Gruneisen parameter of the target is then

$$G = \frac{P_t}{\rho E} = \left(\frac{Z_{bs} + Z_t}{2} \right) \left(\frac{\lambda \dot{F}}{\rho_t E} \right)$$

or

$$G = 9.45 \times 10^{-7} \left(\frac{\dot{F}}{E} \right)$$

$\dot{F}$ and F are understood to be the maximum fringing rate and maximum energy density, respectively.

For 2DCP, Table 8 lists maximum fringing rates, gives mirror velocities, and reports Gruneisen constants calculated from the expression above. Cumulative uncertainty in the Gruneisen due to statistical variation in dose and to limits on the accuracy with which fringe rate can be read is about ± 10 percent. Mean values of G were determined to be 0.25 at 18 cal/gm peak dose and 0.41 at 54 cal/gm.

While the analysis used here is approximate, it should not be far in error for the small stresses involved. To check this point, the stress history measured on shot 2041 has been compared with a PUFF calculation made as a portion of the pretest analysis to support experiment design[6]. The calculation assumed a Gruneisen of 0.4, and was made for

TABLE 8

RESULTS OF GRUNEISEN MEASUREMENTS
ON 2DCP

Shot Number	Nominal Fluence, cal/cm^2	Peak Dose, cal/gm	Maximum Velocity, cm/sec	Maximum Fringing Rate, sec^{-1}	Gruneisen
2097	10	18	126	4.0×10^6	0.21
2106	10	18	195	6.2×10^6	0.28
2020	40	54	788	2.5×10^7	0.43
2041	40	54	725	2.3×10^7	0.40
2076	40	54	725	2.3×10^7	0.40

a 50 cal/cm^2 beam; in Figure 9, this calculation has been scaled to 40 cal/cm^2. It can be seen that calculated and measured waveforms are in good agreement.

Attempts to determine the Gruneisen of 3DCC using a high voltage geam indicated that G must be small compared to that of fused silica; recorded fringe trains resembled those obtained with pure fused silica targets. This implies a number which is considerably less than 0. 1.

Experiments with the 2. 6 MeV beam could not be made more definitive than this because stresses generated in the fused silica beam stop dominated the measured response. To circumvent this problem, a second experiment was undertaken in which 3DCC was pulsed with a 120 cal/cm^2 beam having a mean energy of about 750 keV. In this configuration, target thickness exceeded electron range and the recorded stress history corresponded solely to a thermomechanical shock originating in the 3DCC. This experiment suffered, however, from the fact that the wave was propagated across the target before reaching the measuring site, and attenuation may therefore have taken place. Nevertheless, the data should define a lower limit to the Gruneisen.

Experiments were carried out with FX-35 operating at an average fluence of about 120 cal/cm^2 over a 0. 5-inch diameter spot. Targets consisted of 0. 095-inch 3DCC bonded to a 0. 125-inch fused silica. To this buffer plate was bonded a mirrored fused silica backer; motion of the mirror was monitored with a laser interferometer operating in the displacement mode. Although several shots were taken, only one of these produced a clean trace. This was shot 2143, for which the interferometer record has been reproduced in Figure 10.

In this figure the slight baseline disruption that occurred near the left hand side of the trace corresponded to beam emergence; the shock arrived at the mirror location about one microsecond later. Information relating to the main shock is contained in the first fringe and indicates a wave with symmetrical positive and negative components, the classical

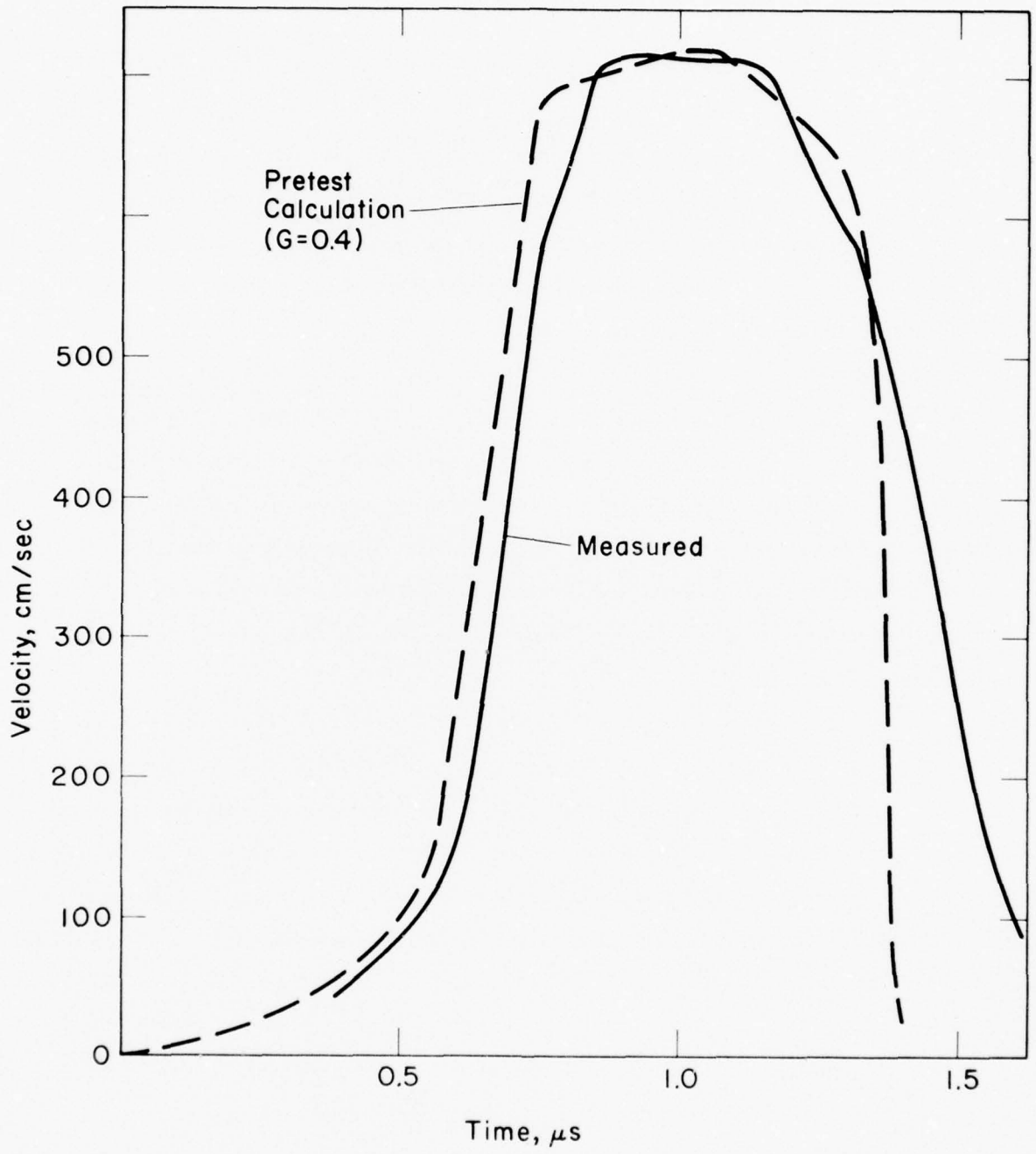

Figure 9. Comparison of Measured and Calculated Stress Histories for 2 DCP

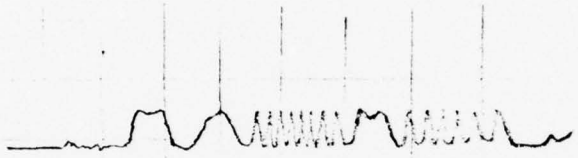

Scale:	1 μsec/div
Target:	0.095-in 3DCC
	0.125-in fused silica
Mean Energy:	750 keV
Fluence:	120 cal/cm^2

Figure 10. Displacement Interferometer Output for Shot 2143.

shape of a non-blowoff history.

To deduce a Gruneisen constant from this record, it must first be reduced to velocity versus time; the approximate treatment outlined below can then be used to estimate G.

For instantaneous energy deposition without blowoff, the peak stress which will be propagated into a target is

$$P = \frac{G\rho E}{2} \tag{10}$$

where ρ is density and E the peak energy density. If there is an acoustic mismatch between the locations at which stress is generated and measured, then pressure will be modified by a transmission factor to give stress at the mirror as

$$P_M = TP, \tag{11}$$

with

$$T = \frac{2Z_1}{Z_1 + Z_2} \tag{12}$$

Quantities Z_1 and Z_2 are impedances of the backer and target respectively.

From the Hugoniot relations, pressure can be approximated as

$$P = Zu \tag{13}$$

with Z and u the impedance and particle velocity of the backer.

Combining (10), (12), and (13), and solving for the Gruneisen gives

$$G = \frac{2TZu}{\rho E} \tag{14}$$

Particle velocity, u, is determined from the interferometer record; the remaining quantities are characteristic of the materials and the electron beam. The following values were used:

Fluence, ϕ :	120 cal/cm^2
Normalized peak dose, k:	4.5 cal/gm/cal/cm^2
Peak energy density (ϕ x k):	540 cal/gm
3DCC density, ρ :	1.6 gm/cm^3
Fused silica impedance, Z_1 :	1.3 gm/cm^2 μsec
3DCC impedance, Z_2 :	0.98 gm/cm^2 μsec

To obtain the impedance value quoted above for 3DCC, sound speed was estimated from the shock arrival time noted on Shot 2143 and the known thicknesses of 3DCC and fused silica. Arrival time was 0.95 μsec after beam emergence; transit time over 0.125-inch of fused silica should be about 0.54 μsec (using a bulk acoustic velocity of 0.59 cm/μsec, determined from the Hugoniot data given by Bade[6]. Velocity in 0.095-inch 3DCC was therefore

$$c = \frac{0.241 \text{ cm}}{(.95 - .54)\ \mu\text{sec}} = 0.59 \text{ cm}/\mu\text{sec}$$

The corresponding product of sound speed and density was found to be 0.98 gm/cm^2 μsec.

Transmission factor from 3DCC to fused silica was therefore T = 1.13.

Figure 12 shows velocity versus time resulting from the interferometer record of Shot 2143. Peak velocity measured was 104 cm/sec. Using this peak velocity, a transmission coefficient of 1.13, and other data as listed earlier gives a Gruneisen equal to 0.0085.

Accordingly it is concluded that the Grueneisen constant of 3DCC must lie in the range $.008 \leq G \leq .04$. The upper limit is the Gruneisen of fused silica.

Because the stresses measured were small (~ 0.1 kb peak in 3DCC), attenuation may have been slight, the wave behaving elastically. On the assumption that this was the case, it is anticipated that the effective Grueneisen is nearer the lower limit than the upper and probably is on the order of 0.01.

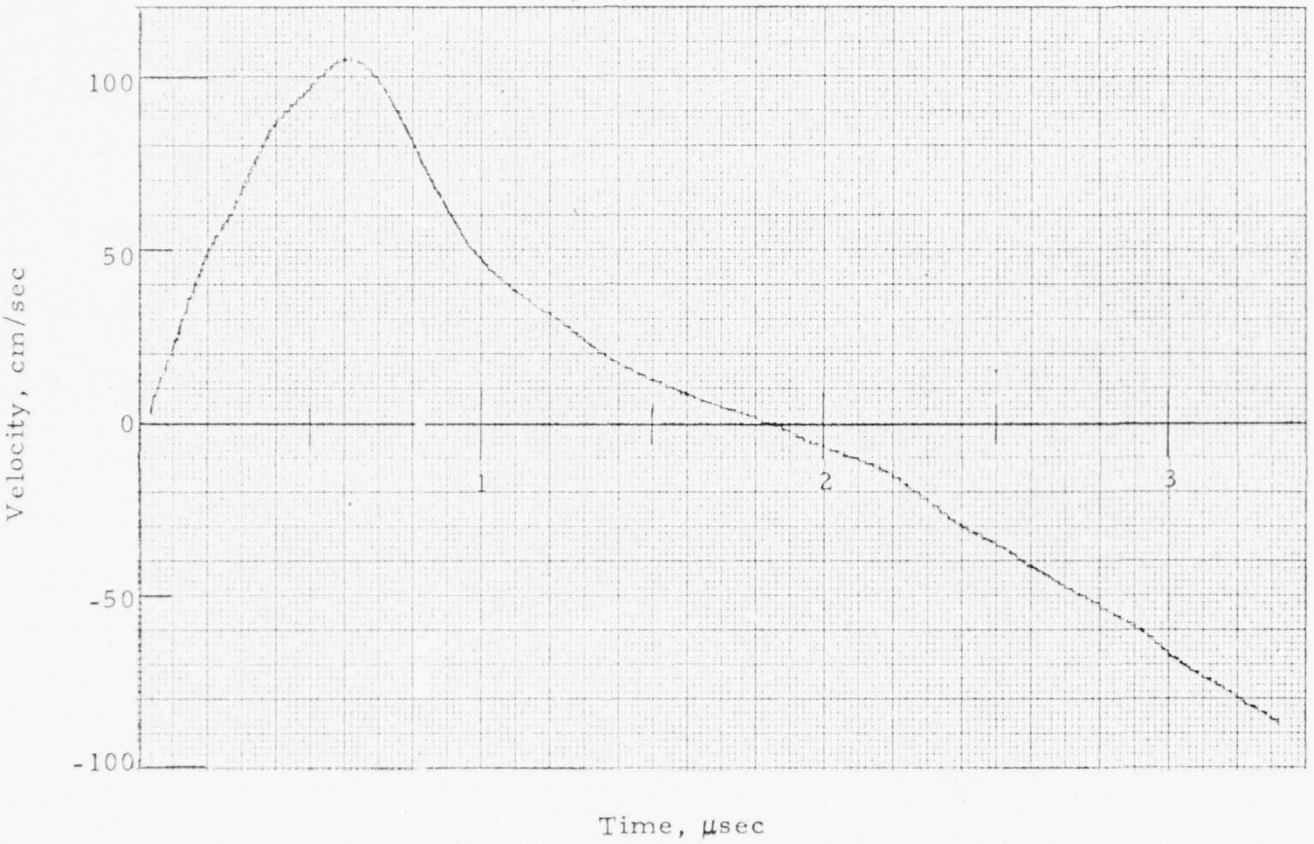

Figure 11. Particle Velocity History for FX-35
Shot No. 2143 on 3DCC.

SECTION IV
IMPULSE MEASUREMENTS

Blowoff impulse measurements were preceded by an experimental program designed to minimize anode debris on Neptune, to measure its amplitude, and to optimize configuration of the guide cone termination and pendulum bob. The latter can be particularly important, for it has been shown that introduction of area effects and/or spurious pressure buildup between stationary and rotating portions of the measuring system can result in an error a factor of two or more in impulse.

4.1 Cone and Pendulum Configuration Studies on Neptune

Four configurations were investigated; these are illustrated in Figure 12 where each is given a numerical designation. Configuration one was used at IPC until about 1971, when it was abandoned in favor of a guide cone termination shaped as in Figure 12 (4). Subsequently, "hat" shaped targets, such as that shown in Figure 12(3) were adopted to give the standard setup used throughout the PREDIX testing program[2] conducted at IPC in 1972 and early 1973.

Experiments reported upon in this section were intended to re-evaluate the basic approaches to utilizing a ballistic pendulum and to study a new technique (configuration 2) which was first proposed several years ago[8] but which had not been attempted in earnest until this effort. It was hoped that configuration two could be engineered into a system which would allow meaningful data to be taken even at doses in excess of the vaporization threshold of graphite. In standard methods, a plug of target material is located flush with the face of a carbon washer, and the entire assembly is mounted on a ballistic pendulum. Both the plug and the innermost portion of the washer are irradiated; the washer must be struck by electrons to give correct scattering conditions at the target perimeter. This approach will work well as long as peak doses remain below the threshold for production of impulse in the washer; for materials which produce impulses much larger than that from graphite, it can be used above this threshold. While evaporation from the washer will introduce a systematic error at these levels, this error

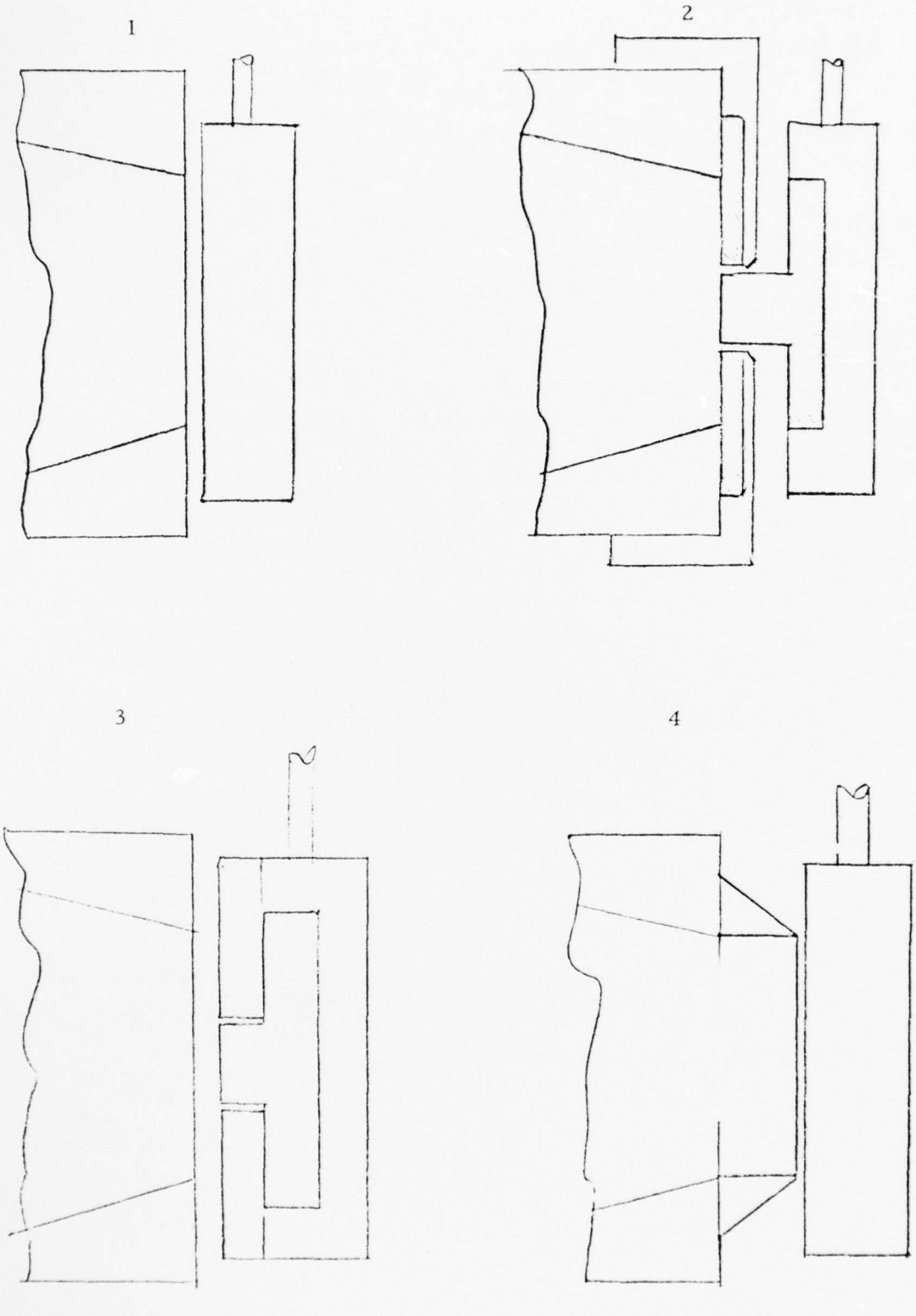

Figure 12. Guide Cone and Pendulum Configuration Studied

will be small if the momentum generated by blow-off from the target is large. A correction can be made for impulse contributed by the washer if the relationship between impulse and fluence is known for graphite.

When the washer and target produce similar impulse levels, as in the case of 3DCC, accuracy of the correction controls accuracy of the measurement unless exposed graphite is minimized in area or an alternate scheme, not requiring correction, can be employed. Configuration two represents such an alternative.

While it is somewhat more complex and requires a larger volume of target material than the standard method, it should record target impulse directly, without the need for a washer correction. It would do this while maintaining appropriate boundary conditions, and it would have the additional advantage of unequivocally monitoring one dimensional flow in vapor evolved from the target.

Simply put, the method calls for fixing the washer to the guide cone while the target remains free to recoil backward through the hole. Used in this way, the washer takes on much the same significance as a guard ring in matched boundary gas gun experiments, and we therefore refer to it as a guard ring in the ensuing pages. Figure 13 shows details of the experimental configuration.

Cylindrical targets 0.5-inch long by 0.5-inch in diameter were bonded into carbon plates and affixed to a pendulum bob as shown. Bonding in this fashion was adequate to prevent sample loss from the bob, and the carbon plate prevented blowoff from electrons which penetrated the space between target and guard ring.

A necessary condition for the success of this technique is that pendulum motion should be slow compared to the time over which mass is evolved from the target. If this condition is not met, then the still spouting target may swing through the hole and blow vapor into the space between the pendulum and guard ring holder. The net effect would be to raise the pressure in this volume; because it would act over the entire area of the bob, pressure exerted here would cause an erroneously high impulse to be read.

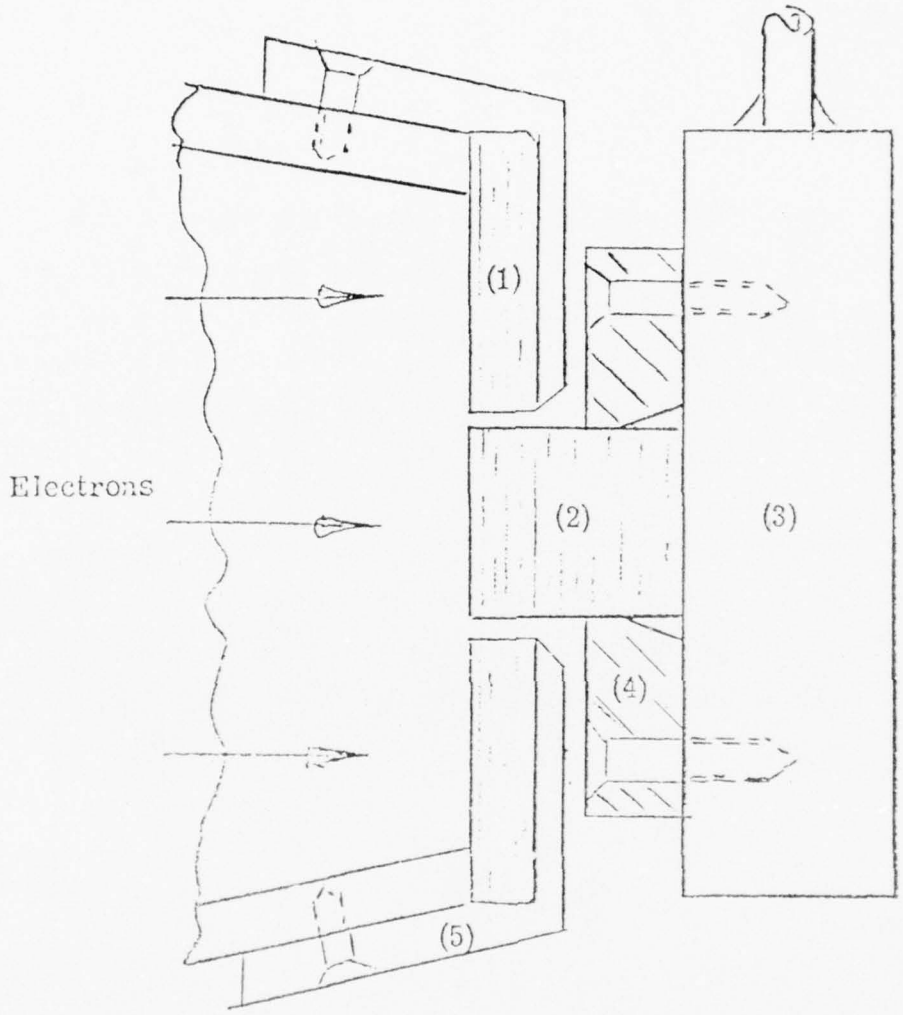

(1) Guard Ring
(2) Target
(3) Pendulum Bob Body
(4) Carbon Plate
(5) Guard Ring Holder

Figure 13. Details of Guard Ring Configuration.

To estimate the initial velocity of the target, we note that this can be computed from:

$$v = \frac{I}{M} \tag{15}$$

Here, I is total momentum and M is the mass of the pendulum bob. For a pendulum which is properly set up, M will be chosen to limit the swing angle to a value which is within the small angle approximation, thus giving a system which oscillates in simple harmonic motion. This requirement fixes the mass at a value which can be determined in the following way. Initial angular momentum of the pendulum is given by:

$$J\dot{\theta} = IR$$

where J is the moment of inertia and the pendulum arm. Equating the initial kinetic energy of the system with its potential energy at maximum amplitude gives a second relationship in $\dot{\theta}$,

$$J\dot{\theta}^2 = MgR\,(1-\cos\theta)\ .$$

Using the approximation

$$\cos\theta \sim 1 - \frac{\theta^2}{2}$$

and introducing the expression for $\dot{\theta}$ from above results in the relationship

$$M = \sqrt{\frac{1}{Rg}}\ \frac{I}{\theta_L} \tag{16}$$

The angle θ_L is the limiting swing angle.

In the process of getting to this result we have also employed the fact that $J = MR^2$.

Using equation (16) in the expression for initial velocity gives:

$$v = \sqrt{Rg}\ \theta_L \qquad (17)$$

For a typical experimental configuration on our machines, swing angle would be limited to 0.1 radians, and shaft length would be about 30 cm. For these parameters, initial velocity is 17 cm/sec. Assuming a guard ring assembly having an overall thickness of 0.125-inch (0.3 cm), about 20 milliseconds would be required to withdraw the target from the hole at this velocity. Blowoff occurs over a time span which is short compared to 20 milliseconds, so that vapor evolution behind the guard ring should not be a problem.

As the target swings backward it will drop slightly because it moves on a radius rather than translating linearly; to accommodate this drop, clearance must be provided between it and the guard ring. To estimate the clearance needed, an approximate computation of the drop can be made. Referring to the geometry of Figure 14, it can be seen that the drop, d, is smaller than the quantity L-R. By computing L-R, an upper limit on d can therefore be obtained. Defining f as the ratio T/R, then we can write

$$L\text{-}R = R\left(\sqrt{1 + f^2} - 1\right)$$

Typically, T will be about 1 cm and R will be 30 cm; f, therefore is on the order of 0.01. When f^2 is small, the approximation can be made that

$$\sqrt{1 + f^2} = 1 + \frac{f^2}{2}$$

this leads to the result

$$d < L\text{-}R \simeq \frac{Rf^2}{2}$$

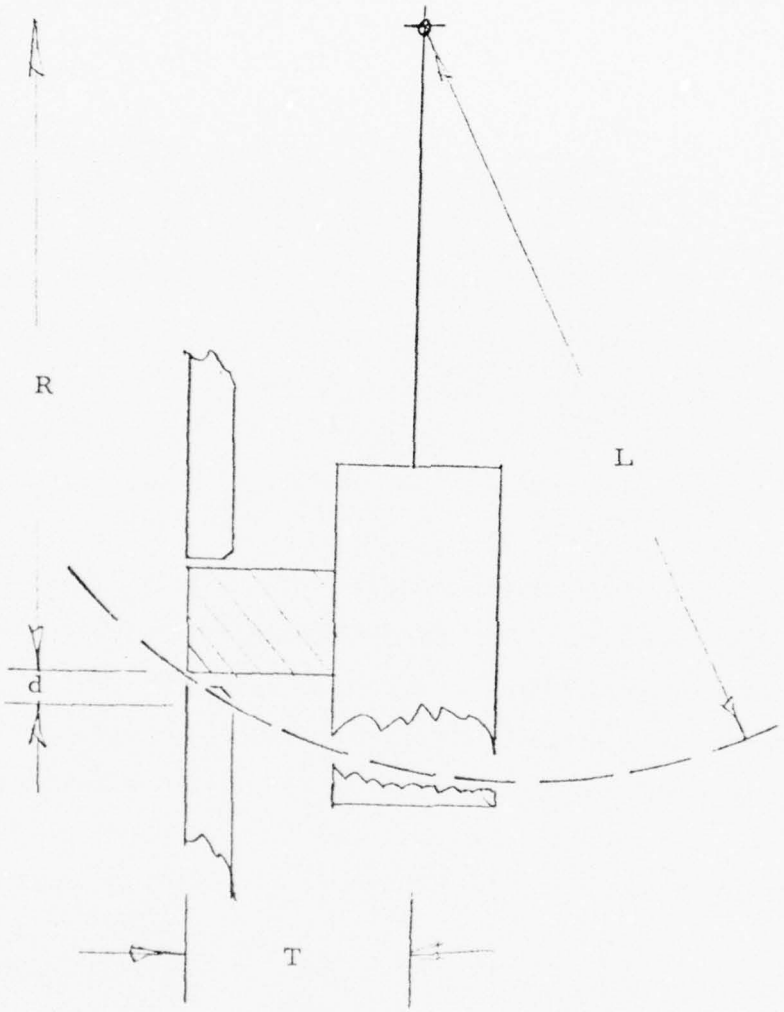

Figure 14. Geometry of Target Drop upon Withdrawal from Guard Ring.

Using R = 30 cm and f ≃ .01 , this expression estimates that the drop will be less than .0015 cm, or about half a mil. The nominal clearance necessary to permit an unobstructed swing through the hole is therefore very small.

The actual clearance was made larger than this nominal value to prevent binding due to lateral expansion of the target under the action of stress waves. A rough guess as to the magnitude of target expansion resulting from radial relief suggests that this would not exceed 15 mils. This estimate was arrived at by making the approximations:

$$\frac{\Delta v}{v_o} \approx \frac{P}{C}$$

and

$$\frac{\Delta v}{v_o} \approx \frac{2\Delta r}{r_o}$$

Here P is pressure and C is target modulus; r is target radius and V stands for volume. Combining these gives

$$\Delta r \approx \frac{P r_o}{2C}$$

The modulus of TWCP is about 0.2×10^{12} dynes/cm^2 and that of 3DCC about 0.4×10^{12}. The highest pressure estimated in pretest calculations was approximately 30 kilobars; accounting for mismatch, this corresponds to 25 kb or less in the target. Taking a radius of 0.25-inches, a pressure of 25 kb, and using the TWCP modulus gives $\Delta r \approx 15$ mils.

In practice the guard ring will also expand, and the clearance would probably have to be about twice that indicated by the calculations above to accommodate this.

These considerations suggested a clearance of about 1/32-inch on the radius would be needed.

The guard ring was made a range thick (this thickness is not

critical as long as it exceeds the potential crater depth) and was held in place by a steel guard ring holder which served to:

- stop electrons leaking through the guard ring.
- hold the guard ring in place without allowing significant rearward deflection due to blowoff.
- shield the pendulum from material which might spall from the guard ring.

The holder was chamfered aft of the aperture to prevent blowoff from electrons collected in the steel. It was necessary to assure that the guide cone was rigidly fixed to the drift chamber, so that the impulsive load exerted on it by vaporization of the guard ring did not cause the entire cone assembly to translate down the chamber. This requirement was easily met by IPC's standard cone mounting arrangement, which secures the cone to the drift pipe through a thick flange.

Evaluation testing was initiated with a series of impulse measurements on ATJ graphite using configuration four with a solid graphite guide cone and a wire rod cone of similar geometry. The wire cone was designed to vent anode debris and deflect it away from the vicinity of the pendulum bob. Measurements were made at about 30, 50, and 100 cal/cm^2 on Neptune, and employed a thick graphite target instrumented with a thermocouple to serve as a calorimeter so that impulse and fluence could be determined simultaneously on any given shot. Results of measurements are listed in Table 9. Conclusion drawn from this testing was that the wire rod cone provides a substantial reduction in background impulse; about 6 kilodyne seconds were measured at 50 cal/cm^2 in the solid cone, while only 1 was recorded when the rod cone was used. At high fluences, this ratio of about 6/1 persisted. Expressed in terms of unit area, background impulse with the wire cone was 240 taps at 50 cal/cm^2 and 500 taps at 85 cal/cm; these values are small compared to the impulse expected from 2DCP at similar levels.

Finally, these values set an upper limit to the impulse from graphite, for if the cone functions as a perfect debris eliminator, then the

TABLE 9

RESULTS OF IMPULSE MEASUREMENTS
ON ATJ GRAPHITE WITH SEVERAL GUIDE CONES

(Note: Cone exit diameter was 1-inch)

Cone Type	Fluence, cal/cm^2	Impulse, kilodynesec
Solid	27	2.6
	29	3.2
	26	3.7
	26	3.8
	28	3.6
	28	3.8
	48	6.0
	49	6.4
	49	5.9
	52	6.0
	85	12.2
	92	11.5
	103	11.0
	109	12.2
Wire Rod	47	0.8
	48	1.3
	49	0.8
	53	1.4
	68	2.0
	81	2.5
	86	1.2

lo· ding must have been due to blowoff or jumpoff.

Having measured background in the two cones, blowoff measurements were made for each of the four configurations in each cone type. Target material was Delrin,* chosen for its low sublimation energy and lack of complexity, characteristics which should make it possible to predict impulses with relatively good success. Experiments were conducted with a standard set of machine parameters, producing 50 cal/cm^2 in the solid cone and 40 cal/cm^2 when the rod cone was used. It has been our experience that rod cones are somewhat more lossy.

Results of measurements using a solid cone are shown in Figure 15. Numbers plotted are net impulse per unit area after correction for background. Curves representing impulse calculated from BBAY theory for several sublimation energies have also been included in the figures for comparison; E_s for Delrin determined from mass loss measurements lies in the range 200 to 300 cal/gm, probably being closer to the high end.

It is the nature of effects related to anode debris that they will cause measurements to record a higher impulse than that due to evaporation of the target alone, hence it would be expected that the technique producing lowest impulse would represent the one giving most nearly correct results. In the solid cone, configuration four produced a net impulse of 7.2 kilotaps; measurements made with the other three techniques were all in excess of 10 kilotaps. This suggests that it is important to prevent a pressure buildup over the bob face by allowing a relief volume into which gaseous debris can be expanded when it moves radially outward after striking the target.

Although configuration two, use of a fixed guard ring, has many advantages on paper, it suffered from blowby. Anode debris passed through the annulus between guard ring and target and piled up between the ring and bob face; while the resulting pressure may not have been great, it acted over a relatively large area hence increased the indicated impulse considerably.

---

* Delrin is the trade name of a proprietary acetal homopolymer manufactured by Dupont.

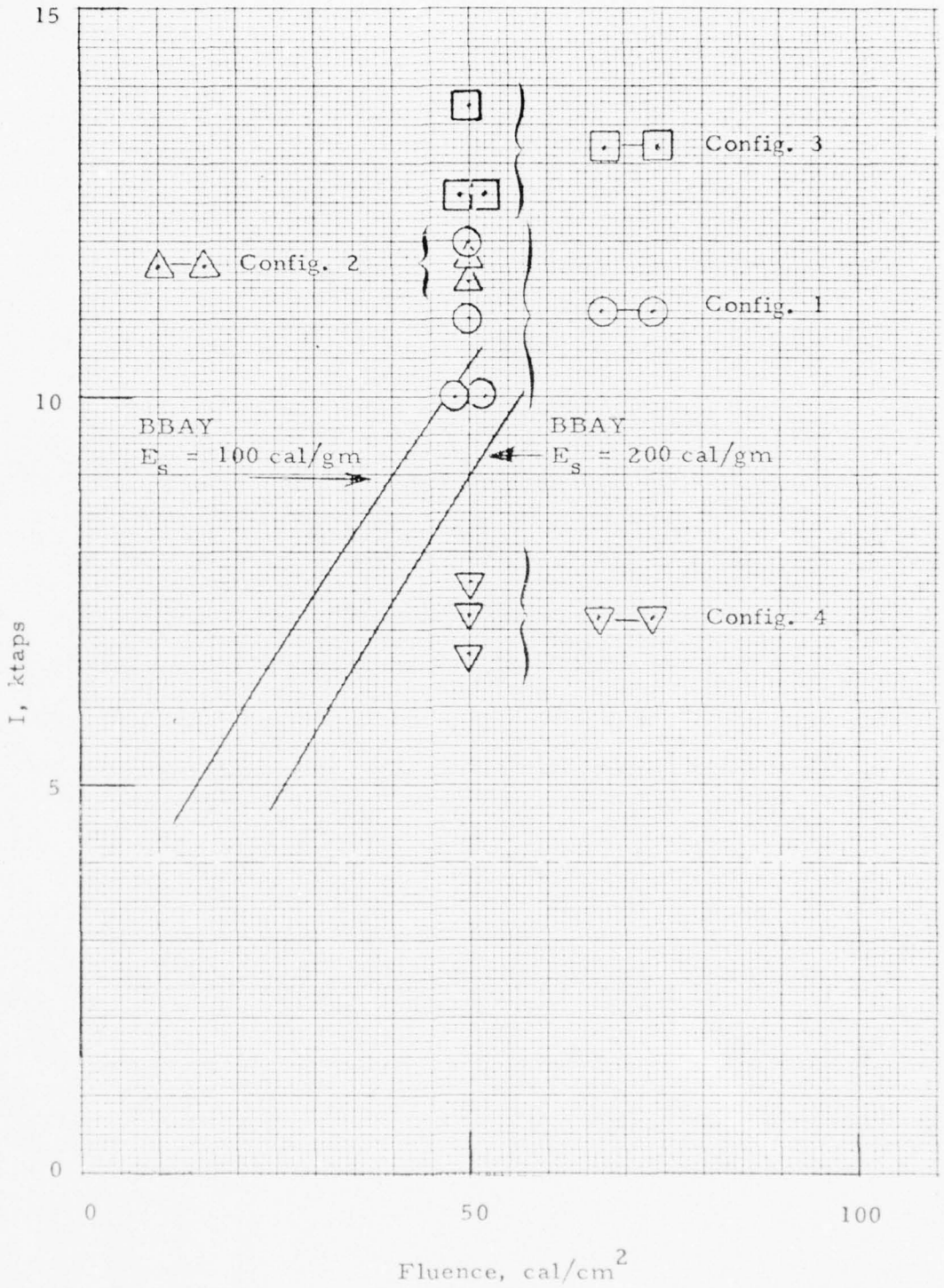

Figure 15. Net Impulse in Delrin with Solid Guide Cone

In the wire rod cone, impulse measured with configurations one and four was 9.3 and 10.3 ktaps respectively. Each value represents the average of three shots. These values were higher than the 7.2 ktaps obtained with configuration four and the solid cone; it was hypothesized that debris vented through the rods was passing outside the cone but still striking portions of the bob. To prevent this, a large disc was added to the cone at its exit plane to act as a blast deflector. Upon redetermining impulse for configuration one with this shield in place, a value of 7.4 ktaps (average of 3 measurements) was obtained.

Conclusions reached from this work were:

- if a solid cone must be used (necessary to obtain maximum fluence), it is mandatory to provide a relief volume over the bob as in configuration four
- in wire rod cones equipped with blast deflector, anode debris is so reduced that any guide cone termination can be used successfully.

In spite of the latter conclusion, general policy was to standardize on the use of a relief volume for all measurements.

4.2 Determination of Impulse from ATJ Graphite

In the previous section it was mentioned that efforts to assign a magnitude to impulse resulting from anode debris in solid and wire rod guide cones led to the conclusion that blowoff from graphite could not be greater than 240 taps at 50 and 500 taps at 85 cal/cm^2 on Neptune. In an attempt to improve upon this estimate, further measurements were made using an experimental configuration designed to distinguish between early and late time impulse (blowoff and anode debris). The method consisted of rigidly mounting a graphite target in a pendulum bob and affixing to it an impedance matched flyer in good hydrodynamic contact, but secured with a zero strength bond. In theory, if the stress wave generated by blowoff is purely compressive and if flyer thickness is greater than half pulsewidth, this system will result in blowoff impulse being trapped in the flyer and spalled away from the bob, leaving the pendulum stationary. Upon its subsequent arrival, anode debris will strike the pendulum and be duly recorded in the usual manner. By making a sequence of measurements with and without flyers, it should therefore be possible to determine both blowoff and background impulses.

If the sum of blowoff, J_f, and background, J_b, impulses is designated J_t, then

$$J_t = J_f + J_b .$$

This is the quantity measured by the pendulum when no flyer is affixed. With a flyer, J_f is carried away and J_b is recorded. Accordingly, background is read directly on such shots. Blowoff can be found by difference as

$$J_f = J_t - J_b .$$

In practice this measurement is subject to a number of complications, particularly so if the shock generated by energy deposition is not purely compressive but contains a significant thermal wave. For conditions which

can be obtained with present electron beam accelerators, it can be anticipated that a significant thermal shock will accompany blowoff from graphite. The resulting nonblowoff impulse is characterized by compressive and tensile portions of equal magnitude, the compressive wave proceeding at the head of the shock. This raises the possibility that flyer separation will not occur upon arrival of the reflected compression wave from the flyer free surface, but at an earlier time when tensile portions of the thermal shock reach the flyer-target interface. If this happens, then the flyer will trap both blowoff impulse and positive portions of nonblowoff; treating the data as above will then overestimate blowoff and underestimate background.

A second problem pertains to the "zero strength bond", which must provide sufficient adhesion to secure the flyer in place until it is shocked from the bob. If the bond is strong enough to pass tensions back to the target, the flyer will trap something less than full blowoff impulse.

Finally, edge effectsand shear waves excited on the interface may affect the time at which the flyer is launched, hence the momentum it carries.

In view of these defects in the technique, the basic approach taken was to make a large number of shots and hope for the emergence of a statistical pattern in the data. Results of measurements are summarized in Figure 16; data have been plotted with separate symbols indicating cases in which there either was no flyer or the flyer did not spall from the bob (hence J_t was measured), and instances in which separation occured (and J_b was read). Curves representing rough fits through the solid symbols (no spall) and open ones (flyer separated) have been made; these are seen to converge at a fluence of about 50 cal/cm^2 and to diverge at higher fluences. The upper curve represents J_t, the lower J_b, hence the difference between them should be J_f, the blowoff impulse from graphite. With this interpretation, and with limits placed as in Figure 16, values of blowoff impulse inferred from the data are those listed in Table 10. In addition to a "most probable" impulse, a maximum has been listed which corresponds to the upper curve of Figure 16. The figure implies no blowoff at 50 cal/cm^2 and 500 taps at 85 cal/cm^2, both values being consistent with measurements reported in the previous section.

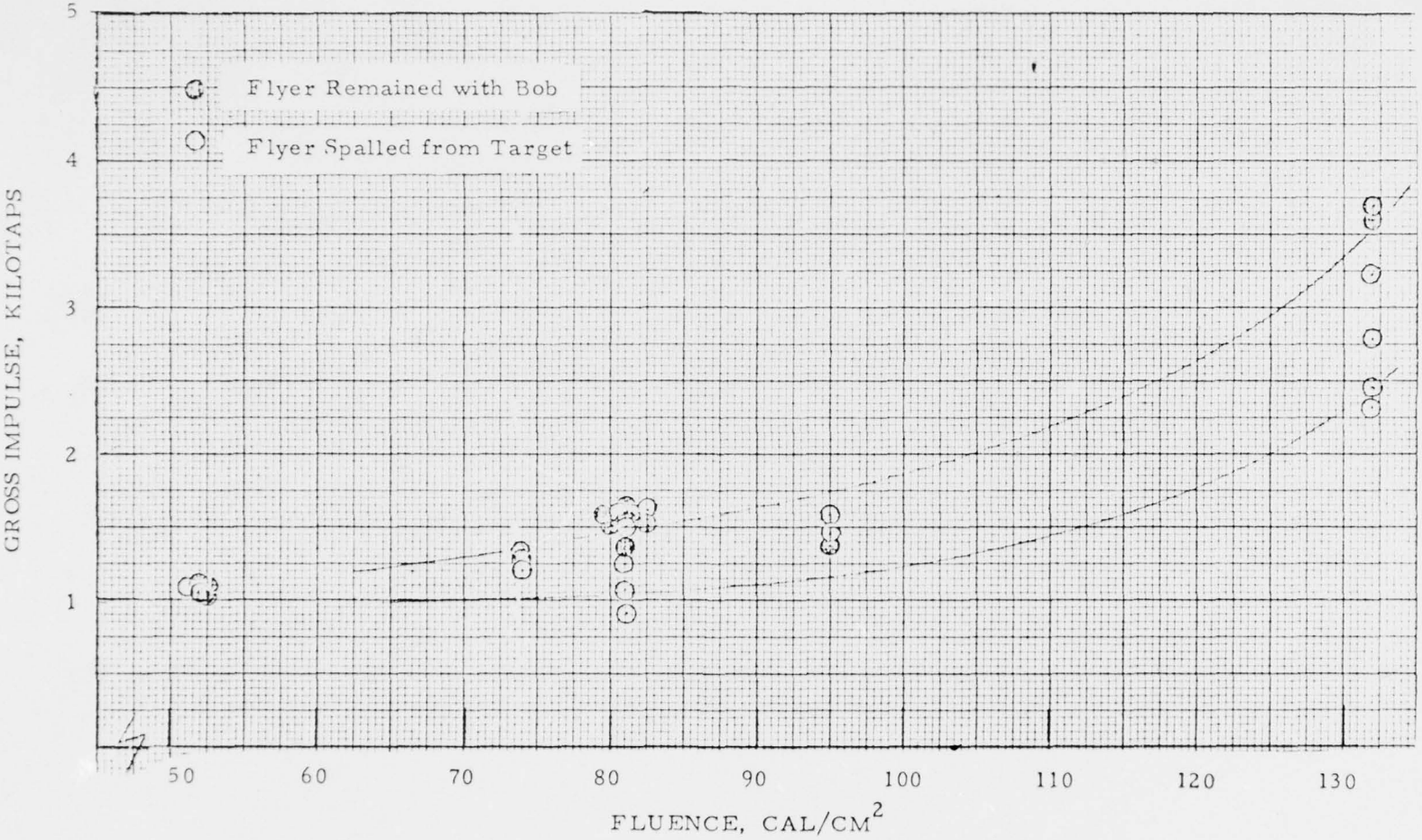

Figure 16. Summary of Graphite Impulse Data

TABLE 10

BLOWOFF IMPULSE IN GRAPHITE

Fluence, cal/cm^2	Graphite Blowoff, taps	
	Most Probable	Maximum
50	0	1050
85	500	1550
130	1050	3350

4.3 Results of Impulse Measurements

4.3.1 Neptune

Table 11 and Figure 17 summarize impulse measurements made on 2DCP with Neptune. Data have been corrected for anode debris. Triangles plotted in Figure 18 are stress-time integrals from quartz gage records. These were integrated to the limit of gage read time (1.1 microseconds and mismatched from quartz to 2DCP using linearized theory. From a comparison of stress and pendulum data it appears that a substantial fraction of total impulse is developed within the first microsecond. At 130 cal/cm^2, mean impulse from stress gages was 5.7 ktaps while the pendulum read an average of 6.7 ktaps. During gage readtime, 85 percent of ultimate impulse was therefore transferred to the target, and late-time blowoff could not have exceeded 15 percent of overall impulse.

Table 12 lists dose at removal depth for 2DCP impulse targets where mass loss was measured. Mean values were 396 cal/gm at 22 cal/cm^2, 399 at 55 cal/cm^2, and 520 cal/gm at 130 cal/cm^2.

Impulse measurements were made on 3DCC only at 130 cal/cm^2, it was decided to begin testing at this level and proceed to lower fluences only if there was a clear prospect of obtaining measureable impulse. The program consisted of alternating shots on 3DCC and ATJ graphite. Graphite data were taken to provide a control and a standard against which 3DCC could be compared; shots on graphite were repeated here rather than relying on results of the preceding section to protect against the possibility of inadvertent changes in the experimental setup or variability in machine performance. Three shots each were made on 3DCC and ATJ; an additional four shots were made on graphite targets with a flyer to determine background impulse. Results are given in Table 13. Mean impulses (not corrected for anode debris) were the following:

TABLE 11

SUMMARY OF 2DCP IMPULSE MEASUREMENTS ON NEPTUNE

Shot	Fluence, cal/cm^2	Mass Loss, gm	$\frac{\Delta m}{A}$, $\frac{gm}{cm^2}$	J, kds	J_{net}, kds	I, ktaps	Area, cm^2
2044	22	NM	-	3.8	2.9	0.6	4.66
2046	22	NM	-	6.7	5.8	1.2	
2047	22	NM	-	7.1	6.2	1.3	
2049	22	0.093	0.020	6.4	5.5	1.2	
2066	55	0.225	0.048	15.2	14.5	3.1	
2069	55	0.245	0.052	19.3	18.6	4.0	
2071	55	0.200	0.043	15.2	14.5	3.1	
2413	130	-	-	22.9	15.8	6.2	2.56
2414	130	-	-	29.8	22.7	8.9	
2420	130	0.143	0.056	20.4	13.3	5.2	
2421	130	0.187	0.073	24.2	17.1	6.7	

TABLE 12

DOSE AT REMOVAL DEPTH FOR 2DCP ON NEPTUNE

Shot	Fluence, cal/cm^2	Δm	Δm/A	Dose, cal/gm
2049	22	0.093	0.020	396
2066	55	0.225	0.048	406
2069	55	0.245	0.052	352
2071	55	0.200	0.043	468
2420	130	0.143	0.056	702
2421	130	0.187	0.073	338

TABLE 13

COMPARISON OF 3DCC AND ATJ
IMPULSE

Shot	Material	Uncorrected Impulse, kds	Uncorrected Impulse, ktaps
2423	3DCC	5.3	1.9
2424	ATJ	6.8	2.4
2427	3DCC	7.0	2.5
2430	ATJ	4.7	1.6
2432	3DCC	6.9	2.4
2433	ATJ	6.1	2.1
2435	ATJ + Flyer*	4.3	1.5
2436	ATJ + Flyer	5.9	2.1
2437	ATJ + Flyer	5.3	1.9
2438	ATJ + Flyer	5.1	1.8

*In all cases the flyer spalled from the target.

Background:	1.8 Ktaps
ATJ:	2.1 Ktaps
3DCC:	2.2 Ktaps

These results indicate that there was little if any difference between ATJ and 3DCC and that absolute impulse was small. Table 14 summarizes net impulse values for the three 3DCC shots and gives mass loss data. On the two shots for which impulse was significantly different from zero, the mean was 230 taps.

Average dose corresponding to mass loss depth was 2210 cal/gm.

4.3.2 FX-35

Impulse measurements made on 2DCP with a nominal 750 keV beam are summarized in Table 15 and Figure 18.

At the two higher fluence levels, mylar windows were employed; hence a correction for anode debris was necessary. Background impulse recorded at the nominal 60 and 100 cal/cm^2 conditions is summarized in Table 16; background corresponding to 150 taps at 60 cal/cm^2 and 810 taps at 100 cal/cm^2 was found. At 30 cal/cm^2 a metal window was employed and there was no background impulse.

A good deal of difficulty was encountered with beam centering at 30 cal/cm^2, and on only one shot was the target fully irradiated (number 2200). The remaining two points have been corrected for reduced area, and they scatter about the 3.7 ktaps recorded on 2200.

Dose profile at 60 cal/cm^2 was somewhat shallower than that at 30 (see section 4.4) because mean energy was set too high when the change of fluences was made; for this reason peak dose increased by only 40 percent rather than doubling; data cannot properly be plotted in terms of fluence for this reason. A more appropriate correlator might be peak dose, in which case the presentation would appear as in Figure 19.

Mass loss data are summarized in Table 17; target delamination occured in most cases, and mass was lost through mechanisms other than

TABLE 14

3DCC IMPULSE SUMMARY FOR NEPTUNE 130 CAL/CM^2 STATION

Shot	Area, cm^2	Mass Loss, gms	Mass Loss, gm/cm^2	Dose at Removal Depth, gm/cm^2	Net Impulse, kilodynesec	Net Impulse, kilotaps
2423	2.85	0.084	0.029	1870	~0	~0
2427	2.85	0.047	0.016	2860	0.7	0.25
2432	2.85	0.081	0.028	1790	0.6	0.21

TABLE 15

2DCP IMPULSE SUMMARY FOR FX-35 TESTING

Shot	ϕ	Area, cm^2	Δm, gm	$\frac{\Delta m}{A}$, $\frac{gm}{cm^2}$	J, kds	J_{net}, kds	I, ktaps	Comments
2195	33	2*	.139	0.069	8.5	8.5	4.2	(1) off scale (2) off center
2198	33	2*	.088	0.044	4.5	4.5	2.2	off center
2200	33	2.56	.219	0.086	9.4	9.4	3.7	OK
2266	64	2	.323	0.161	6.2	5.9	3.0	OK
2268	64	2	.190	0.095	4.4	4.1	2.1	OK
2269	64	2	.225	0.112	5.3	5.0	2.5	OK
2289	97	1.05	.090	0.086	-	-	-	self fire below voltage
2290	97	1.05	.221	0.210	9.06	8.3	7.9	voltage high
2296	97	1.05	.153	0.146	9.73	8.9	8.5	OK

*Nominal 2.56 but beam off center.

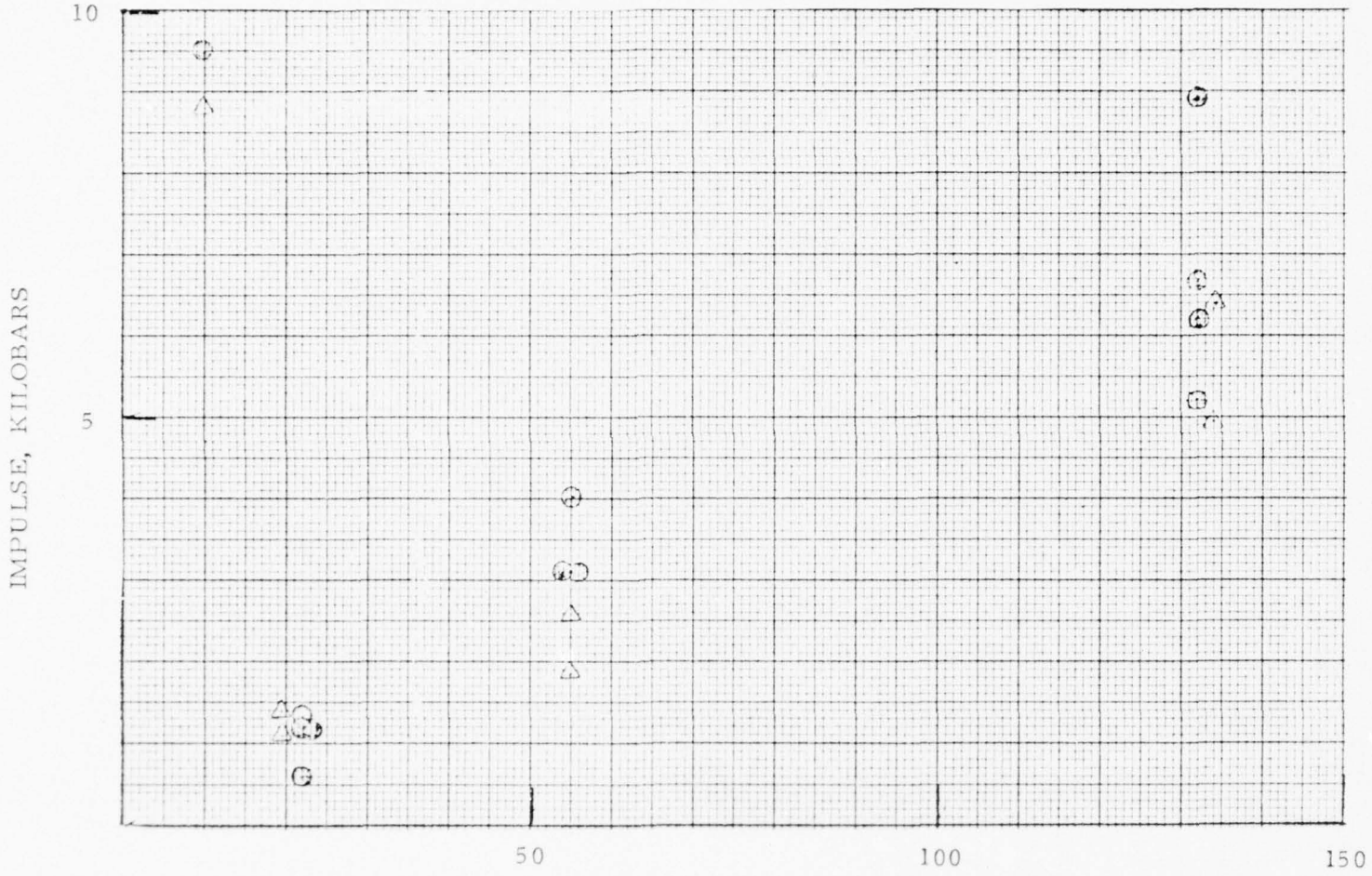

Figure 17. Summary of 2DCP Impulse Measurements on Neptune

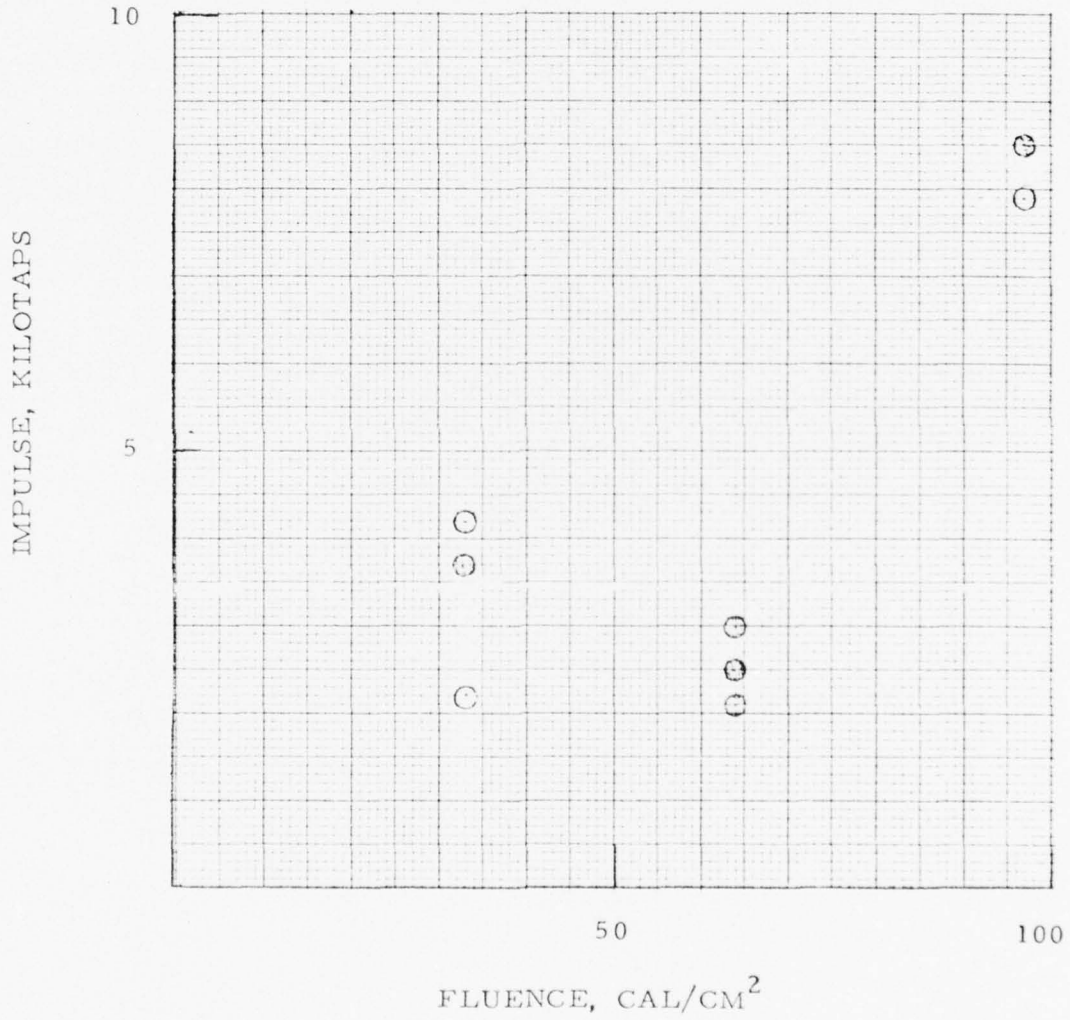

Figure 18. Impulse Vs. Fluence for 2DCP on FX-35

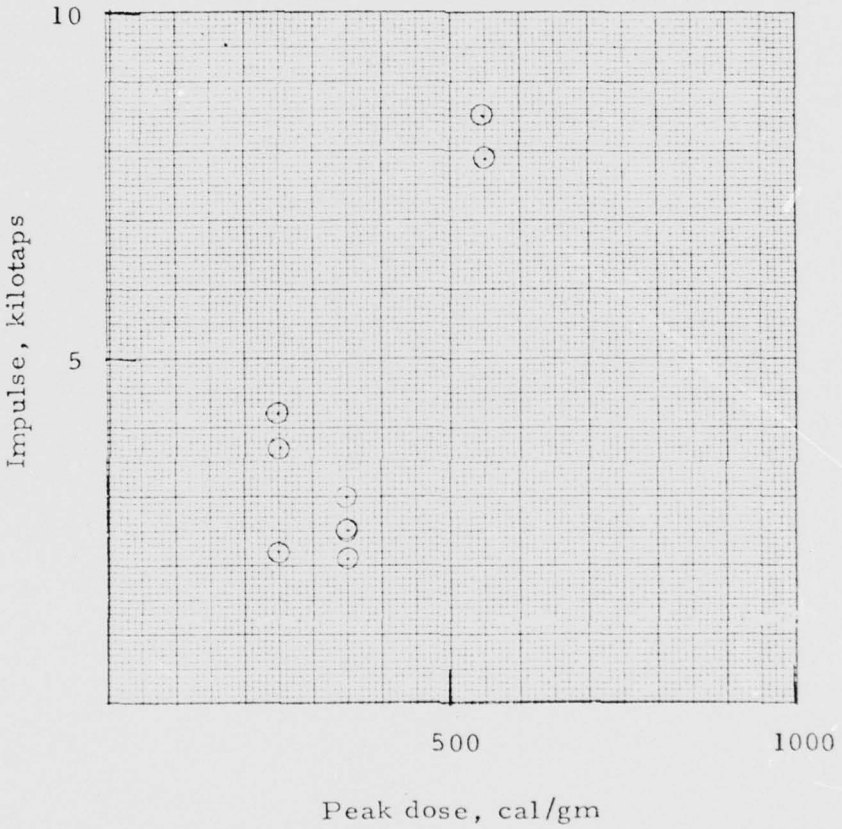

Figure 19. 2DCP Impulse Versus Peak Dose For FX-35

TABLE 16

FX-35 BACKGROUND IMPULSE MEASUREMENTS

Shot Number	Fluence, cal/cm^2	Impulse, kilodyne sec
2262	60	~ 0
2263	60	0.16
2264	60	0.40
2291	100	~ 0
2292	100	0.8

TABLE 17

MASS LOSS DATA FOR 2DCP TESTED ON FX-35

Shot	ϕ	$\frac{\Delta m}{A}$, $\frac{gm}{cm^2}$	Dose at Removal Depth, cal/gm	Comments
2195	33	0.069	150	Beam off center
2198	33	0.044	190	Beam off center
2200	33	0.086	140	Delamination at target edge
2266	64	0.161	115	Delamination at target edges
2268	64	0.095	235	Delamination at target edges
2269	64	0.112	190	Delamination at target edges
2290	97	0.210	70	Large delamination at target edge
2296	97	0.146	147	Large delamination at target edge

vaporization. Doses corresponding to mass loss depths therefore represent lower limits on effective sublimation energy. Most values fell between the limits 100 and 200 cal/gm.

4.4 Beam Diagnostics for Neptune and FX-35

This section reviews diagnostic measurements made on beams used to take impulse and stress-time data on Neptune and FX-35.

4.4.1 Neptune

Calorimeter shots were made regularly as testing progressed at each level, and these were used to verify machine stability and determine operating fluence. It was general practice to employ a flat faced graphite calorimeter at fluences below 100 cal/cm^2; above this level, a conical "bomb" calorimeter patterned after that first used by Cooperstein on Gamble I at the Naval Research Laboratory was used.

An intensive and complete job of reporting upon reproducibility, uniformity, and dose profiles for Neptune beams at fluences below 100 cal/cm^2 has been done by Schallhorn et al[9]; accordingly, only data for the 130 cal/cm^2 condition is reported here.

Figure 20 plots calorimeter measurements made with flat faced and conical calorimeters at the highest testing station on Neptune. From a comparison of the two it is clear that an energy loss mechanism was at work in the case of the flat calorimeter; it indicated an average fluence of 91 while the conical device read 132 cal/cm^2. Scatter about the 132 cal/cm^2 was minimal, less than ± 10 percent RMS.

Dose profile at 130 cal/cm^2 was determined from a series of transmitted fluence measurements using graphite foils. Results of measurements are plotted in Figure 21, and the depth-dose profile inferred from this curve by piecewise differentiation is shown in Figure 22. The plot is normalized to 1 cal/cm^2 incident. Peak dose corresponding to 132 cal/cm^2 incident with this profile was 4300 cal/gm.

Figure 20. Neptune High Fluence Calorimeter Data

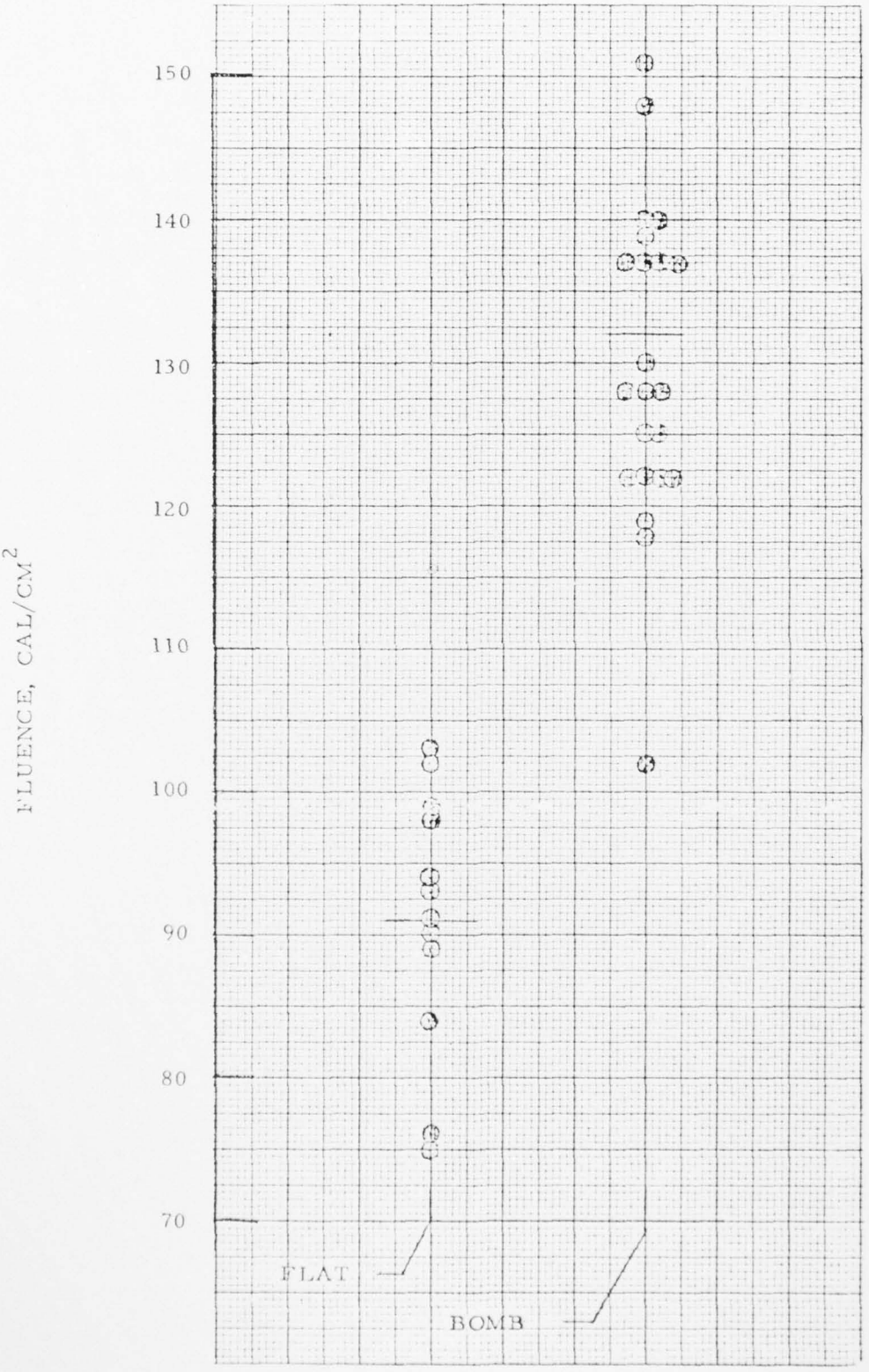

Figure 21. Transmitted Fluence Curve for Neptune
High Fluence Station

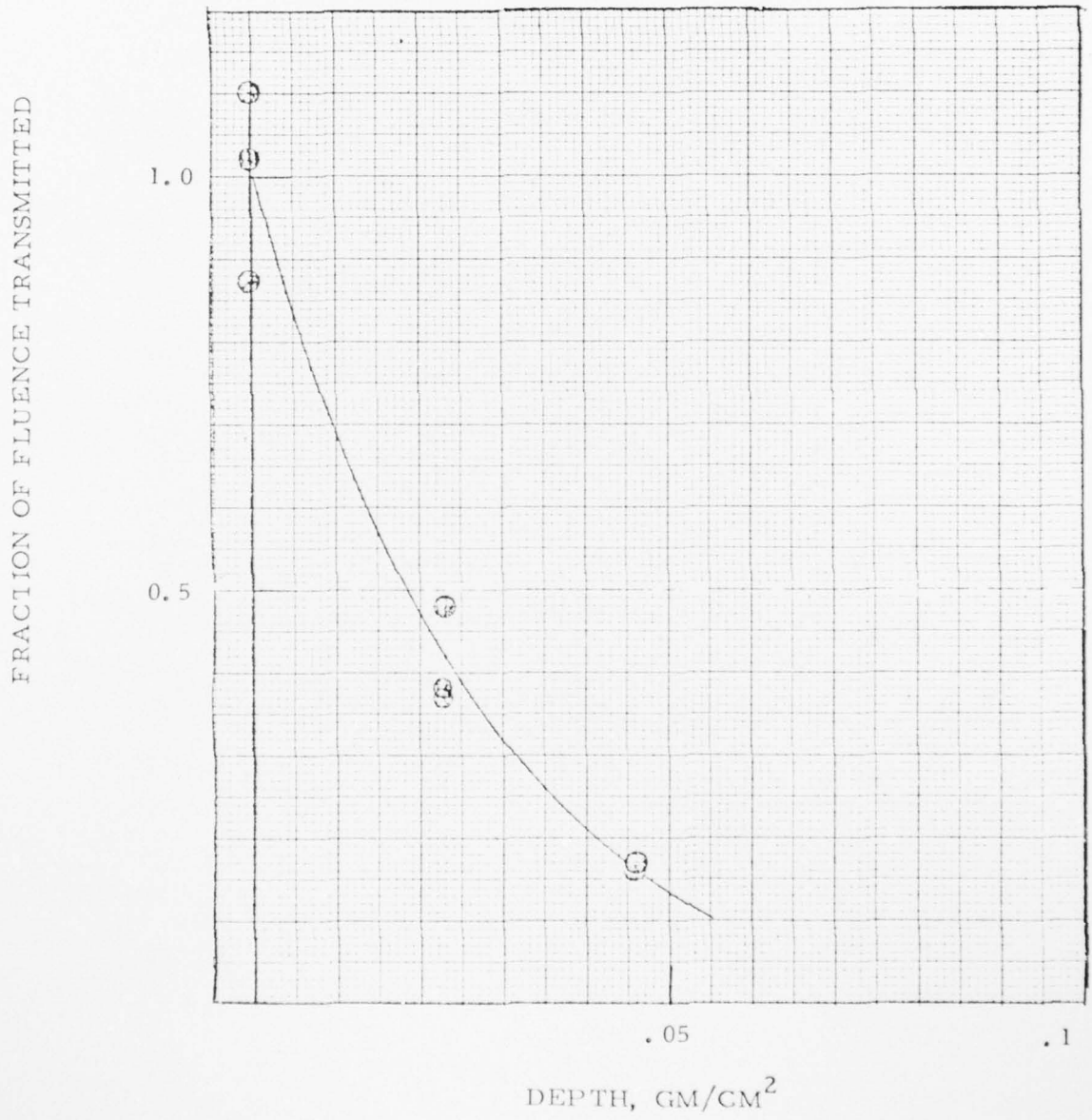

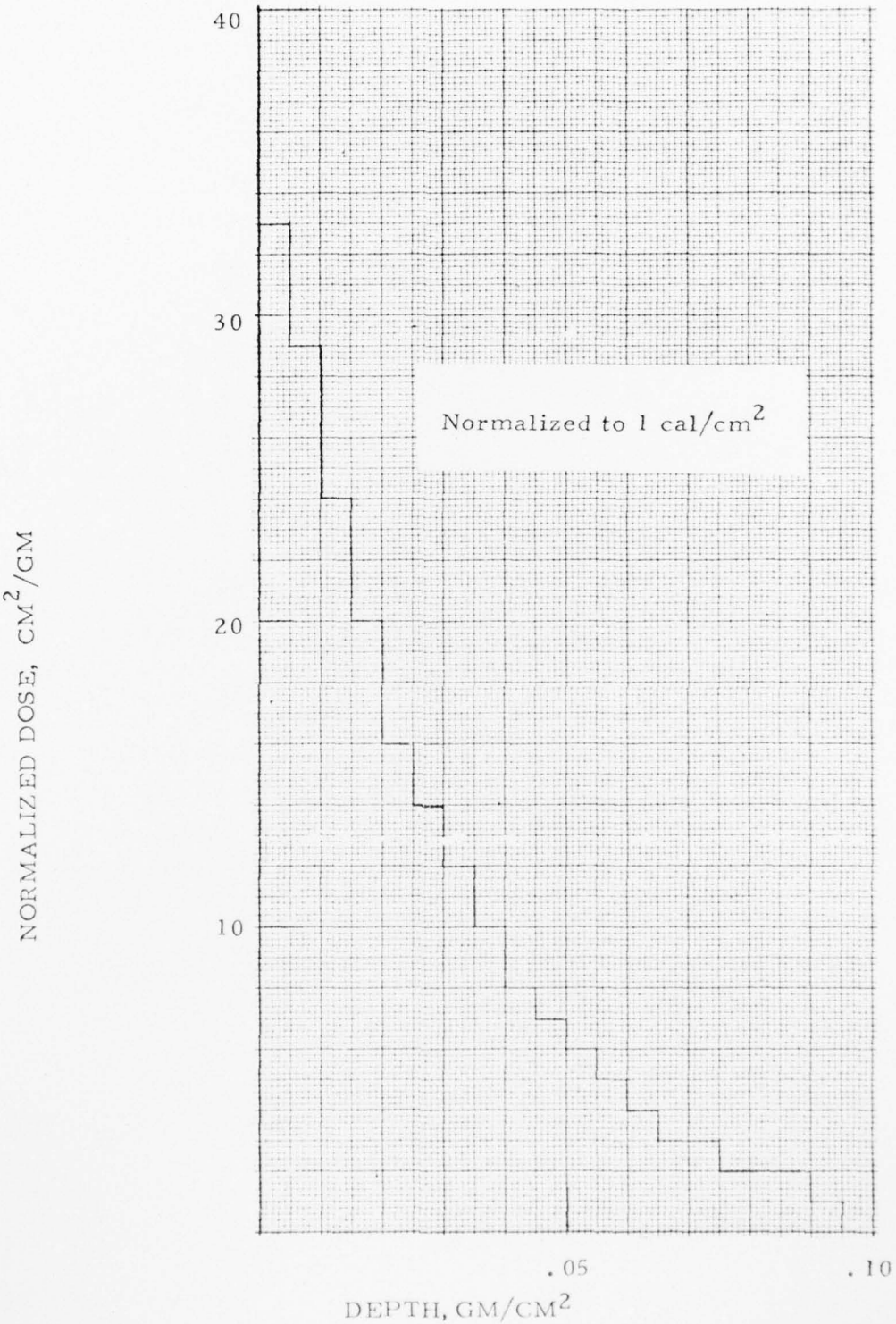

Figure 22. Depth-dose Profile for Neptune 130 cal/cm^2 Station

4.4.2 FX-35

Uniformity measurements were made at 30 and 60 cal/cm^2 by testing with single button calorimeters of differing area, increasing to a diameter equal to that of the target. This approach was impractical at 100 cal/cm^2, where the beam area was only 1 cm^2. No uniformity data were taken at this level. Tables 18 and 19 list results of calorimeter data for 30 and 60 cal/cm^2; these show that uniformity was relatively good for both beams. Reproducibility of fluence for a given calorimeter size was generally 10 percent or better.

Reproducibility of fluence measurements made with a 1 cm^2 calorimeter at 100 cal/cm^2 is shown in Table 20.

Using the transmitted fluence technique, dose profiles were measured for the 30 and 60 cal/cm^2 beams. Because peak voltage at 100 cal/cm^2 was similar to that at 60, the same profile should apply to both.

Dose profiles deduced from transmission experiments using graphite foils are shown in Figures 23 and 24 for 30 and 60 cal/cm^2.

TABLE 18

BEAM UNIFORMITY DATA FOR FX-35
(30 cal/cm^2 BEAM)

Shot No.	Calorimeter Area, cm^2	Fluence, cal/cm^2
2175	2.85	32
2176	2.85	32
2178	2.00	33
2179	2.00	37
2180	1.25	35
2181	1.25	37
2182	2.85	31
2183	2.00	35
2187	2.85	38
2188	2.85	34
2193	2.85	31
2194	2.85	31
2196	2.85	34
2197	2.85	35

Area, cm^2	Mean Fluence, cal/cm^2
1.25	36
2.00	35
2.85	33

TABLE 19

BEAM UNIFORMITY DATA FOR FX-35
(60 cal/cm^2 BEAM)

Shot No.	Calorimeter Area, cm^2	Fluence, cal/cm^2
2233	1.25	75
2234	2.00	64
2245	2.00	70
2246	2.00	64
2247	2.00	60
2248	2.00	70
2249	1.25	73
2250	1.25	73
2252	1.25	75
2255	1.25	74
2265	2.00	68
2267	2.00	65
2270	2.00	60
2273	2.00	58
2274	2.00	62
2277	2.00	67

Area, cm^2	Mean Fluence, cal/cm^2
1.25	74
2.00	64

TABLE 20

REPRODUCIBILITY OF 100 cal/cm^2 FX-35 BEAM

Shot Number	Calorimeter Area, cm ^{2}	Fluence, cal/cm^2
2285	110	94
2286	110	102
2287	110	94
2288	110	98
2293	110	75
2294	110	85
2295	110	95

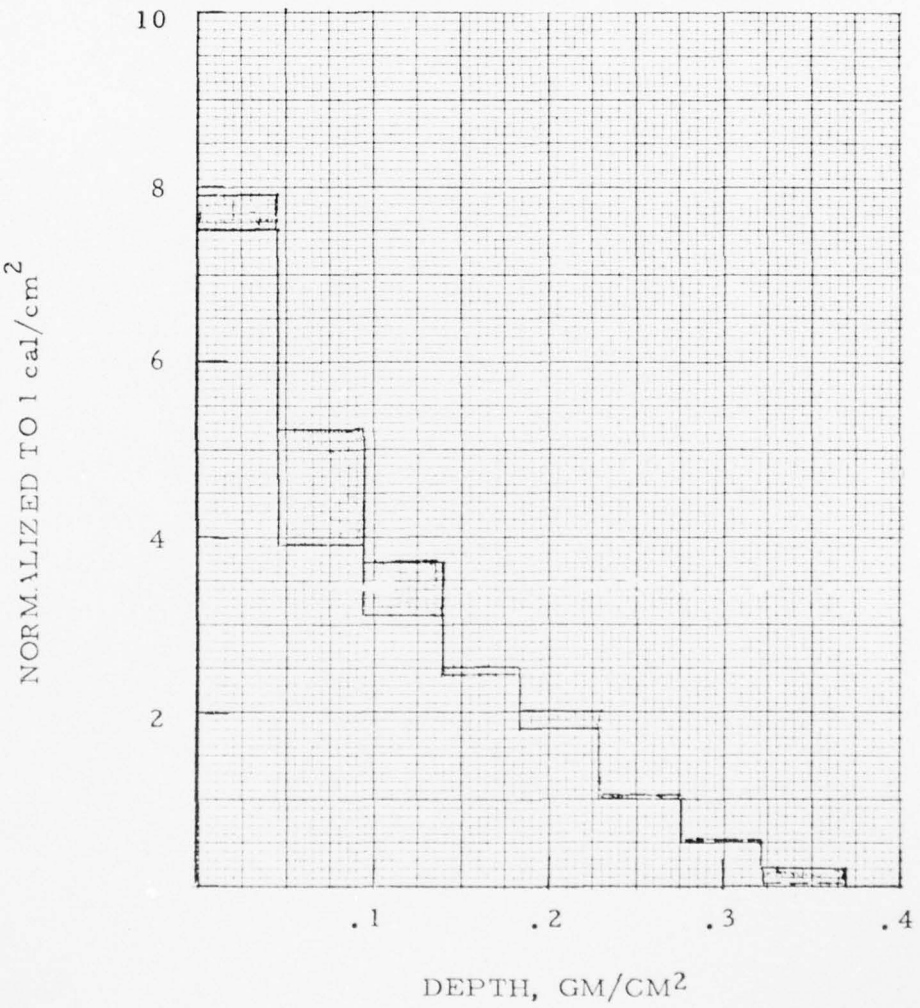

Figure 23. Depth-Dose Profile Measured in Graphite Foils for 32 cal/cm^2

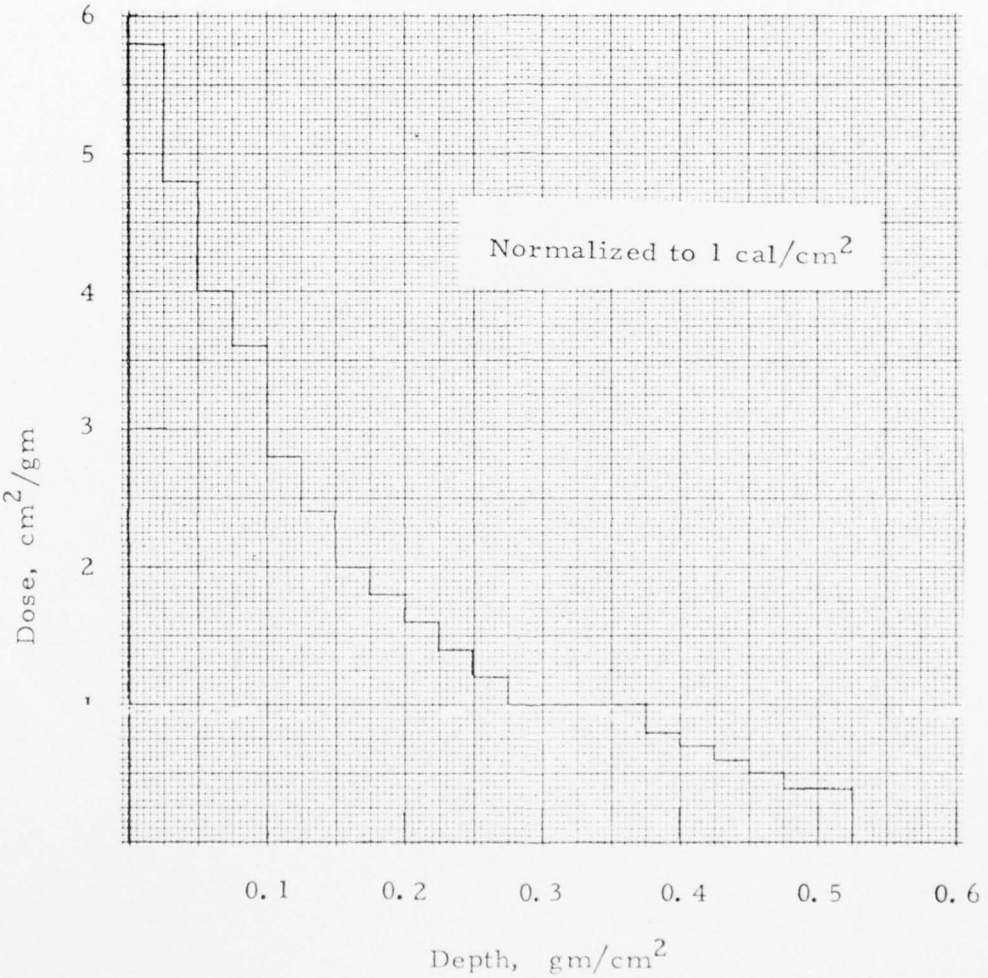

Figure 24. Depth-dose Profile in Graphite Foils for 60 cal/cm^2

SECTION V

STRESS WAVE MEASUREMENTS

Because high dose electron beams can presently be generated only over relatively small areas, selection of gaging technique requires some care if one dimensional read time is to be maximized. Consideration was given to using either quartz gages or miniature carbon gages. Because little was known about the response of miniature carbon gages to electron beam generated shock waves, it was necessary to conduct an evaluation of these devices before making a final selection of gage type. It was ultimately decided that demonstrating the applicability of miniature carbon gages consisted of a program in itself, and quartz gages were chosen as the basic measuring technique.

In the hope that our experience with miniature carbon gages might prove useful to others who wish to employ them in electron beam environments, results of work with them is discussed in the following section.

The chapter closes with presentation of quartz gage results and discussion of measurements.

5.1 Carbon Gage

Carbon gages require active monitoring; sensitivity is therefore dependent upon both the functional relationship between pressure and resistance change and the background noise level through which output must be read. As a minimum, the signal-to-noise ration should be 5:1. At this level, the amplitude of excursions centered on the fundamental as a dc base will be 20 percent peak-to-peak, corresponding to an uncertainty of ± 10 percent in the main wave. If good resolution of detailed structure in the wave is required, a higher minimum signal-to-noise ratio may be necessary.

Background noise levels associated with the operation of carbon gages on IPC's Neptune-C and FX-35 machines were not known at the start of the program; to determine these levels, noise testing was conducted. Initial experiments employed the standard, low noise system used at IPC with quartz gages. In this system, the gage and its output cable form a continuous

system which is shielded everywhere except over the active element itself; the outer conductor of this triaxial arrangement is grounded to the machine and to the screen room. Noise is typically cut down to about 0.1 volt peak-to-peak on Neptune and 0.05 volt on the FX-35. Lower levels can be obtained by placing a skin depth thick conducting layer over the gage to terminate the triax. In the past we have employed 1/2 mil thick copper to good effect for this purpose with manganin gages. Additional noise reduction gained in this way is obtained at the expense of an increase in the time required for the gage to come to mechanical equilibrium, but this increase is small. Standard Dynasen carbon gages resolve 20 nanosecond rise times*; equilibration time in 1/2 mil copper is about 5 nanoseconds. Performance degradation by this amount is an important consideration only for very sharp pulses.

In lieu of noise data on actual carbon gage configurations, it was projected that background levels would be the same as those measured with quartz crystals. This implied that a minimum signal of 0.5 volt would be necessary for experiments on Neptune and 0.25 volt on the FX-35.

To put these minimum voltage requirements in terms of stresses a calibration curve is needed, and it is necessary to know the operating characteristics of the gages. Calibration curves have been published by Effects Technology Inc. and by Dynasen; in both instances calibrations were determined from impact experiments on gages whose active elements were relatively large[10,11], ETI gages were 1.0-inches long by 0.4-inch wide by 0.001-inch thick; gages calibrated by Dynasen were 0.5-inch by 0.2-inch by 0.0004-inch thick. The ETI calibration included a number of shots at stress levels below 10 kb, some as low as 2 kb. The Dynasen calibration is based upon data taken at stresses ranging upward from 12 kb.

It was our understanding that a low stress calibration for Dynasen gages was to become available as a result of gas gun testing at EG&G, Santa Barbara under contract to the AFWL†, but this was not in hand at the start of CADRE.

---

*Dynasen Data Sheet No. 2, Dynasen Inc., 20 Dean Arnold Place, Goleta, Cal.

†Personal communication, Dr. Jacques Charest, August 22, 1973.

An estimate of the effect which gage size might have on the calibration can be made by considering the processes by which resistance is changed during shocking. Two effects contribute to this change. The first is variation in resistivity of the gage material due to crowding together of the fine carbon particles which make up the element, and the second results from changes in gage geometry. If gage length, width, and thickness are defined as ℓ, w, and t, then resistance is given by the expression

$$R = \frac{\rho \ell}{wt} ,$$

for a gage with current flowing through the cross sectional area wt. This is the standard configuration. Differentiating, the fractional change in R when ρ and t vary as the gage is placed in uniaxial strain is

$$\frac{dR}{R} = \frac{d\rho}{\rho} - \frac{dt}{t} .$$

This relation depends only on fractional changes in thickness and resistivity, length and width canceling out. As a first approximation, therefore, it would appear that gage calibration should be independent of physical dimensions other than thickness. Preliminary data obtained at EG&G on small gages suggest that this is the case. On the basis of this evidence we have used available calibration data as if it were universally applicable to gages of all sizes.

ETI fitted a cubic to their data and found the following relationship between stress and resistance change:

$$P = -26.8 \left(\frac{dr}{r}\right) - 21.0 \left(\frac{dr}{r}\right)^2 - 287 \left(\frac{dr}{r}\right)^3$$

We have made a similar fit to the Dynasen data; the expression obtained was

$$P = -39.8\left(\frac{dr}{r}\right) - 98.6\left(\frac{dr}{r}\right)^2 - 247.6\left(\frac{dr}{r}\right)^3$$

It is clear that the two are not the same, the Dynasen gage being somewhat more sensitive at low stress levels.

AFWL has evaluated gages fabricated by these two sources and by SRI and has concluded that the gage most technically advanced is that sold by Dynasen. Discussion is therefore limited to gages of this type.

Dynasen gages are presently being manufactured in the standard dimensions listed below. Energy dissipation by joule heating in each type must be held within limits implied by current and pulsewidths indicated in the table.

Gage Dimensions, inches	Maximum Current, amps	Maximum Current Duration, μsec	Bridge Voltage Limit, volts
0.5 x 0.2	6	40	815
0.25 x 0.130	6	40	815
0.2 x 0.1	3	20	405
0.075 x 0.035	1.5	15	205

In practice the gage is operated as one arm of a bridge circuit; because gage current would be controlled by adjusting the driving voltage applied to the bridge, it is desirable to restate the heating limits tabulated above in terms of bridge voltage. Figure 25 shows a schematic of the bridge employed in the standard metrophysics power supply. When the bridge is balanced no current flows through the resistance R_4 and we can write the following expression for gage current:

AD-A043 433 ION PHYSICS CORP BURLINGTON MASS F/G 11/4
ELECTRON BEAM TESTING FOR CARBON DYNAMIC RESPONSE PROGRAM (CADR--ETC(U)
MAY 77 R D EVANS F29601-73-C-0075
UNCLASSIFIED IPC-7604-TR-447 AFWL-TR-76-138 NL

2 OF 2
ADA
043433

END
DATE
FILMED
9-77
DDC

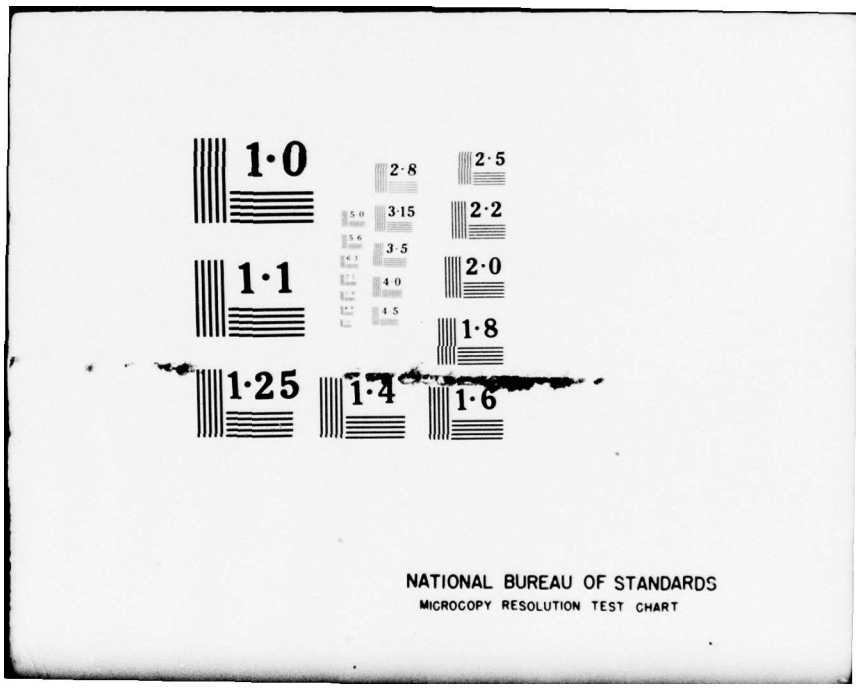
1·0
1·1
1·25
1·4
1·6
1·8
2·0
2·2
2·5
2·8
3·15
3·5
4·0
4·5
5·0
5·6
NATIONAL BUREAU OF STANDARDS
MICROCOPY RESOLUTION TEST CHART

$$V = (R_3 + R_g)\, i = (136)\, i .$$

Here V is the applied voltage.

Under stress the gage resistance decreases and current therefore increases to a value higher than that estimated from the expression above. Fractional change in resistance is small, however. Driving voltages estimated in this way will maintain a current through the gage which is approximately equal to the limiting value. For the standard Dynasen gage sizes, bridge voltages corresponding to the limiting currents have been listed in column four of the table above.

Dynasen reports that their gages have a temperature coefficient of resistance equal to 9×10^{-4} $\Omega/\Omega\,^{\circ}$C at room temperature. At higher temperatures, this coefficient decreases. To estimate the pressure equivalent of a power pulse at the limiting current, temperature rise can be computed and used to determine the fractional resistance change. Temperature rise can be found from

$$\Delta T = \frac{I^2 R T}{\rho c_p x y t}$$

where
- I = limiting current
- R = 50 Ω
- T = pulse width
- ρ = density of gage element, equal to 1.3 gm/cm^3
- x, y, t = gage dimensions
- c_p = specific heat, given as 0.25 by Dynasen

From the expression above we find a temperature rise of about 80°C; this equates to an energy density of 20 cal/gm in the gage. The change in resistance resulting from a temperature increase of this magnitude is

$$\frac{\Delta R}{R} = 0.072 \ \frac{\Omega}{\Omega} .$$

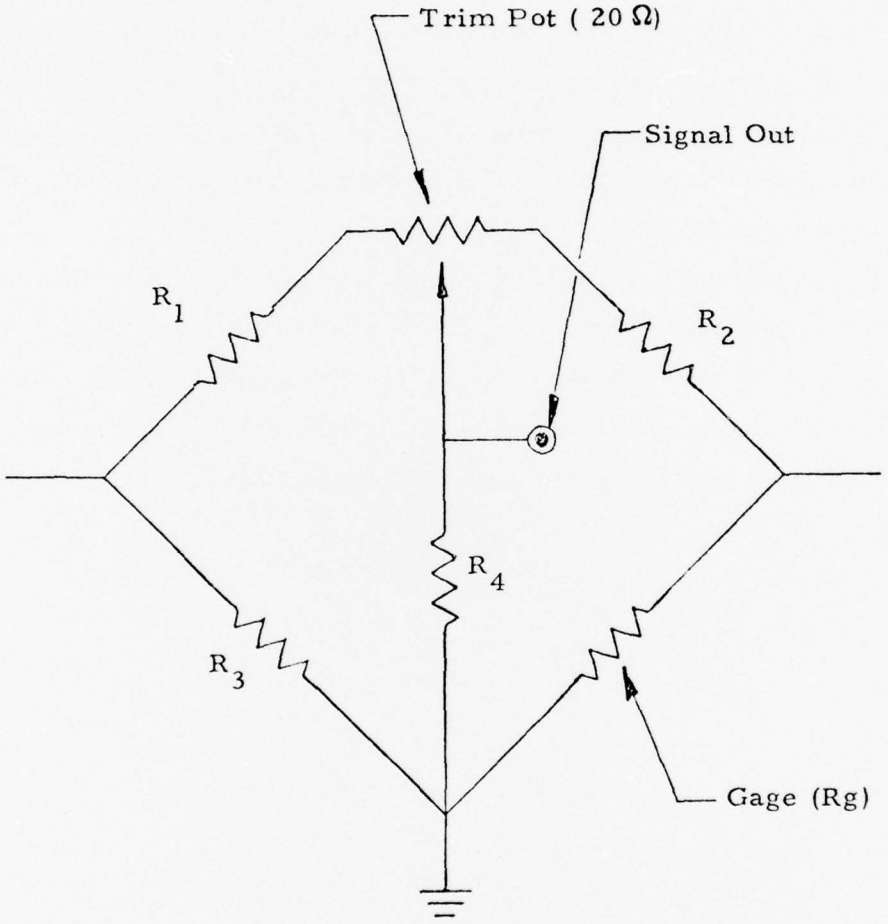

R_1 = 106.6 Ω
R_2 = 60 Ω
R_3 = 86.6 Ω
R_4 = 75 Ω

Figure 25. Schematic of Metrophysics Power Supply

This gives an equivalent pressure of 2.4 kb. To reach this value, the gage must be heated adiabatically through a complete pulse. In operation, conduction losses to the encapsulating material and target probably reduce the resistance change due to heating; passing a current smaller than the limiting value through the gage would further reduce this effect. For example, pulsing the 75 mil by 35 mil gage at the lower voltage limit of the unmodified metrophysics supply (180 v) would reduce current from 1.5 to 1.3 amps and would cut the temperature increase from 80 to 60°C. This in turn would cause the thermal equivalent pressure to drop to 1.8 kb. With modification to the power supply, bridge voltage can be further reduced and thermal background diminished.

Resistance change due to I^2R heating represents essentially a dc bias which can be determined for each gage prior to pulsing it. Gage sensitivity is affected by heating, however, as signal strength must be comparable to or greater than the thermal pressure equivalent to minimize uncertainty introduced in the process of determining stress by difference between shock and thermally generated resistance changes.

In a report describing calibration of the metrophysics supply, Rice[12] formulated the bridge equations necessary to solve for output voltage as a function of fractional resistance change in the gage arm. According to Rice, output can be calculated from the expression

$$E_o = E_s \frac{R_s}{k_1} \left[\frac{\Delta R}{(R_g + R_s)(R_g + R_s + \Delta R)} \right]$$

where

$$E_s = VR_1 \left[\frac{(R_g + R_s)}{R_3 (R_1 + R_2)} \right]$$

$$R_s = \frac{R_3 R_4 (R_1 + R_2) + R_3 R_1 R_2}{(R_3 + R_g)(R_1 + R_2) + R_1 R_2}$$

$$k_1 = \frac{R_4 (R_1 + R_2) + R_1 R_2}{R_4 (R_1 + R_2)}$$

R_1, R_2, R_3 and R_4 are bridge resistances defined in Figure 25

R_g = Gage resistance, 50 Ω

V = Voltage applied to bridge.

Solving the E_o relation for voltages ranging from 180 to 400 volts with R_1 = 116.6 Ω, R_2 = 70 Ω, R_3 = 86.6 Ω, R_4 = 75 Ω, the curves plotted in Figure 26 were obtained*. These curves can be entered at output voltages of 0.25 and 0.5 volt to obtain the corresponding fractional resistance changes for each operating voltage. These resistance changes can then be used to find pressures which will give output voltages of .25 and .5 volts. Results of this process provided estimates of the minimum stress which could be read on Neptune and the FX-35 for large and small gages, assuming a signal-to-noise ratio of 5 is required. These stress values are summarized below.

*It was assumed that the trim pot wiper was centered, adding 10 Ω each to R_1 and R_2.

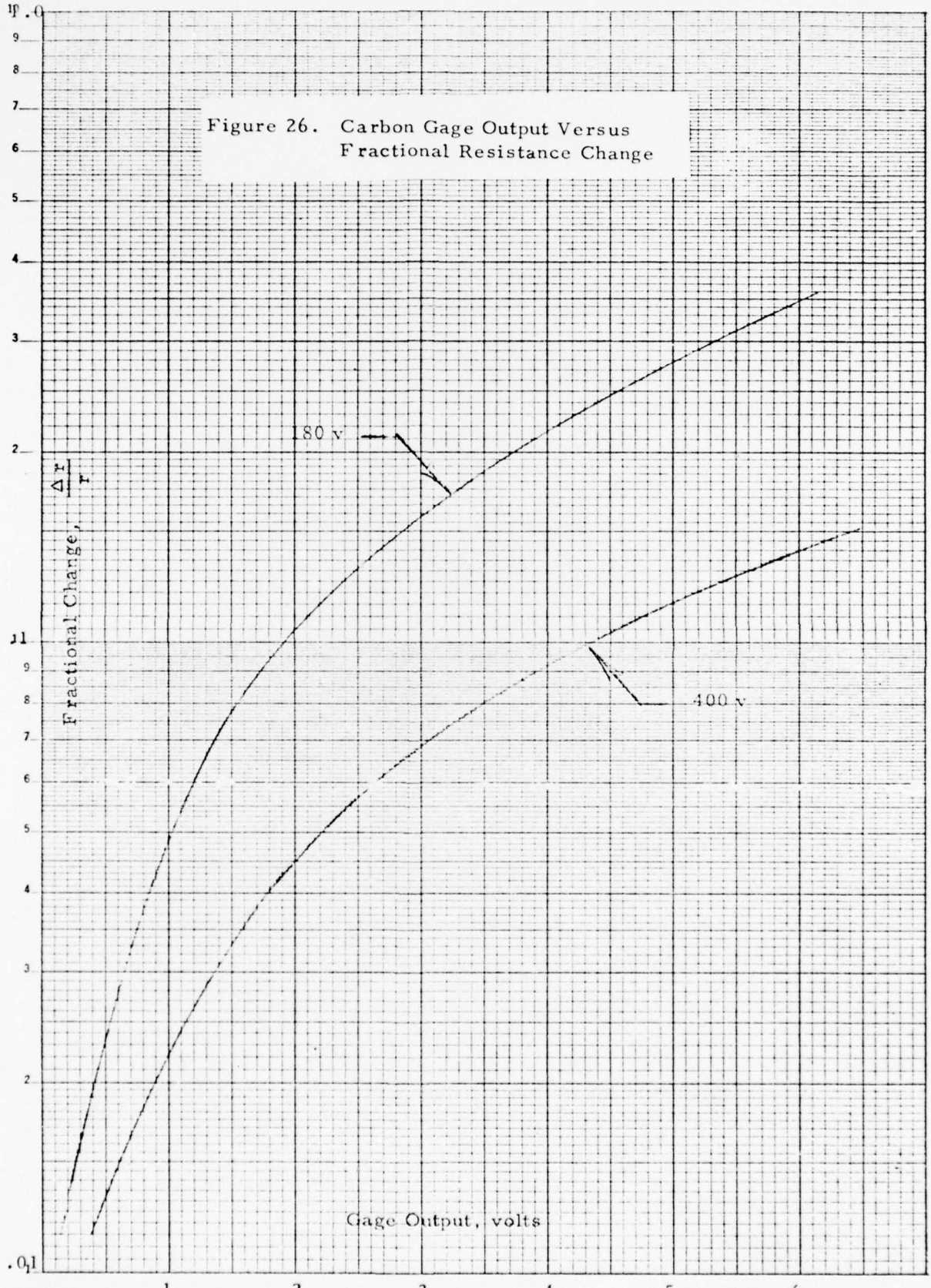

Figure 26. Carbon Gage Output Versus Fractional Resistance Change

Required Output Voltage	Minimum Detectable Pressure, kb	
	75 x 35 mil gage (180 V)	500 x 200 mil gage (400 V)
0.25 V (FX-35)	0.54	0.39
0.5 V (Neptune-C)	0.94	0.50

Carbon gages are limited to reading shocks whose rise time is long compared to the acoustic transit time across the active element and its encapsulation. This requirement stems from the need for the gage to come into mechanical equilibrium with the shock through a series of reverberations across the element. For the gage to follow the shock, applied pressure must not change significantly during the equilibration time.

Acoustic velocities in kapton and composition carbon are approximately equal to 3×10^{-4} cm/ns. The single transit time through two 1 mil layers of kapton and a single 0.4 mil layer of carbon is therefore equal to

$$t = \frac{6 \times 10^{-3} \text{ cm}}{3 \times 10^{-4} \text{ cm/ns}} = 20 \text{ ns.}$$

This is the rise time resolution cited by Dynasen for their carbon gages[11].

5.1.1 Carbon Gage Configuration; Noise Testing; Circuit Calibration

Noise testing was performed with ATJ graphite targets bonded to the gage; the gage and target were then held in a double-shielded target holder. A triax cable carried the gage leads to a special enclosure within a double-shielded screen room. Proper termination of all cables reduced noise in the bridge output signal to approximately 500 mV peak to peak. Noise was reduced to negligibly small levels by complete termination of the triax shield by covering the target with a 0.0005-inch copper foil grounded to the triax shielding. Some noise pickup coincident with the firing of Neptune Switch III was still recorded; however, this noise signal occured well before gage response, so that it did not interfere with the bridge output signal.

Carbon gage configuration (minus copper overlay) is shown in Figure 27.

Figure 28 shows output voltage from the bridge circuit when a small Dynasen carbon gage was put in series with various precision resistances to simulate stress induced changes. The solid curve was obtained from circuit analysis and represents theoretical output. Agreement is seen to be excellent.

5.1.2 Electron Beam Exposure of Miniature Carbon Gage

Miniature gages (0.075 x 0075-in.) were tested with 2DCP targets on Neptune at 22 cal/cm^2; comparative results were also obtained with quartz gages. A typical carbon gage record is shown in Figure 29, and quartz gage traces taken with similar targets under identical conditions are shown in Figure 30. Carbon gage indicated a peak stress of 6.5 kb and a pulsewidth of about 0.25 μs; main pulse was trailed by a second shock of 1.2 kb amplitude. Quartz gages read a peak stress of 5.5 kb in the gage; width of the main pulse was .25 to .30 μs wide. Main shock was followed by a "tail" in which stress

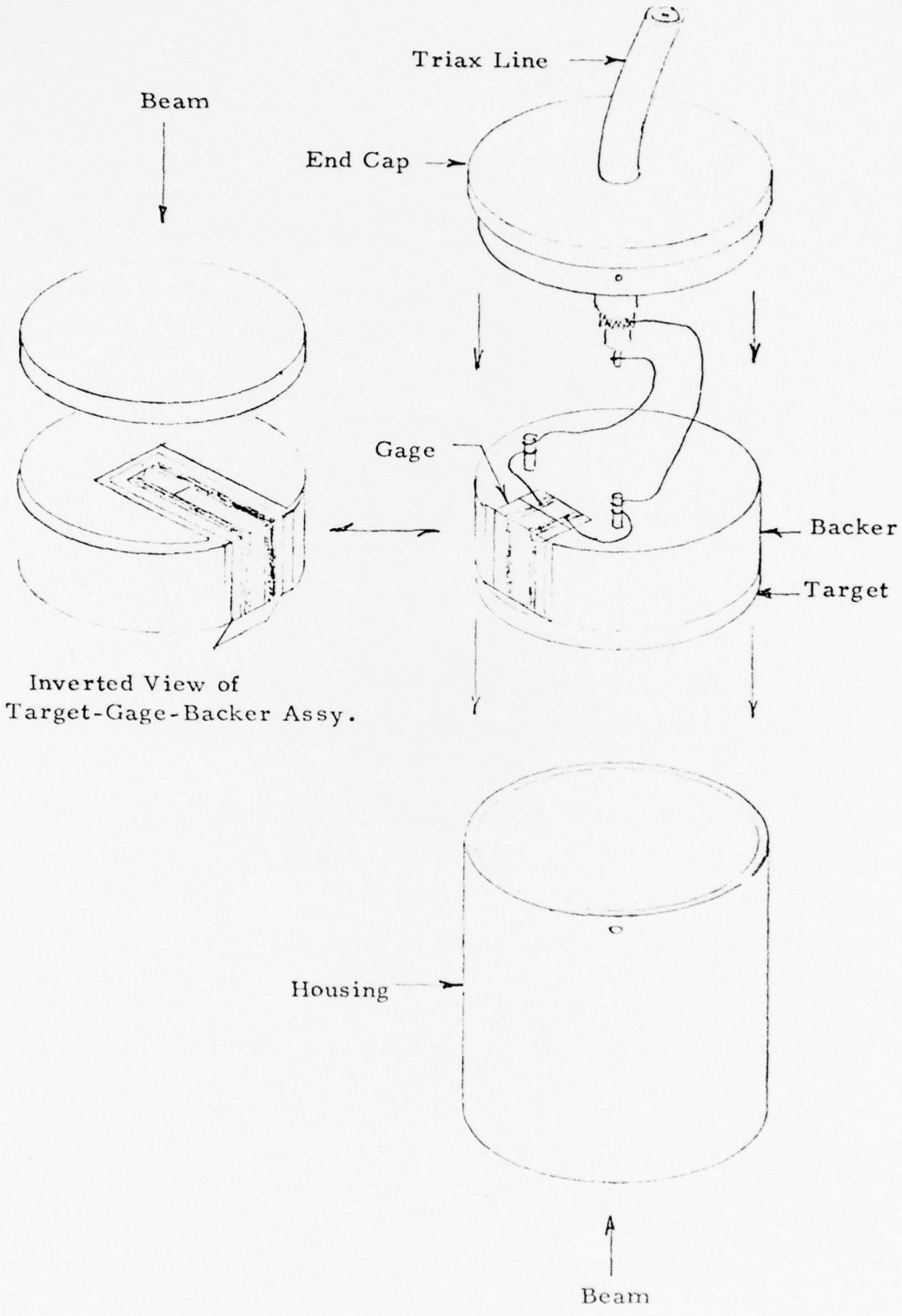

Figure 27. Exploded View of Carbon Gage Assembly

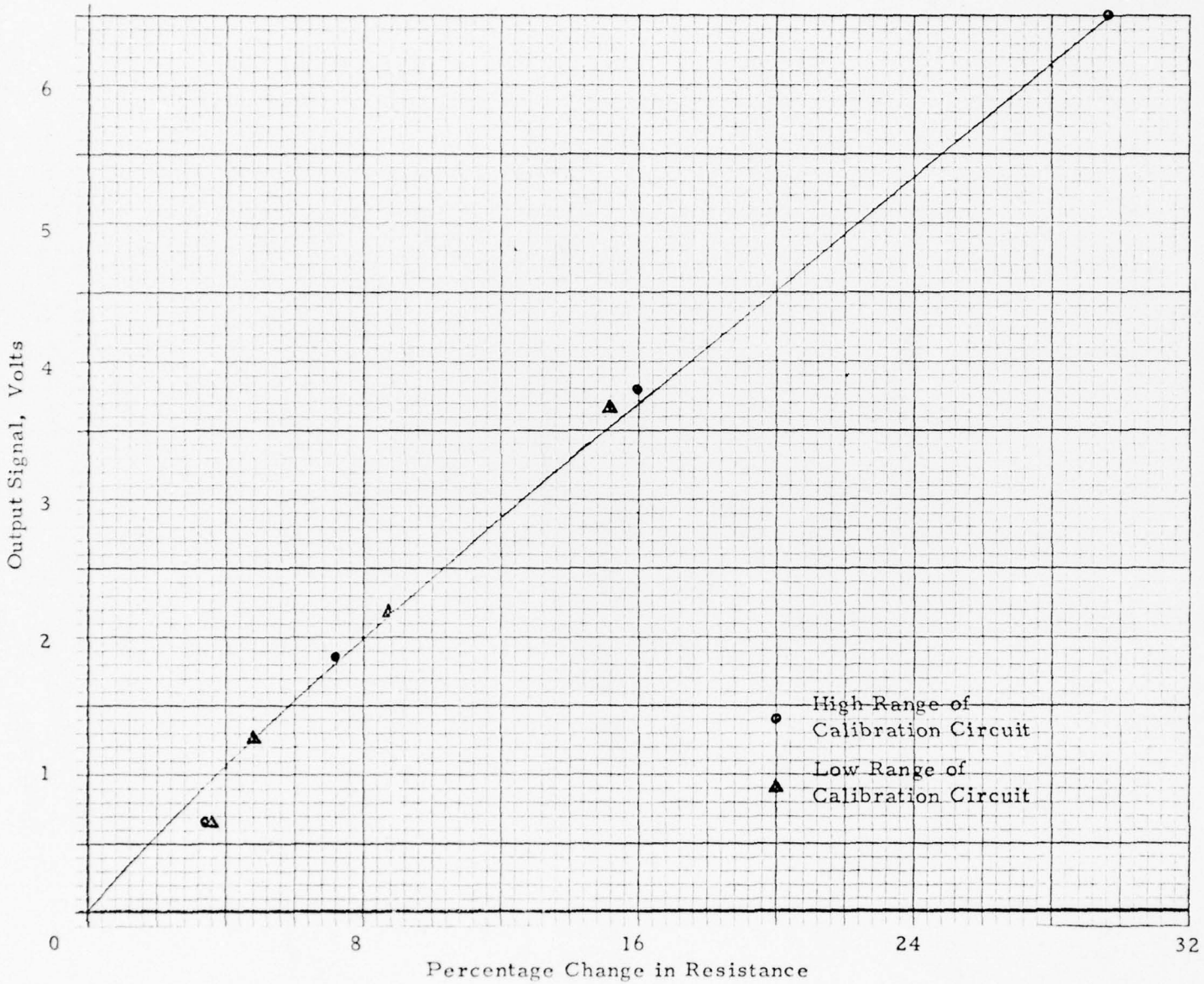

Figure 28. Calibration Curve for Small Dynasen Carbon Gage(Note: 100 V applied to bridge)

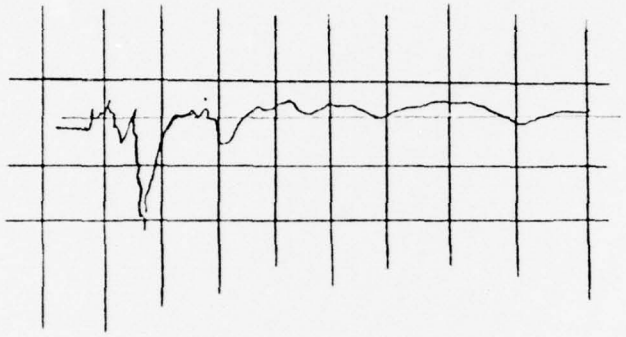

Shot 2050
0. 060-in 2DCP
22 cal/cm^2

Figure 29. Oscilloscope Record for Miniature Carbon Gage - 2DCP at 22 cal/cm^2 on Neptune

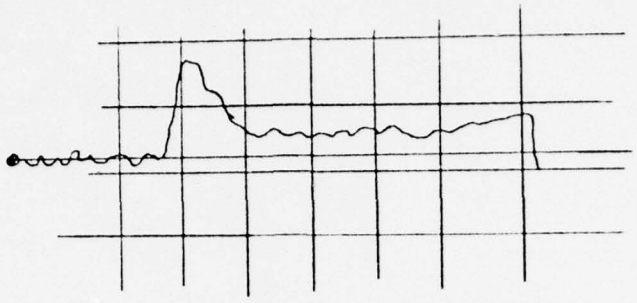

Shot 2038
0.060-in 2DCP
22 cal/cm^2

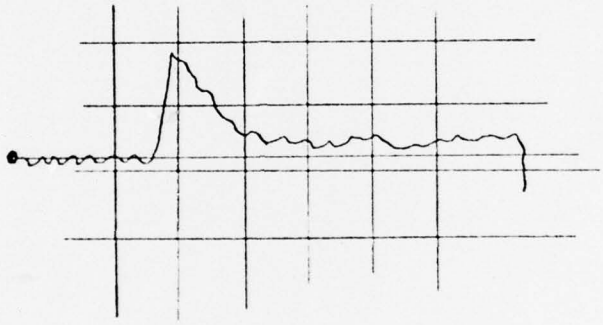

Shot 2040
0.060-in 2DCP
22 cal/cm^2

Figure 30. Oscilloscope Records for Quartz Gages - 2DCP at 22 cal/cm^2 on Neptune

was essentially constant out to the gage cutoff point. Mismatching stress back to the 2DCP using linear theory, quartz gages suggested a target stress of approximately 3.5 kb, or about half the value recorded with Dynasen gages.

Because there was substantial disagreement between the gage types regarding both shock magnitude and details of the late time pulse shape, it was concluded that miniature carbon gages should be abandoned in favor of making all stress measurements with quartz.

The necessary gages were purchased from Valpey-Fisher Corp., Holliston, Massachusetts, as their standard part number OC-100. Active diameter of the crystals was 0.25-inches across the guard ring; thickness was 0.20-inches.

5.2 Results of Quartz Gage Measurements on Neptune and FX-35

Quartz gage records were taken on 2DCP at 22, 55, and 134 cal/cm^2 with Neptune and 30, 60, and 100 cal/cm^2 with FX-35. Results are summarized in Table 21. The table lists fluence, peak stress in quartz, sample thickness, and shock arrival times corresponding to first detectable distrubance and to peak stress.

A series of measurements was attempted on 3DCC at 130 cal/cm^2 using Neptune. Traces showed early time noise typical of that seen on 2DCP targets, but no discernible pressure wave arrived within the gage read time. It is therefore concluded that either the shock reached the gage later than 1.1 μsec after irradiation or peak stress was below the detectable limit. This limit is about 0.25 kb for Neptune.

For a shock to be delayed beyond gage read time, its velocity must have been less than 0.14 cm/μsec. This figure was computed from target thickness (0.060-in.) and gage read time (1.1 μsec). In practice, a wave arriving after one dimensional read time should still cause a signal to be read; although its magnitude may not be readily determinable, its presence should be evident. No indication of such a late wave appeared within the sweep time of our oscilloscopes (set to 5 μsec for these measurements). The conclusion appears to be that stress generated in 3DCC under the highest doses

TABLE 21

SUMMARY OF QUARTZ GAGE MEASUREMENTS ON 2DCP

Machine		Shot No.	Arrival Time, μs			Target Thickness		Shock Velocity,	
			Peak Stress in Gage, kb	Peak Stress	Leading Edge	inches	cm	Peak Stress	Foot
Neptune	22	2040	5.6	0.48	0.47	0.062	0.158	0.33	0.34
		2038	5.4	0.52	0.45	0.062	0.158	0.30	0.35
	55	2072	9.6	1.13	1.03	0.125	0.318	0.28	0.31
		2074	9.9	1.13	1.03	0.125	0.318	0.28	0.31
	134	2458	15.7	0.42	0.28	0.062	0.158	0.38	0.56
		2460	17.2	0.46	0.28	0.062	0.158	0.34	0.56
FX-35	35	2210*	6.9	0.85	0.32	0.125	0.318	0.37	0.99
		2212*	9.4	~ 0.90	0.25	0.125	0.318	0.35	1.30
		2213	5.3	0.80	0.30	0.125	0.318	0.40	1.10
	55	2275	7.1	0.85	-	0.125	0.318	0.37	-
		2276*	9.4	0.85	-	0.125	0.318	0.37	-
		2278	7.1	0.90	-	0.125	0.318	0.37	-
	104	2584	13.0	0.82	0.50	0.125	0.318	0.39	0.64
		2585	11.7	0.80	0.50	0.125	0.318	0.40	0.64
		2586	12.1	0.80	0.50	0.125	0.318	0.40	0.64

* Beam was not centered over gage on these shots

employed in this program was not, after propagation through 0.060-inch of material, high enough to be measured. In view of this, tests at other levels were not carried forward.

Detailed plots of stress for each data shot on 2DCP are given in the Appendix to this report.

For comparison with pendulum measurements, areas under quartz gage traces was determined by integration; using linear theory, results were mismatched to the target. Results are given in Table 22.

TABLE 22

IMPULSE DETERMINED FROM QUARTZ GAGES

Machine	Shot No.	Fluence, cal/cm^2	Impulse in quartz, ktaps	Impulse in target, ktaps
Neptune	2038	22	2.1	1.4
	2040	22	1.7	1.1
	2072	54	2.7	1.8
	2074	54	3.8	2.6
	2458	134	7.3	5.0
	2460	134	9.3	6.3
FX-35	2210	33	4.0	2.8
	2212	33	6.4	4.4
	2213	33	3.1	2.1
	2275	63	4.0	2.7
	2276	63	5.7	3.9
	2278	63	3.6	2.4
	2584	104	9.8	6.6
	2585	104	6.7	4.6
	2586	104	9.7	6.6

REFERENCES

1. Tucker, T., Hettchie, R., and Cooperstein, G., Impulsive Response of Graphite Materials to Pulsed Electron Heating, Naval Research Laboratory Report in preparation.

2. Evans, R. D., Ottesen, J. A., and Wenstrup, R. S., Impulse and Particle Velocity Induced by Pulsed Electron Heating of One- and Three-Dimensionally Reinforced Composite Materials, IPC Report No. 7303-TR-425, Ion Physics Corporation, Burlington, Massachusetts, March 1973.

3. Harris, N. W., Evans, R. D., and Milde, H. I., Neptune-C; An Upgraded Low Impedance Pulser , IPC Report 7404-TR-436, Ion Physics Corporation, Burlington, Massachusetts, April 1974.

4. Kohn, B. J., Compilation of Hugoniot Equations of State, AFWL-TR-69-38, Air Force Weapons Laboratory, Kirtland AFB, New Mexico, April 1969.

5. Spencer, L. V., Dissipation of Energy by Fast Electrons, NBS Monograph No. 1.

6. Bade, W. L., Pretest Calculations for CADRE Task 1, Avco Report K500-73-WLB-194, Avco Systems Division, Wilmington, Massachusetts, July 1973.

7. Barker, L. M., and Hollenbach, R. E., "Shock Wave Studies of PMMA, Fused Silica, and Sapphire," JAP 41 , No. 10, 4208, Sept. 1970.

8. Evans, R. D. and Ottesen, J. A., Techniques for Making Impulse Measurements with Small Area Targets in Electron Beams, IPC 7207-TR-420, Ion Physics Corporation, Burlington, Massachusetts.

9. Schallhorn, D. R., et al., Neptune-C Electron Beams, HDL-TR-1723, Harry Diamond Laboratories, Washington, D.C., September 1975.

10. Naumann, W. J., Carbon Stress Gage Development, DNA 3027F, April 1973 (ETI Report).

11. Carbon Shock Pressure Gages, Dynasen Data Sheet No. 2, September 1972.

12. Rice, M. H., Calibration of the Power Supply for Manganin Pressure Gages, AFWL-TR-70-120, Air Force Weapons Laboratory, Kirtland AFB, New Mexico, November 1970.

APPENDIX

PLOTS OF STRESS FOR EACH DATA SHOT ON 2DCP

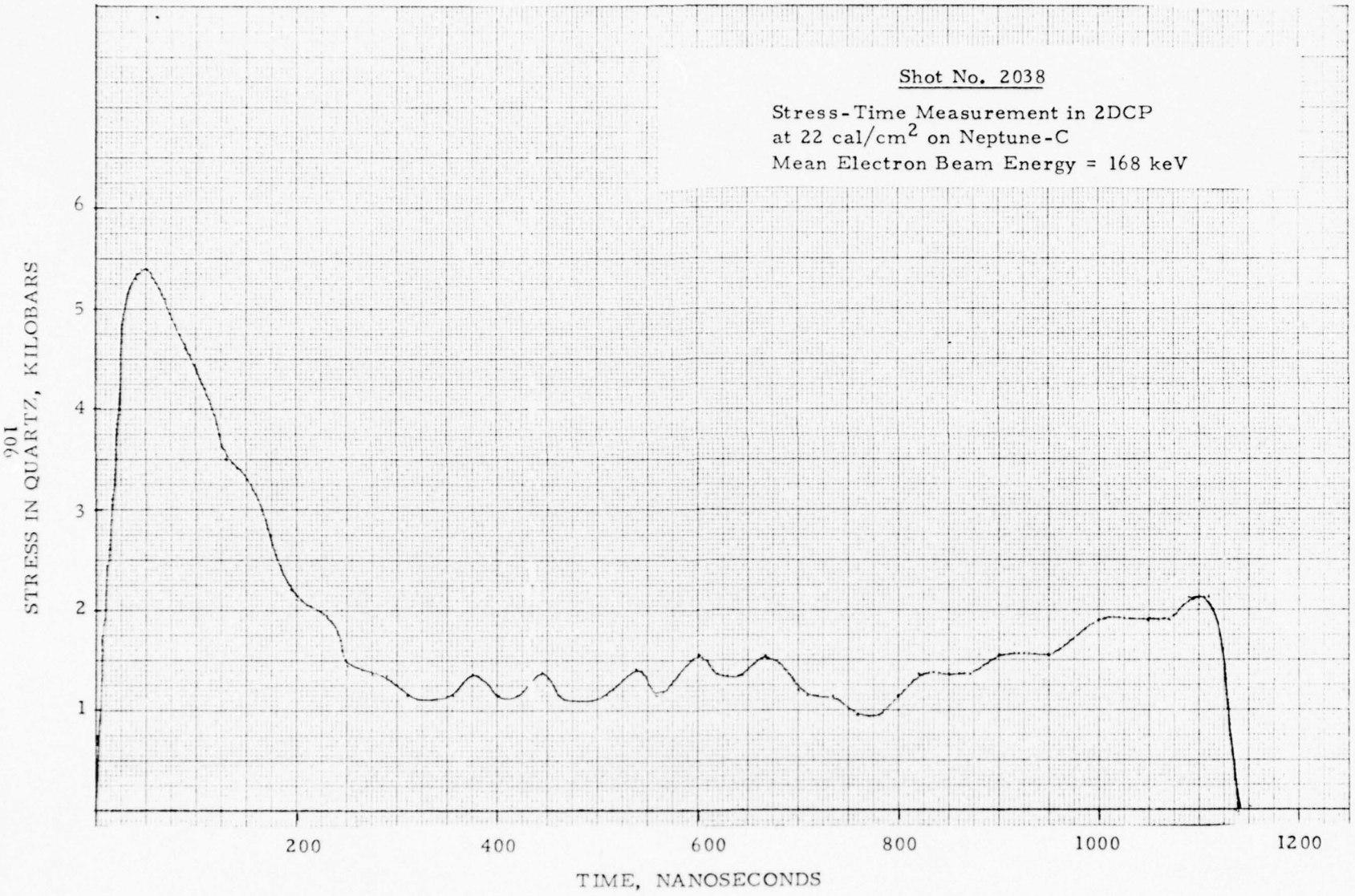
Shot No. 2038
Stress-Time Measurement in 2DCP
at 22 cal/cm2 on Neptune-C
Mean Electron Beam Energy = 168 keV
STRESS IN QUARTZ, KILOBARS
901
1
2
3
4
5
6
200
400
600
800
1000
1200
TIME, NANOSECONDS

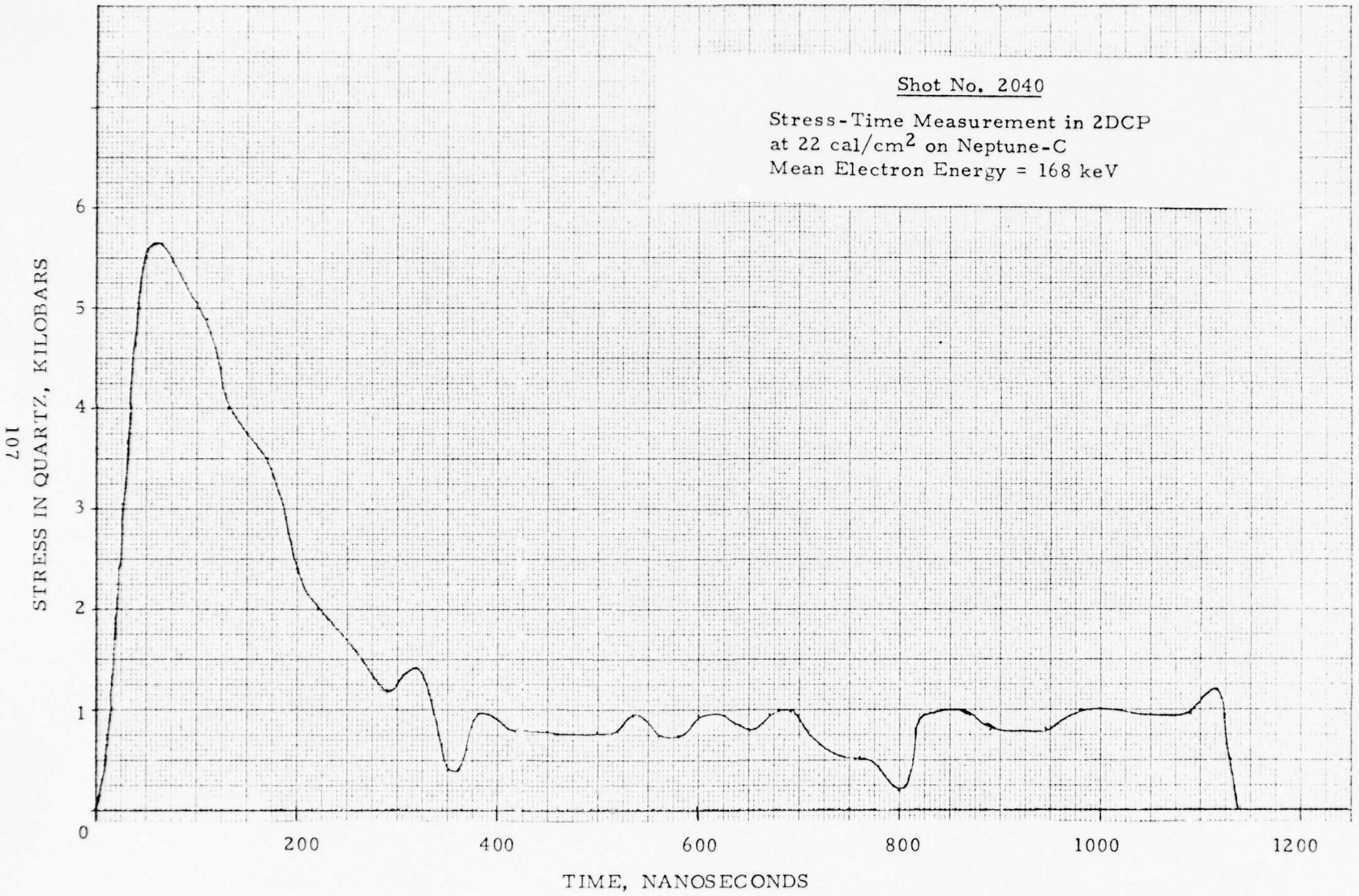
Shot No. 2040
Stress-Time Measurement in 2DCP
at 22 cal/cm2 on Neptune-C
Mean Electron Energy = 168 keV
STRESS IN QUARTZ, KILOBARS
0
1
2
3
4
5
6
200
400
600
800
1000
1200
TIME, NANOSECONDS

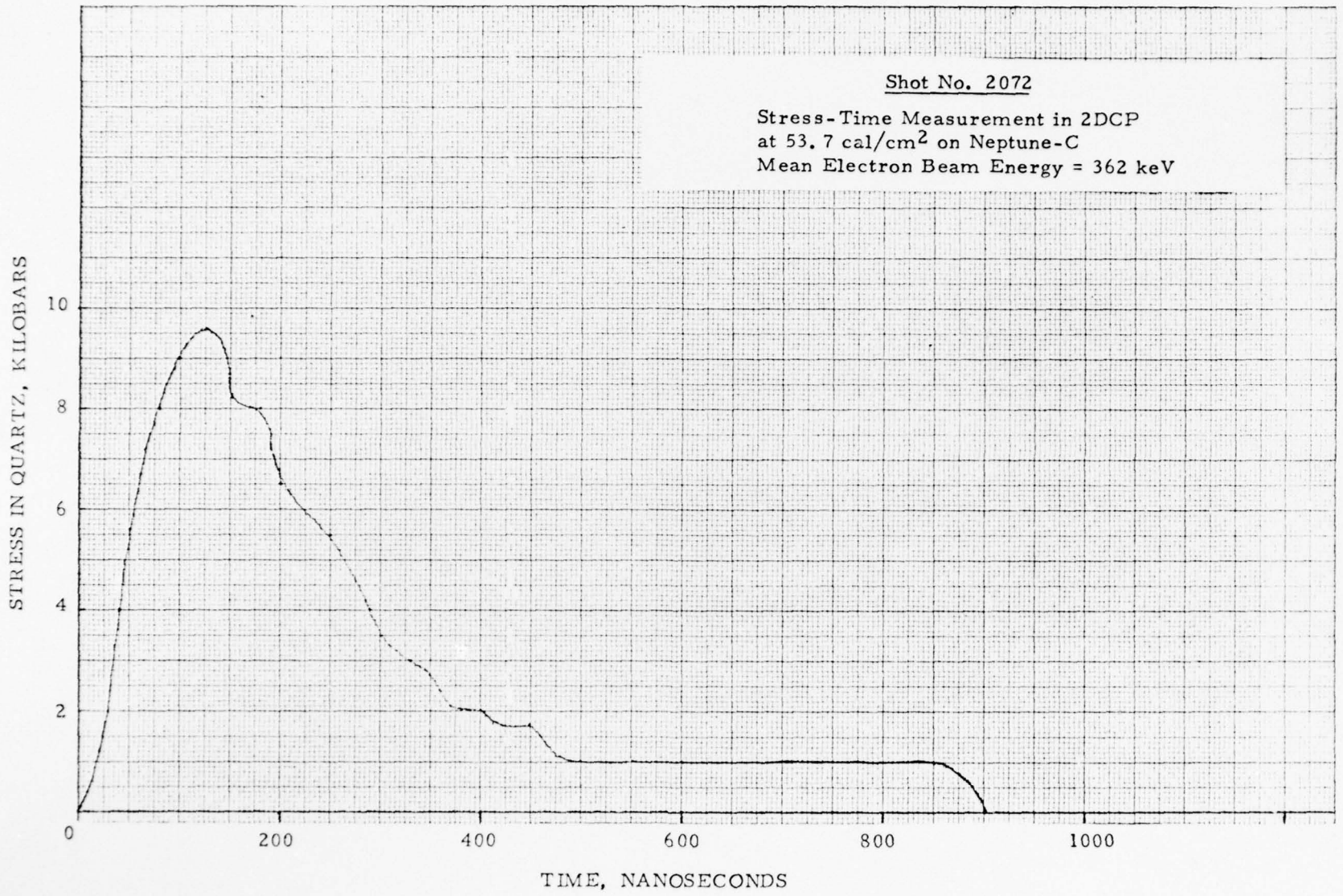
Shot No. 2072
Stress-Time Measurement in 2DCP
at 53.7 cal/cm2 on Neptune-C
Mean Electron Beam Energy = 362 keV
STRESS IN QUARTZ, KILOBARS
10
8
6
4
2
0
200
400
600
800
1000
TIME, NANOSECONDS

Shot No. 2074

Stress-Time Measurement in 2DCP
at 53.7 cal/cm^2 on Neptune-C
Mean Electron Beam Energy = 362 keV

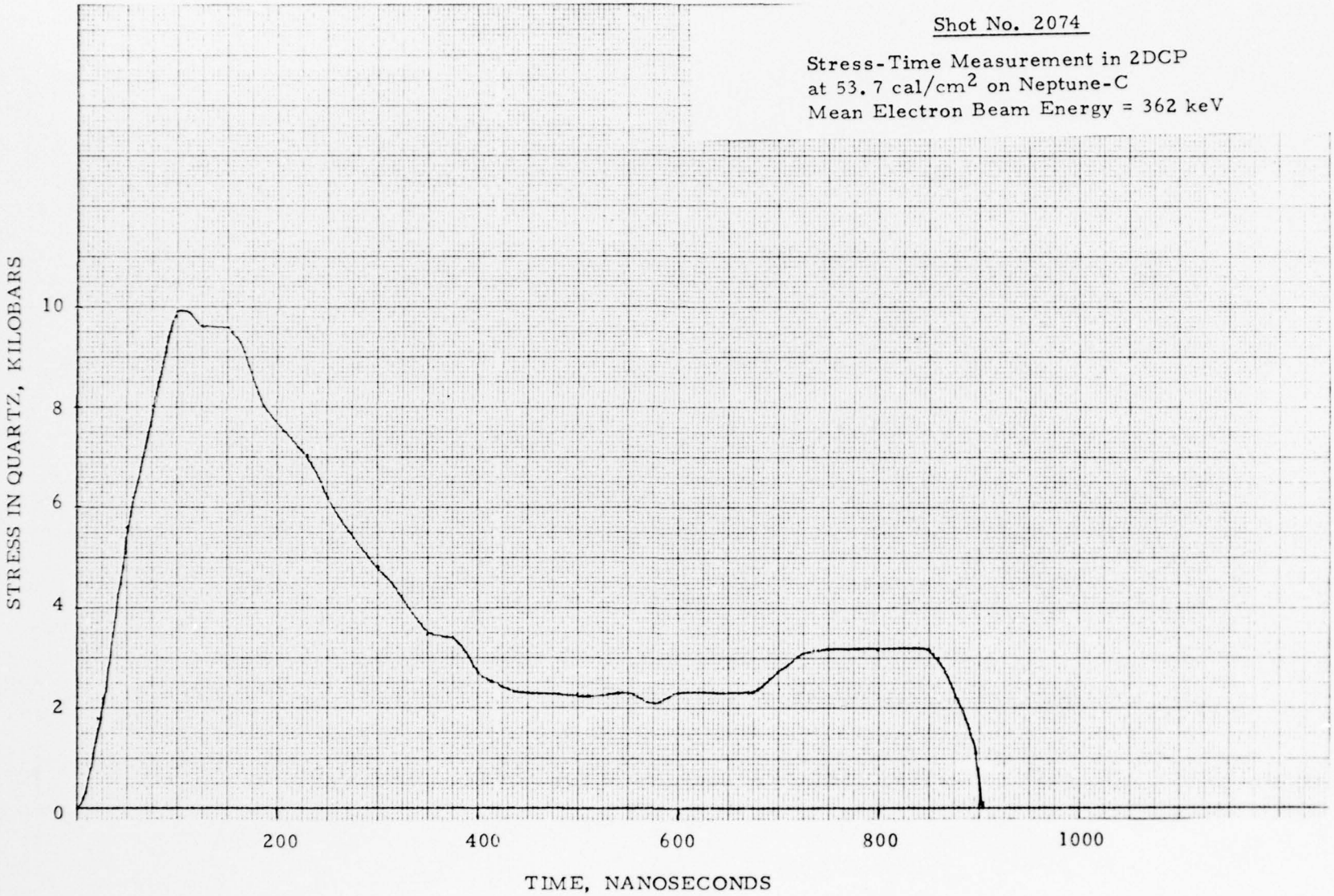

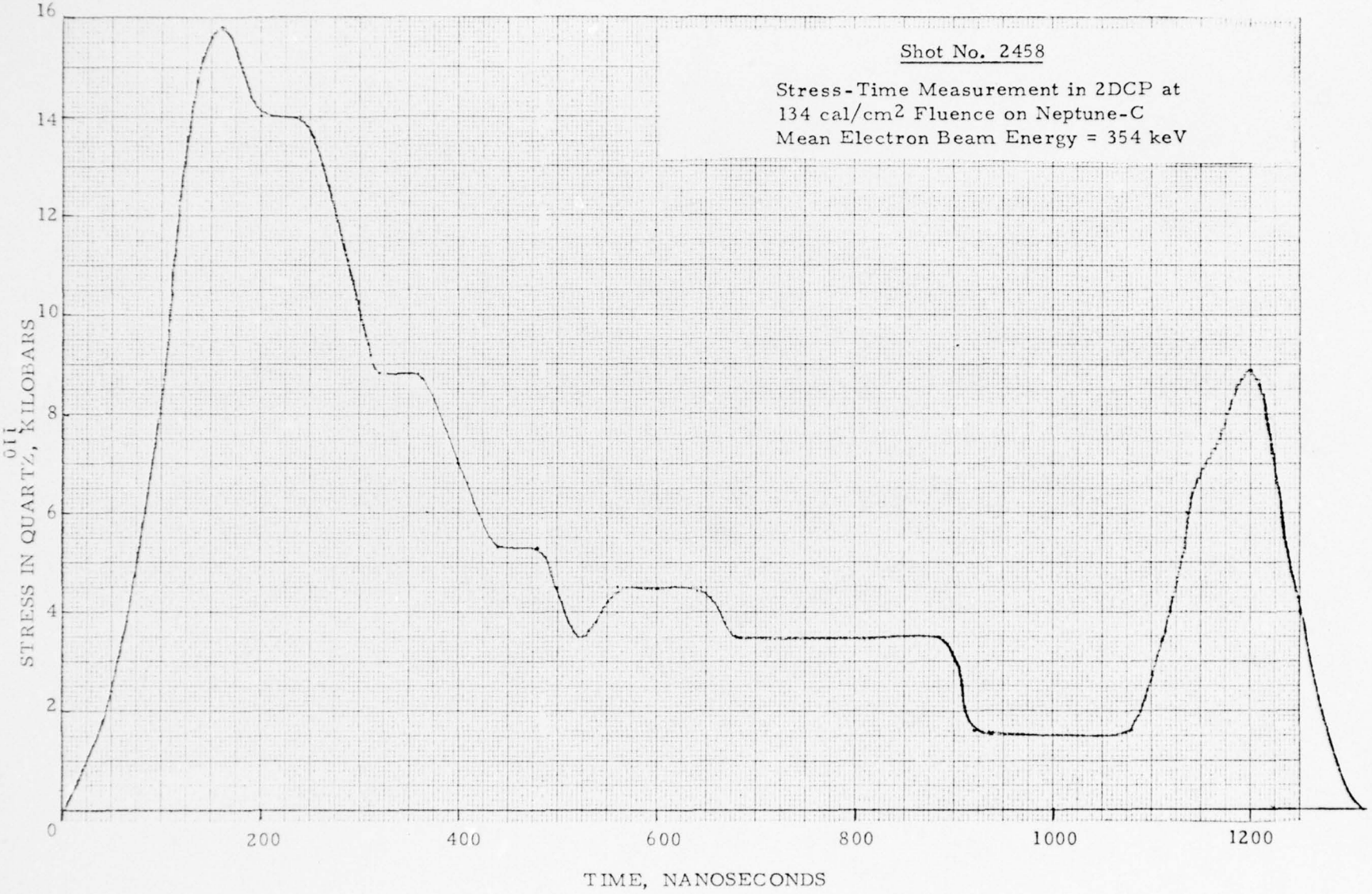
Shot No. 2458
Stress-Time Measurement in 2DCP at
134 cal/cm2 Fluence on Neptune-C
Mean Electron Beam Energy = 354 keV
STRESS IN QUARTZ, KILOBARS
TIME, NANOSECONDS
0
2
4
6
8
10
12
14
16
200
400
600
800
1000
1200

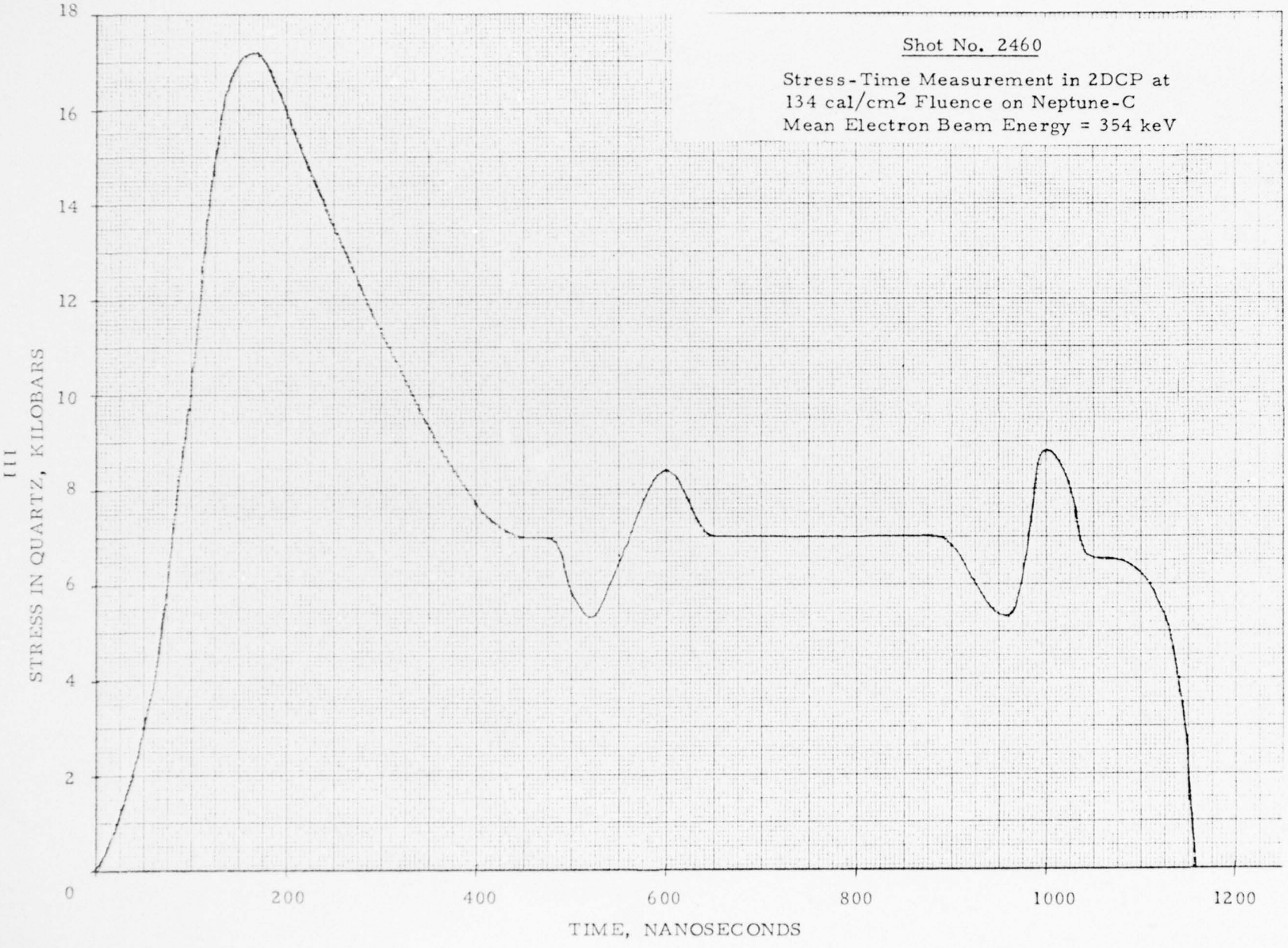
Shot No. 2460
Stress-Time Measurement in 2DCP at
134 cal/cm2 Fluence on Neptune-C
Mean Electron Beam Energy = 354 keV
STRESS IN QUARTZ, KILOBARS
TIME, NANOSECONDS
0
2
4
6
8
10
12
14
16
18
200
400
600
800
1000
1200

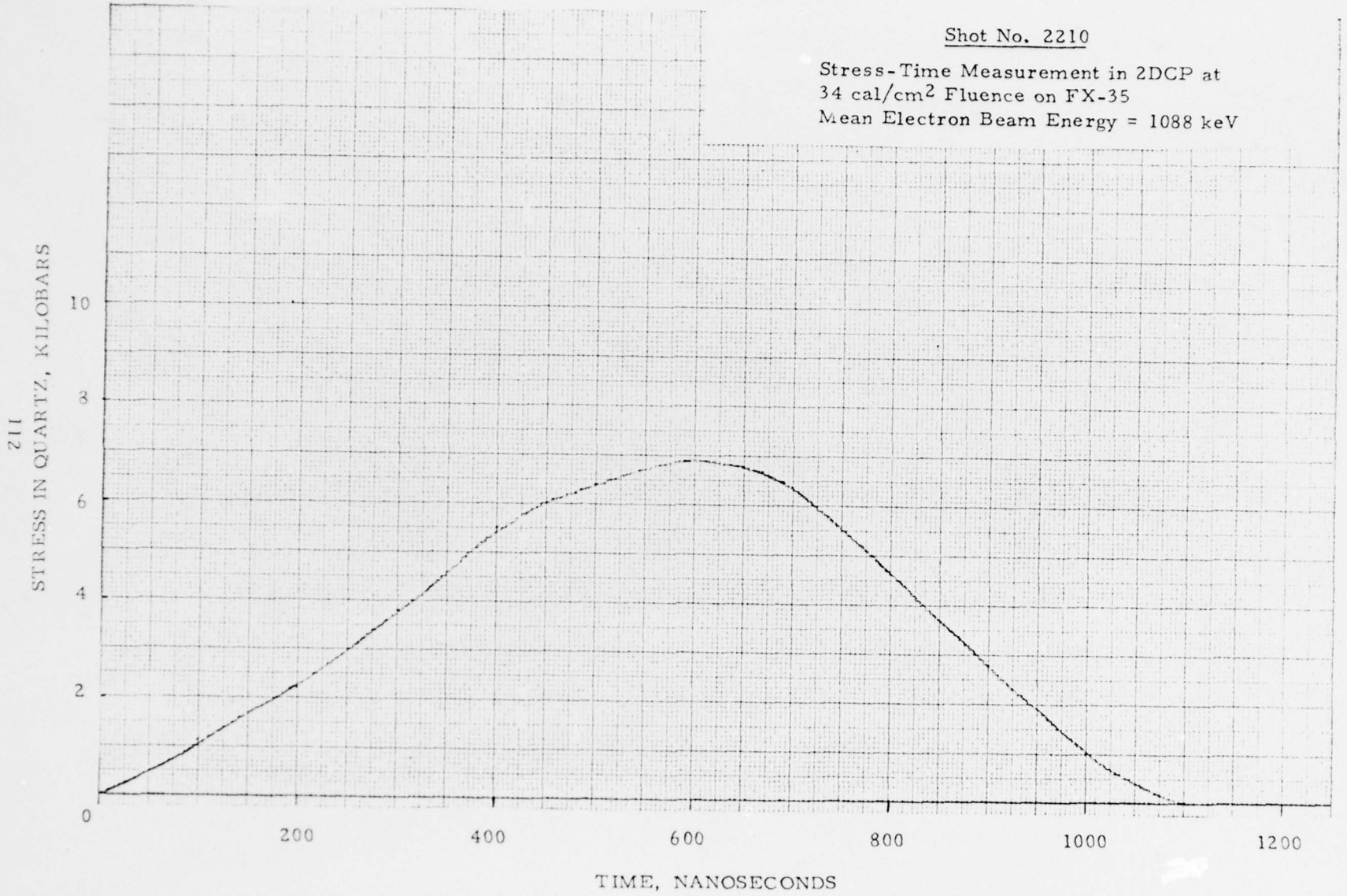
Shot No. 2210
Stress-Time Measurement in 2DCP at
34 cal/cm2 Fluence on FX-35
Mean Electron Beam Energy = 1088 keV
211
STRESS IN QUARTZ, KILOBARS
0
2
4
6
8
10
200
400
600
800
1000
1200
TIME, NANOSECONDS

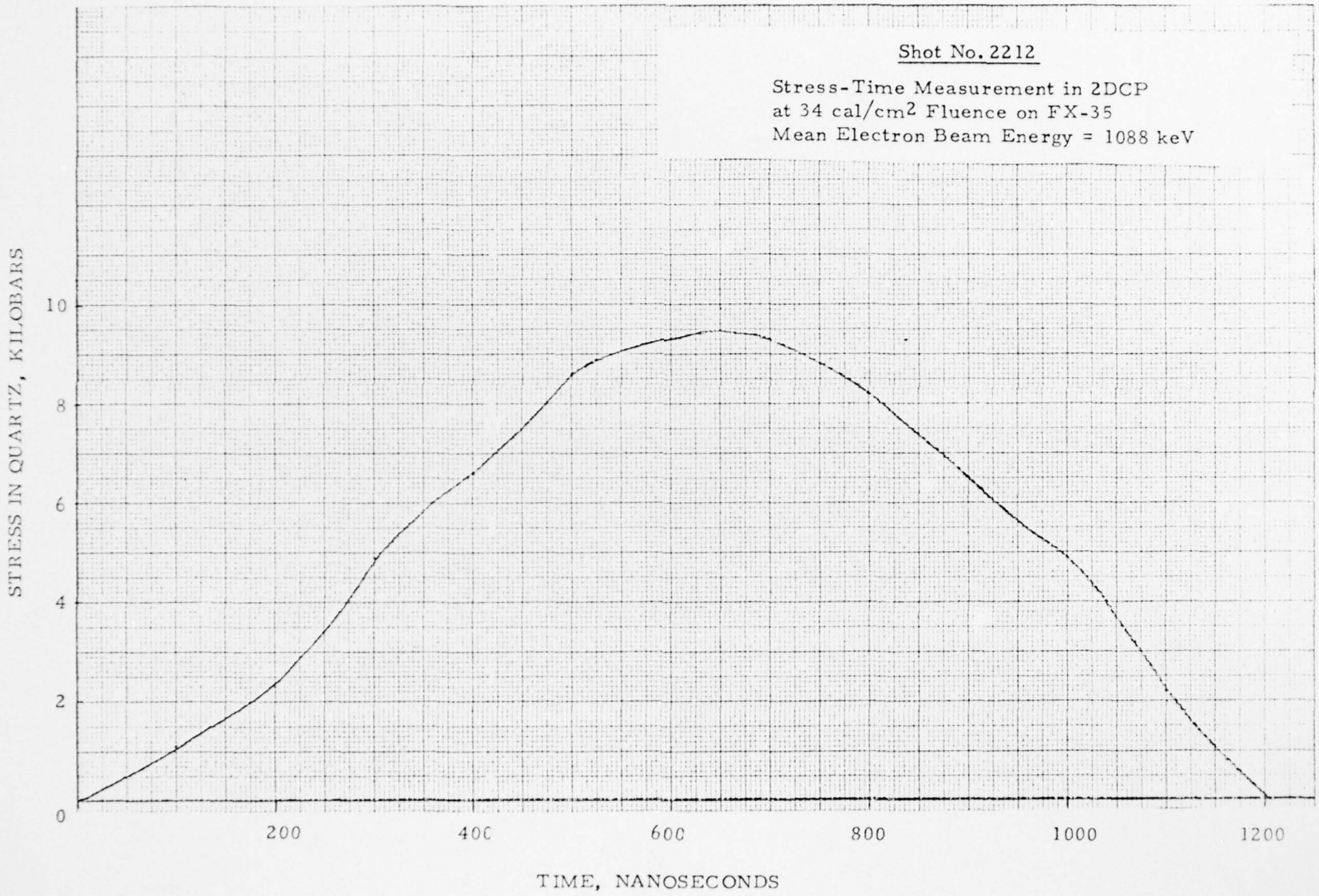
Shot No. 2212
Stress-Time Measurement in 2DCP
at 34 cal/cm2 Fluence on FX-35
Mean Electron Beam Energy = 1088 keV
STRESS IN QUARTZ, KILOBARS
0
2
4
6
8
10
200
400
600
800
1000
1200
TIME, NANOSECONDS

Shot No. 2213

Stress-Time Measurement in 2DCP at
34 cal/cm^2 Fluence on FX-35
Mean Electron Beam Energy = 1088 keV

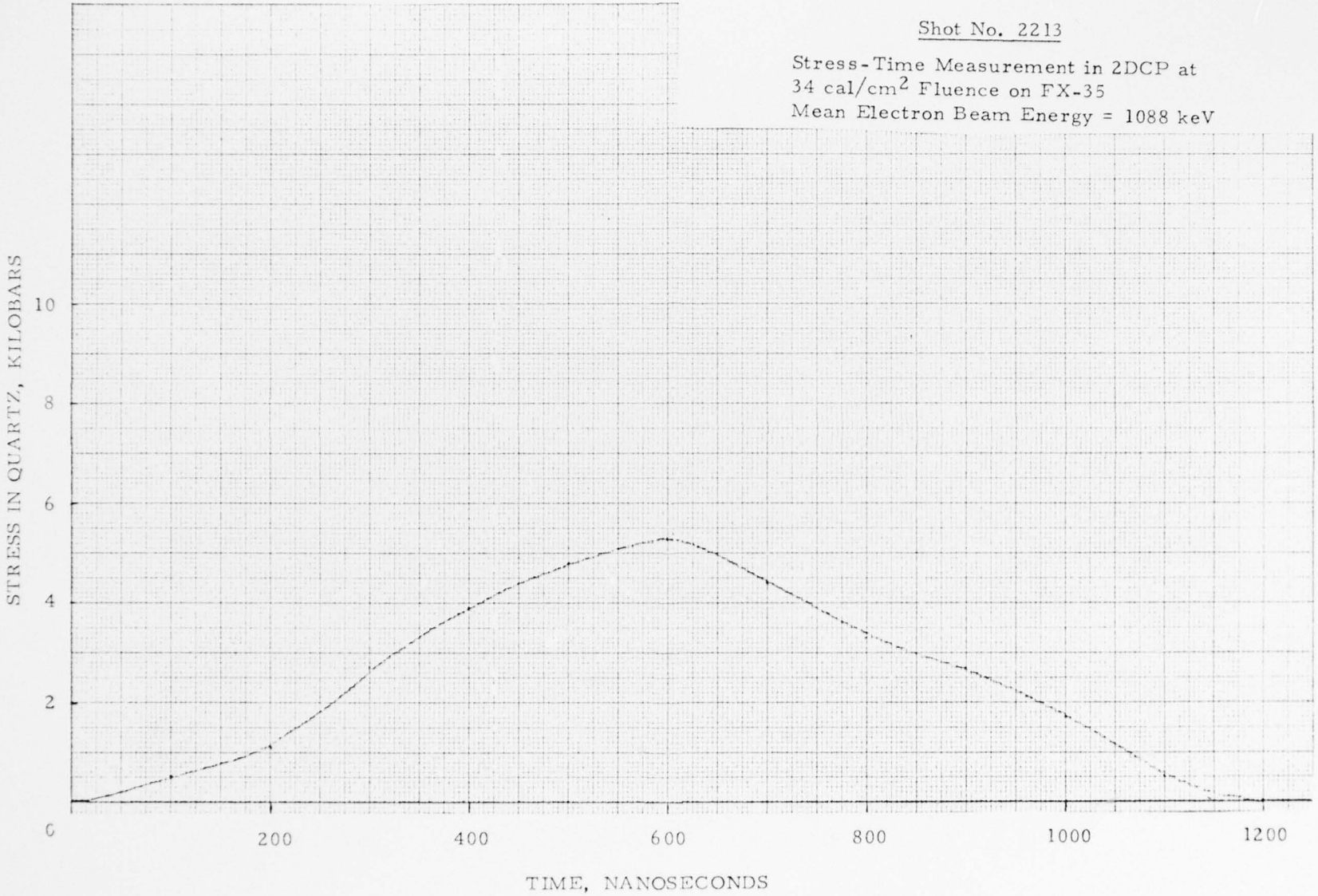

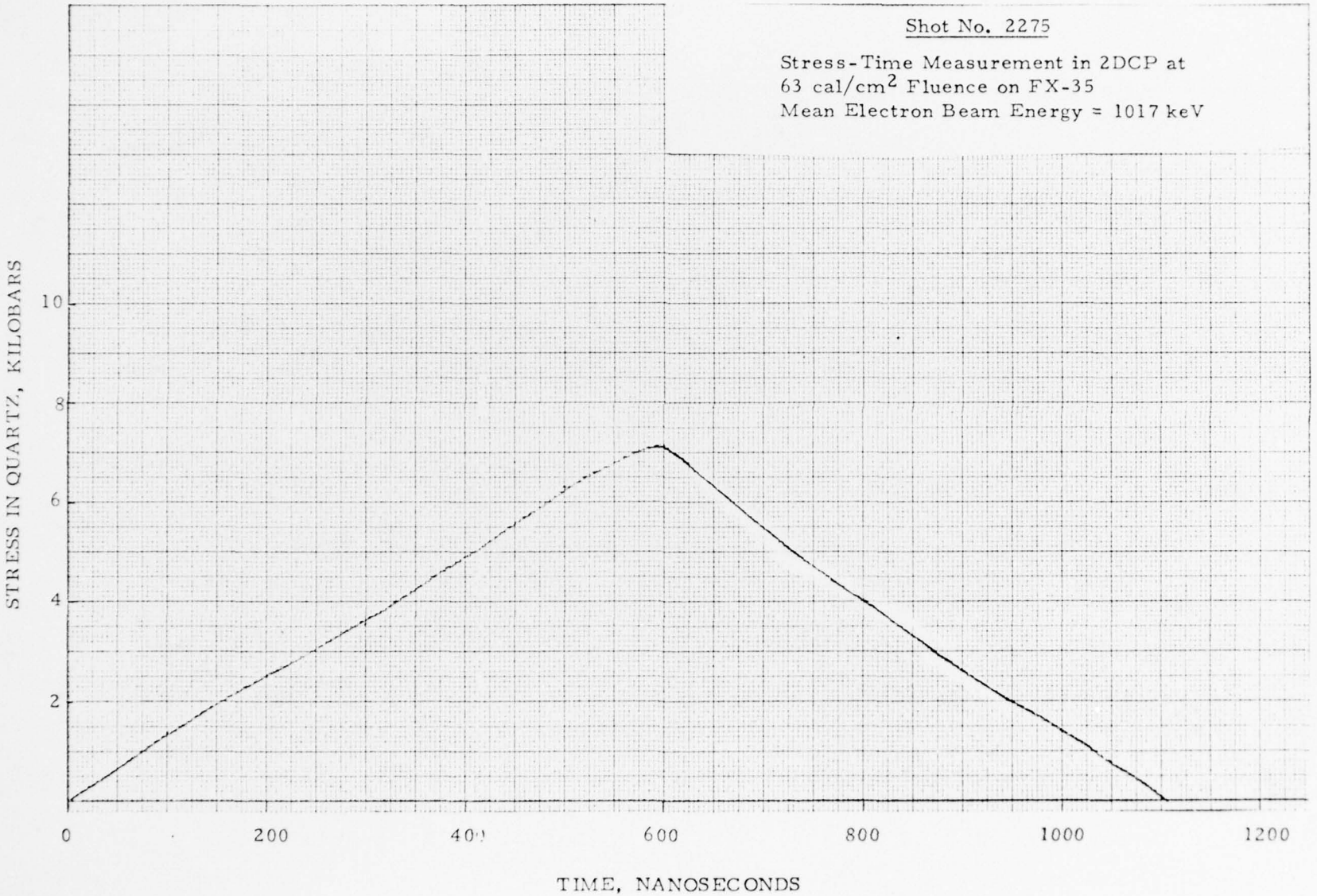
Shot No. 2275
Stress-Time Measurement in 2DCP at
63 cal/cm2 Fluence on FX-35
Mean Electron Beam Energy = 1017 keV
STRESS IN QUARTZ, KILOBARS
10
8
6
4
2
0
200
400
600
800
1000
1200
TIME, NANOSECONDS

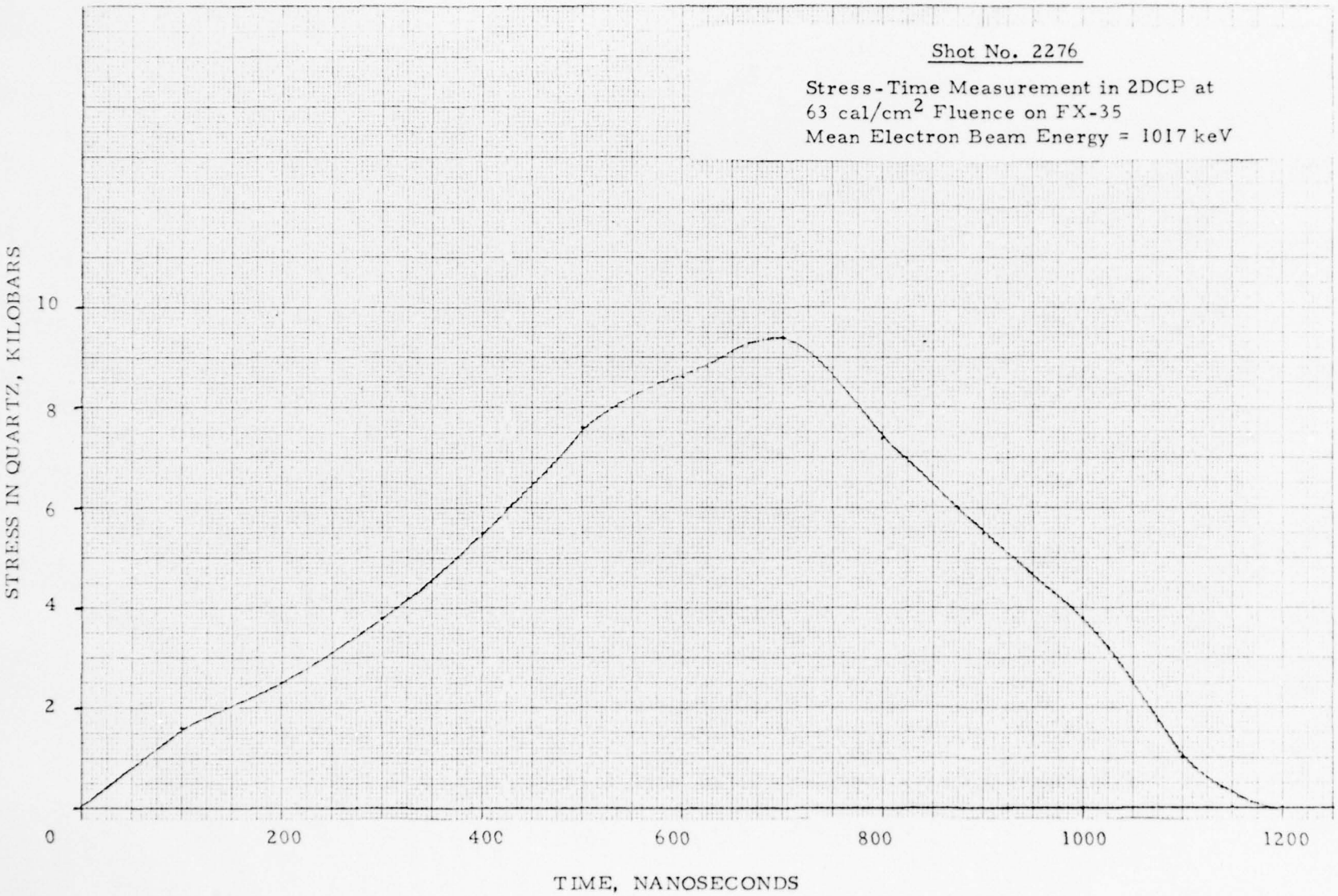
Shot No. 2276
Stress-Time Measurement in 2DCP at
63 cal/cm2 Fluence on FX-35
Mean Electron Beam Energy = 1017 keV
STRESS IN QUARTZ, KILOBARS
0
2
4
6
8
10
0
200
400
600
800
1000
1200
TIME, NANOSECONDS

Shot No. 2278

Stress-Time Measurement in 2DCP at
63 cal/cm^2 Fluence on FX-35
Mean Electron Beam Energy = 1017 keV

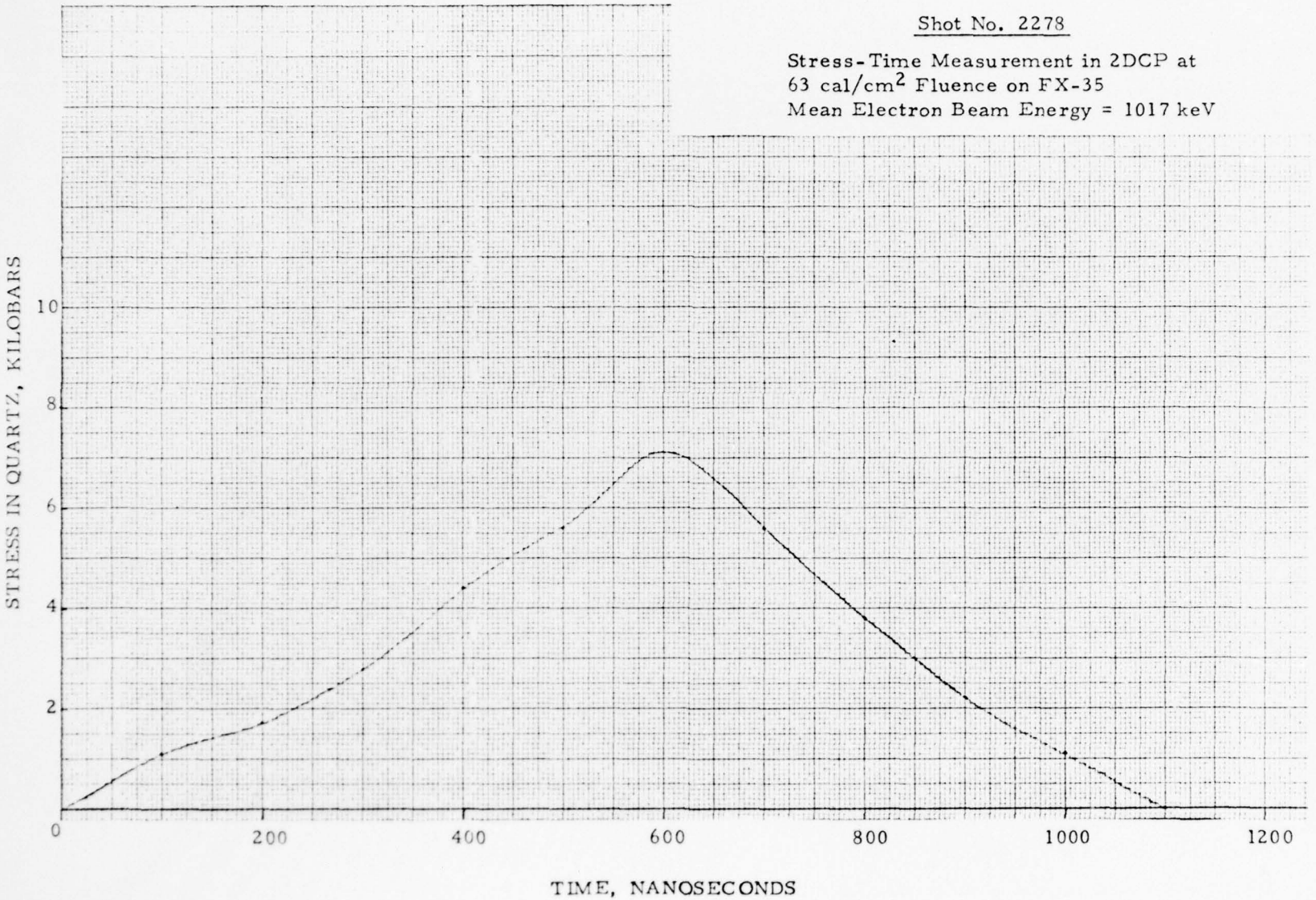

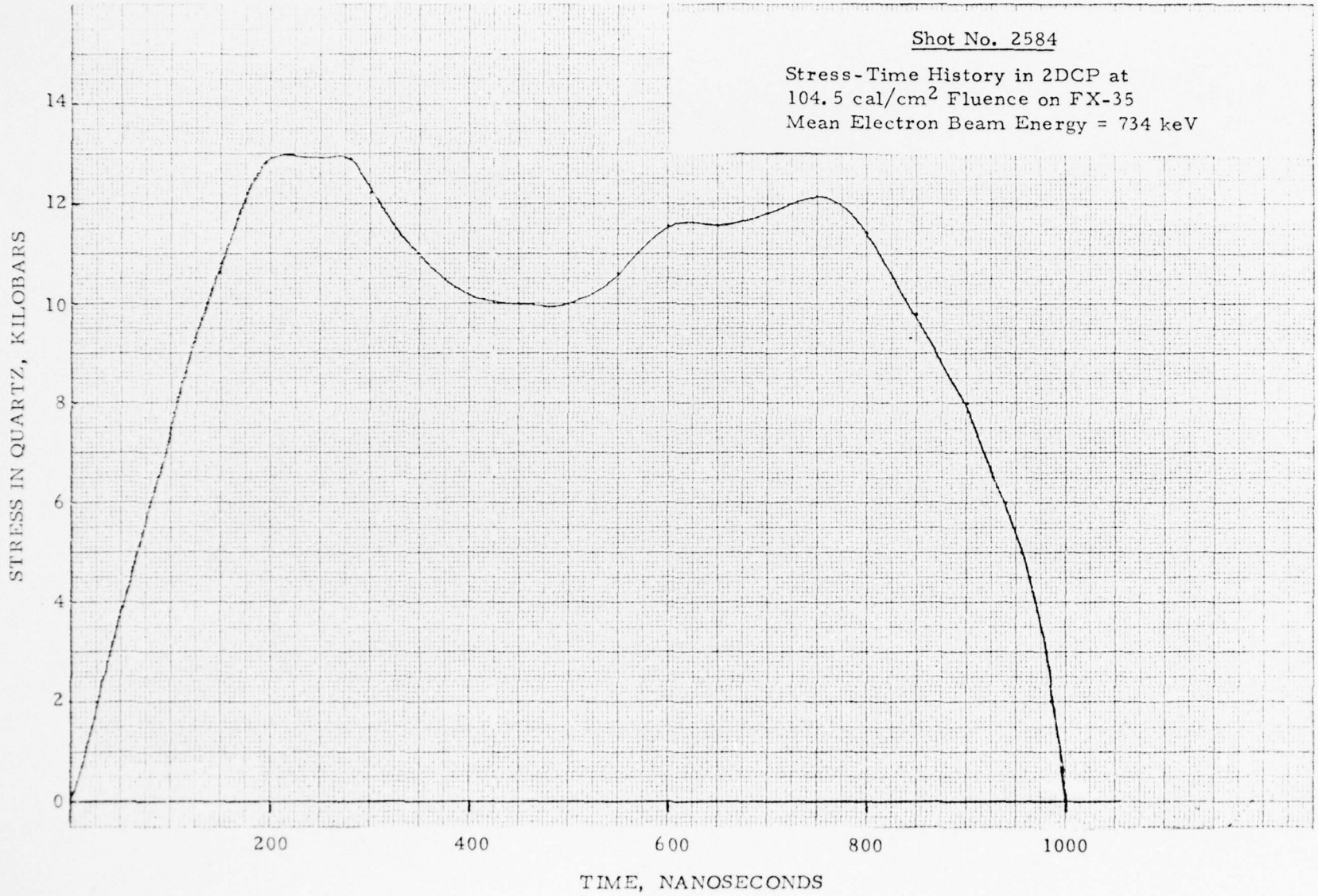
Shot No. 2584
Stress-Time History in 2DCP at
104.5 cal/cm² Fluence on FX-35
Mean Electron Beam Energy = 734 keV
STRESS IN QUARTZ, KILOBARS
0
2
4
6
8
10
12
14
200
400
600
800
1000
TIME, NANOSECONDS

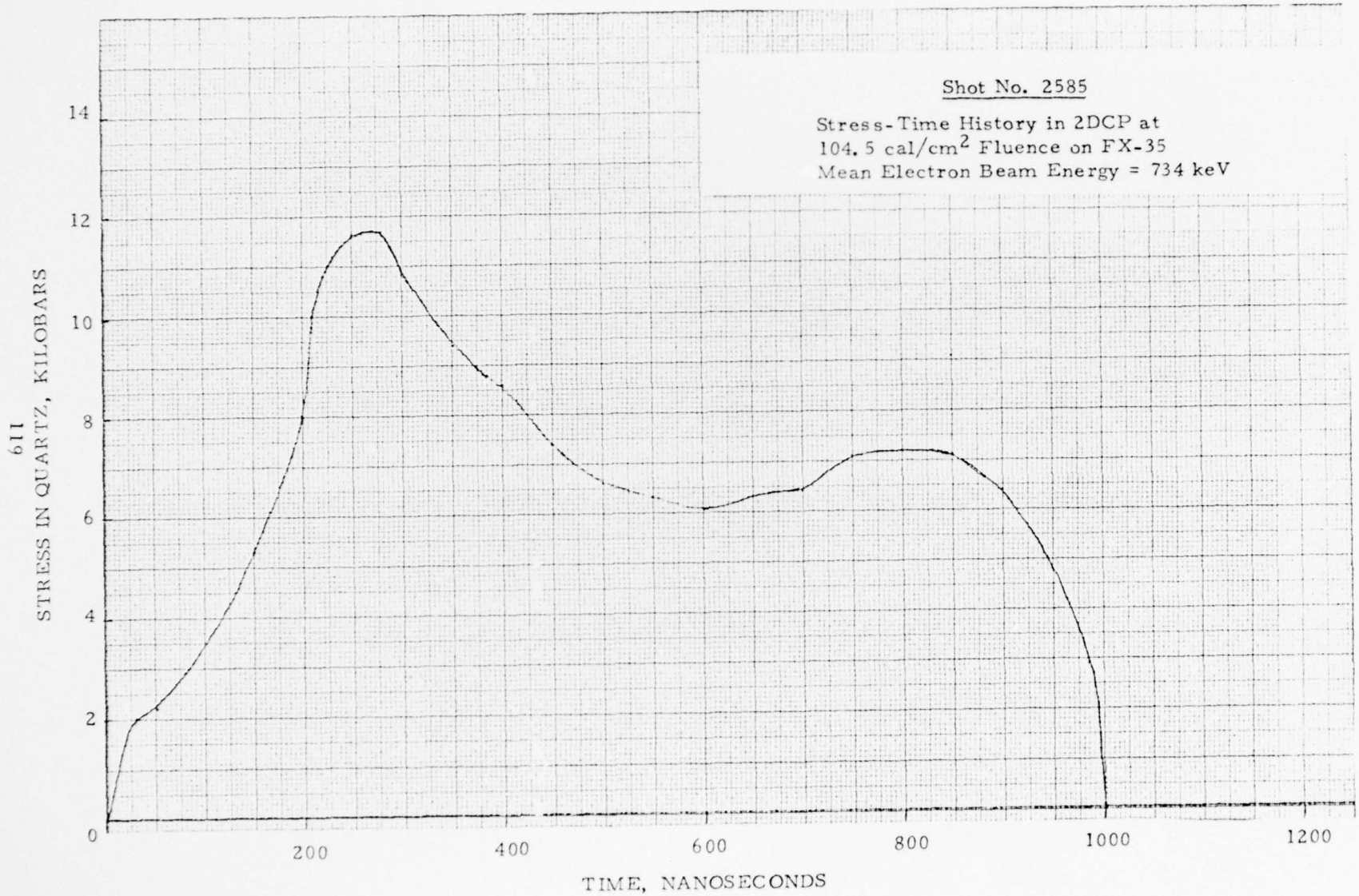
Shot No. 2585
Stress-Time History in 2DCP at
104.5 cal/cm^2 Fluence on FX-35
Mean Electron Beam Energy = 734 keV
611
STRESS IN QUARTZ, KILOBARS
0
2
4
6
8
10
12
14
200
400
600
800
1000
1200
TIME, NANOSECONDS

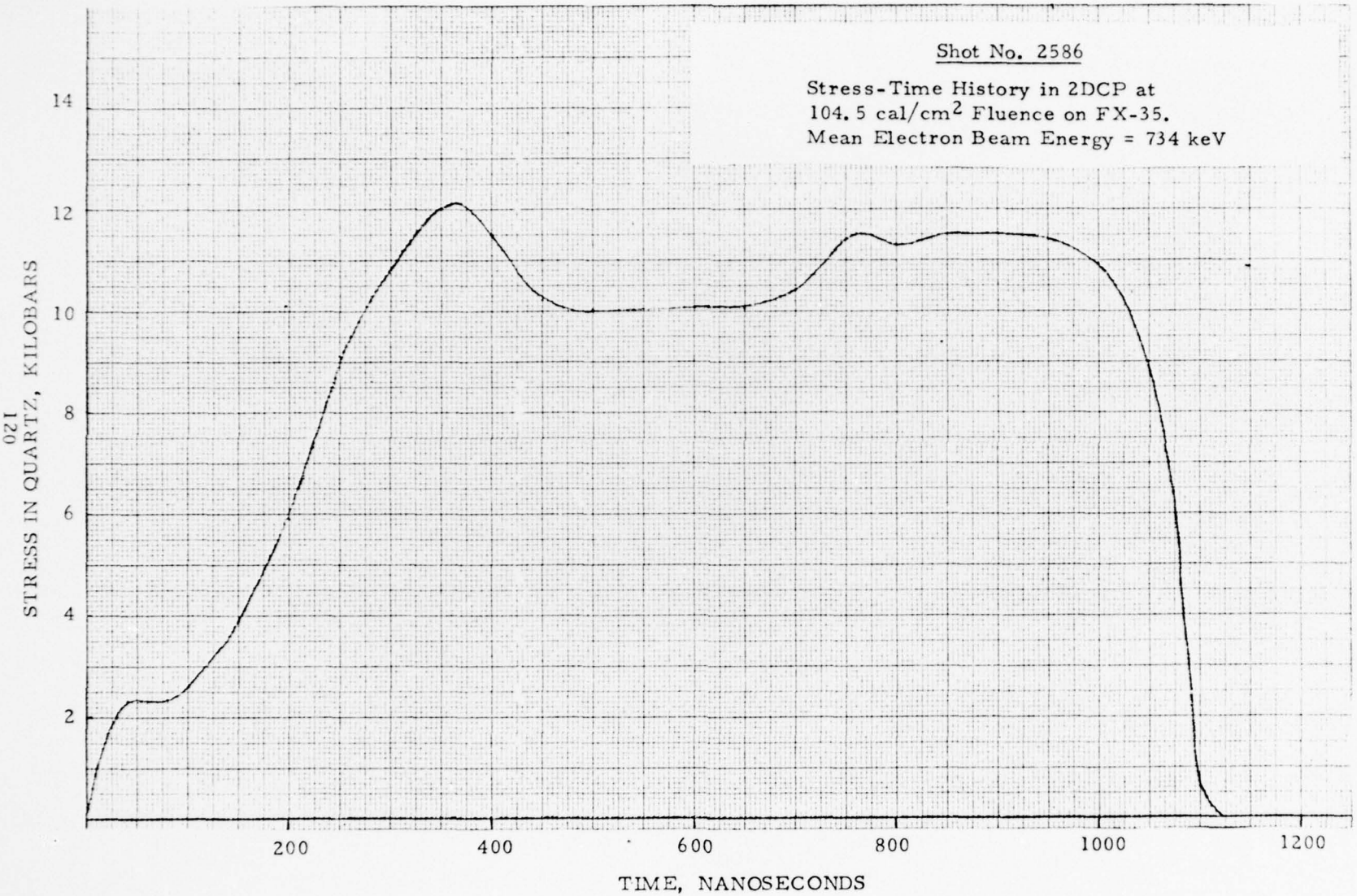
Shot No. 2586
Stress-Time History in 2DCP at
104.5 cal/cm² Fluence on FX-35.
Mean Electron Beam Energy = 734 keV
STRESS IN QUARTZ, KILOBARS
021
120
14
12
10
8
6
4
2
200
400
600
800
1000
1200
TIME, NANOSECONDS

DISTRIBUTION LIST

No. Cys.	
1	Hq. USAF, AFTAC (TAP)
1	AFISC (PQAL)
1	AUL (LDE)
1	AFIT (Tech. Library, Bldg. 640, Area B)
1	USAF, SCLO (Major J. H. Pierson, Chief, LO)
	Air Force Materials Lab.
1	Tech. Library
1	Dr. Robert Craig
	SAMSO
1	Tech. Library
1	RSSE
1	MNNR
1	AFATL (DLOSL)
1	AFRPL (DYSN)
	AFWL
1	HO/Dr. Minge
2	SUL
1	DY
1	DYV/Major C. D. Stuber
1	DYV/Major R. F. Mitchell
10	DYV/Mr. K. D. Smith
1	DYV/Mr. C. D. Newlander
1	DYS/Dr. W. Baker
1	ELS/Mr. B. Kline
	Army Materials & Mechanics Rsch. Center
1	Mr. J. Dignam
1	Dr. T. Chou
	Harry Diamond Laboratories
1	HDL Library
1	Mr. D. Schallhorn
1	Mr. P. Caldwell
1	Mr. S. Graybill
1	Mr. R. Oswald
1	Mr. J. Gwaltney
1	Comdg. Officer, BRL (AMXBR-ED, Mr. H. Burden), Aberdeen Proving Ground
1	Picatinny Arsenal, Dr. P. Harris
	Director, Naval Research Laboratory
1	Technical Library
2	Dr. G. Cooperstein
	Naval Surface Weapons Center
1	Mr. L. Gowan
1	Dr. J. Pastine
1	Dr. J. Sazama (CASINO)
1	Code 730, Technical Library

No. Cys.	
1	CO, NWEF (ADS)
	Director, DNA
2	APTL
2	SPSS
1	PPSR
1	SPAS/Mr. J. Moulton
5	SPAS/Mr. D. Kohler
5	RAEV/Mr. J. Farber
1	RAEV/Captain J. Van Prouyen
1	DDR&E (Asst. Dir., Strat. Wpns.)
	Dir., DIA
1	(DI-7D)
1	(DI-3)
1	Dir., OSD, ARPA (MMR)
1	Comdr., FC DNA (FCTA)
1	Chief, LVLO (FCTD-N-DNA)
1	Dir., Wpn. Sys. Eval. Gp. (Doc. Cont.)
1	JSTPS (JLTW)
2	DDC (TCA)
	Sandia Laboratories
1	Tech. Library, Orgn. 3141
1	Dr. L. Posey
1	Dr. B. Butcher
1	Dr. A. Toepfer
	Lawrence Livermore Laboratory
1	Dr. J. Keller
1	Dr. J. Moyer
	Los Alamos Scientific Laboratory
1	Report Library
1	Dr. R. Skaggs
1	Dr. R. Dingus
1	Aeronutronic Ford Corp., Mr. K. Attinger
	Aerospace Corporation, ABRES Program
1	Dr. B. Barry
1	Dr. M. Kausch
1	Dr. J. Benveniste
	AVCO Corporation
3	Dr. W. Bade
1	Mr. W. Broding
	The Boeing Aerospace Company
1	Dr. B. Lempriere
1	Mr. J. Adamski
1	Mr. J. Shrader

No. Cys.	
	Effects Technology, Inc.
1	Mr. B. Wengler
1	Mr. M. Rosen
1	Mr. W. Isbell
	General Electric Co., TEMPO-Center for Advanced Studies
1	DASIAC
	General Electric Company Space Division Valley Forge Space Center
1	Mr. G. Harrison
1	Mr. J. Hannabeck
1	Mr. R. G. Peterson
10	ION Physics Corp., Mr. D. Evans
	Kaman Sciences Corp.
1	Dr. F. Shelton
1	Mr. T. Meagher
	K Tech. Corp.
1	Dr. D. V. Keller
1	Mr. N. Froula
1	Mr. L. Lee
	Lockheed Missiles & Space Company, Inc.
1	Dr. M. Miller
1	Dr. A. O. Burford
1	Mr. R. Smith, Dept. 81-14
1	Mr. R. Walz
1	Mr. T. Kellcher

No. Cys.	
	Maxwell Laboratories, Inc.
1	Dr. V. Fargo
	McDonnell Douglas Astronautics Co.
1	Dr. R. J. Reck
1	Dr. H. Berkowitz
	Physics International Company
1	Dr. J. Shea
1	Mr. K. Childers
1	Dr. S. Putnam
	Prototype Development Associates, Inc.
1	Mr. T. McKinley
	R&D Associates
1	Dr. P. Rausch
1	Dr. A. Field
	Science Applications, Inc.
1	Dr. O. Nance
	Science Applications, Inc.
1	Dr. J. Cramer
	Simulation Physics, Inc.
1	Mr. R. Little
	Southern Research Institute
1	Mr. Colt Pears
	Stanford Research Institute
1	Mr. A. Lutze
	Systems, Science & Software
1	Dr. G. Gurtman
	Official Record Copy
1	Mr. C. D. Newlander, AFWL/DYV